Novel Concepts for the Characterization of the Delamination Resistance of Fiber Reinforced Polymer Laminates

Master's Thesis

Georg Singer, BSc

prepared at the

Chair of Materials Science and Testing of Plastics
Montanuniversitaet Leoben, Austria

and the

Department of Construction and Manufacturing Engineering
University of Oviedo, Spain

Thesis Supervisor: Dipl.-Ing. Steffen Stelzer

Academic Supervisor: Univ.-Prov. Dipl.-Ing. Dr.mont. Gerald Pinter

Leoben, September 2011

Master's Thesis

Mister Georg Singer, BSc

Novel concepts for the characterization of the delamination resistance of fiber reinforced polymer laminates

Work definition:

High performance fiber composites feature outstanding specific properties and therefore have an indisputable potential for applications in lightweight design. Nevertheless their susceptibility to delamination limits their applicability in primary structures, because delaminations can grow to a critical size and lead to the failure of a component made out of fiber reinforced composites. The most critical load case is cyclic loading due to the possibility of crack growth even below the static strength of the material. Based on very strict safety requirements related to the service life of components used for primary structures in the aerospace industry, novel concepts have to be developed in material testing to be able to characterize the delamination properties.

This thesis shall cover work on the interlaminar crack growth behavior of different types of fiber reinforced composites under cyclic loading conditions. In cooperation with the Universidad de Oviedo, Escuela Politécnica Superior de Ingeniería de Gijón, a novel concept to characterize the delamination behavior of unidirectionally reinforced composites under mode I loading conditions shall be developed. Through maintaining a constant stress intensity factor during the test a premature stop of the crack growth can be avoided. This can be realized via a continuous correction of the piston displacement.

Furthermore tests under cyclic mode II loading conditions with two different setups shall be carried out. The results of tests with an end notch flexure test rig, which is

already available at the institute, shall be compared to tests with an end load split set up, which has to be constructed.

The results of the master's thesis have to be demonstrated in a clear manner and have to be debated.

Leoben, September 9th, 2010

Dipl.-Ing. Steffen Stelzer

Univ.-Prof. Dipl.-Ing. Dr. mont. Gerald Pinter

Statutory Declaration

Hereby I state in lieu of an oath, that the presented Master's Thesis has been written by me and that no illegitimate aid but the literature cited and the support indicated has been used.

Leoben, September 14th, 2011

Georg Singer

Acknowledgement

First and foremost I want to express my gratitude to Univ. Prof. Dipl.-Ing. Dr. Gerald Pinter and Prof. Dr. Alfonso Fernández Canteli for making it possible to do parts of my research work at the Department of Construction and Manufacturing Engineering of the University of Oviedo in Spain. This was not only an academic, but also a personal enrichment.

Prof. Dr. Alfonso Canteli and Prof. Dr. Anonito Argüelles guided me during my measurements in Gijón and we had some constructive discussions regarding my results. In this regard I have to express my gratitude to Ms. Patricia Coronado Sáez for her supervision and her patience. She always helped me with any problem that occurred during my tests and also apart from working together I appreciate her hospitality.

During the whole project Univ. Prof. Dipl.-Ing. Gerald Pinter was available at any time to give me feedback to my work and to give inputs for further steps to be done. Especially I wish to thank Dipl.-Ing. Steffen Stelzer who did a great job in supervising me during all the months I worked for this thesis. Without him it would have been difficult to bring up all the motivation throughout the project. He was always available for discussions, provided a lot of constructive input to my work and was always interested in any question that occurred.

Further I want to thank Mr. Jürgen Föttinger who helped me a lot with the construction of the test device that was developed within this thesis. He also realized subsequent changes fast and practical. Special thanks also go to Dipl.-Ing. Florian Müller who helped me with all concerns regarding programming with MatLab.

Finally I want to thank my family and friends who supported me a lot, even during the last few months where I was not always easy to handle as I spent a lot of time to finish this thesis.

Abstract

In times of rising prices for raw materials and the worldwide need of reducing energy consumption, the construction of lightweight components is more relevant than ever. Therefore the use of carbon fiber reinforced polymers plays an extraordinary role and a broad understanding of their properties is of great importance. This thesis deals with fatigue delamination testing of unidirectional carbon fiber reinforced laminates with both epoxy and polyetheretherketone (PEEK) as matrix materials, under mode I and mode II loading conditions.

The goal for the mode I fatigue tests was to develop a test method to measure the crack propagation rate in a Double Cantilever Beam specimen at a constant strain energy release rate. Therefor in a first approach the crack tip opening diplacement was increased step-wise using predefined levels of machine displacement according to certain increments of crack length. This method was evolutionary improved until the energy release rate was held at a constant value by real-time processing of the measured load and displacement data based on a preliminary compliance calibration. This approach yielded the best results but has the problem that by maintaining the maximum and minimum energy release rate constant, the R-ratio of the displacement varies. Based on this problem, further investigations to improve this method should be performed.

The basic idea for the mode II fatigue tests was to compare the tests based on the End Notched Flexural and Calibrated End Loaded Split configuration. The applicability of the Calibrated End Loaded Split test under fatigue loading was the main target of investigation. Therefore an End Loaded Split fixture was constructed and first preliminary tests were performed. In a second stage material for an international round robin for the Technical Committee 4 of the European Structural Integrity Society was tested and the results are presented in this thesis. The tests yielded different results in the plot of energy release rate vs. crack propagation. No effects due to the mounting of the specimens could be proved by measurements of the local strains and heating of the specimen, but the reason for the different results could not be found yet. It will be interesting to see if the results of the other laboratories participating in the round robin show the same tendency. If they do so, the applicability of both test setups for measurements under fatigue loading conditions have to be questioned and further research should be performed.

Kurzfassung

In Zeiten ständig steigender Rohstoffpreise und dem weltweiten Trend zur Verringerung des Energieverbrauchs, erlangt die Konstruktion von Leichtbaukomponenten immer größere Bedeutung. In diesem Zusammenhang spielen kohlenstofffaserverstärkte Kunststoffe eine große Rolle und ein umfassendes Werkstoffverständnis ist für eine effektive Bauteilauslegung unumgänglich. Die vorliegende Arbeit beschäftigt sich mit dem zyklischen Delaminationswachstum unter Modus I bzw. Modus II Belastung. Bei dem geprüften Material handelt es sich um unidirektional verstärkte Laminate mit Epoxidharz bzw. Polyetherehterketon als Matrix.

Ziel der Versuche unter Modus I Belastung war es, eine Testmethode zu entwickeln bei der die Dehnungsenergiefreisetzungsrate bei der Prüfung eines „Double Cantilever Beam“ Probekörpers konstant gehalten wird. In einer ersten Annäherung wurde, abhängig von der Risslänge, der rissöffnende Maschinenweg in vordefinierten Schritten stufenweise erhöht. Das Ziel, eine kontinuierliche Regelung des Maschinenweges im Laufe eines Versuches zu erreichen, wurde durch eine Datenverarbeitung des Kraft- und des Wegsignals in Echtzeit realisiert. Im Vorfeld wurde eine sogenannte Kalibrierung der Nachgiebigkeit durchgeführt, wodurch die Energiefreisetzungsrate basierend auf den Messdaten der Maschine berechnet werden konnte. Die Methode lieferte letztlich konstante Ergebnisse für die Energiefreisetzungsrate, führte aber durch das konstant halten von minimaler und maximaler Energiefreisetzungsrate zu einer Veränderung des R-Verhältnisses während des Versuches. Daher sollte an einer weiteren Verbesserung der Versuchssteuerung gearbeitet werden.

Die Messungen unter Modus II basierten auf der Aufgabenstellung den sogenannten „End Notched Flexural“ Test mit dem „Calibrated End Loaded Split Test“ zu vergleichen. Im speziellen wurde die Anwendbarkeit des „Calibrated End Loaded Split“ Aufbaus für Ermüdungsversuche untersucht. Nach einer Reihe von Vorversuchen wurden schließlich Prüfungen im Rahmen eines internationalen „Round Robin“ Versuchs durchgeführt. Dieser wurde vom „Technical Committee 4“ der „European Structural Integrity Society“ organisiert. Die beiden Testaufbauten lieferten deutlich unterschiedliche Steigungen bei der Darstellung der Risswachstumsgeschwindigkeit über der Energiefreisetzungsrate. Einspanneffekte

der beiden Aufbauten konnten durch optische Dehnungsmessung und Infrarotaufnahmen nicht nachgewiesen werden. Die tatsächliche Ursache konnte bislang noch nicht gefunden werden. Wenn sich diese Ergebnisse im Rahmen des Round Robin Versuchs bestätigen, muss die Anwendbarkeit der beiden Messaufbauten hinsichtlich der Prüfung des zyklischen Delaminationswachstums hinterfragt und weiterführende Untersuchungen angestellt werden.

TABLE OF CONTENT

1. Introduction

With the development of improved manufacturing methods, composite materials have become the material of choice whenever high stiffness and strength at minimum weight are desired. Consequently, many advanced structural applications such as airplane wings, fuselages and aerospace structures now involve composites.

According to the actual trend of saving energy and increasing sustainability in all areas of our daily lives, in combination with rising raw material prices the optimization in construction and design of structural components is inevitable. Fiber reinforced polymers are playing a major role in lightweight components due to their outstanding specific mechanical properties. In aircraft and aerospace engineering their use increases steadily and not only secondary structures, but also primary components of commercial aircrafts are built of composite materials. For effective construction and weight reduction it is necessary to understand failure mechanisms in fiber reinforced polymers and their limits of applicability.

Fiber reinforced polymers show a high dependency of their mechanical strength on the fiber lay-up. A unidirectional reinforced polymer for example, can be highly loaded in the direction of the fibers but shows inferior strength when loaded perpendicularly to the fiber axis. In this case the matrix material has to carry all the load and the fibers even lead to a reduction of the mechanical strength of the matrix material due to the weakness of the fiber-matrix interface. A typical carbon-fiber reinforced epoxy laminate has an in-plane tensile strength of 1500-5000 MPa, dependent on precise layup and fiber type, however the through-thickness tensile strength can be as low as 50 MPa and also the through-thickness shear strength is relatively low. Hence it is clear that through-thickness stresses in a component may give rise to the initiation of delamination if they exceed the through-thickness strength. The subsequent propagation of a delamination however, is not controlled by the through-thickness strength, but by the interlaminar fracture toughness of the composite material (Hodgkinson, 2000; Ehrenstein, 2006).

To describe crack growth in composites under monotonic and fatigue loading conditions, linear elastic fracture mechanics (LEFM) has found the widest acceptance (Cvitkovich, 1995). The most critical loading case is cyclic loading due to the possibility of crack growth even below the static strength of the material. Although

almost three decades have passed since the importance of interlaminar fracture was recognized, interlaminar strength is still one of the design limiting factors in structural composites. Besides a large number of research works on static interlaminar properties of fiber reinforced polymers, numerous papers on delamination properties of laminates under fatigue loading have been published (Hojo, et. al., 2006).

The goal of this thesis is the development and comparison of novel methods of testing the interlaminar fracture toughness within the framework of the Technical Committee 4 (TC4) of the European Group on Fracture (now European Structural Integrity Society, ESIS) to establish a base for international standardization of testing the interlaminar fracture toughness of fiber reinforced polymers.

2. Background

Fracture mechanics was introduced after World War II to analyze fracture, which occasionally occurred at low stresses in high strength steel structures. Fracture mechanics is a science developed to analyze the tendency for a preexisting crack in a structure to grow as a result of applied external loads. Due to the preexistence of a crack, the strength of the structure may be decreased and, depending on the crack size, may fall below the designed limit load and cause structural collapse. Fracture mechanics may be employed to formulate laws on crack extension with an elapsed number of cycles (fatigue). This information leads to structural inspection schedules for monitoring the actual growth of the crack (Carlsson, 1993).

In the field of materials science fracture mechanics is an instrument for characterizing the fracture resistance of a material on a microscopic scale. Material parameters of importance for crack resistance can be isolated and materials with improved fracture toughness can be found. Most work on fracture mechanics is related to isotropic materials, such as metals or polymers. For anisotropic materials, e.g. composite materials, methods of the linear elastic fracture mechanics can be applied (Carlsson, 1993).

2.1 Delamination of fiber reinforced polymers

On a macroscopic level, damage of fiber composites can be grouped into fiber breakages, matrix cracks perpendicular to the fibers and delamination or interlaminar

cracks, which represent cracks between the plies in a composite laminate. The delamination mode of failure has received considerable attention because delamination may significantly reduce the compressive load-bearing capability of a composite structure and may grow under loading (Anderson, 1991; Carlsson, 1993; Hertzberg, 1996).

A basic assumption of fracture mechanics is that each real body or structure contains more or less large cracks which may be a result of production techniques or introduced in service by external stresses (Cvitkovich, 1995). Possible reasons for delamination are imperfections such as inferior fiber-matrix bonding or embedded pollutants, air or humidity, from which micro cracks can initiate and lead to delamination under subsequent loading. Special attention has to be focused on impact damage, because it can lead to invisible delamination inside the laminate. Figure 2.1 shows possible sources of delamination at which normal stresses can occur and lead to delamination.

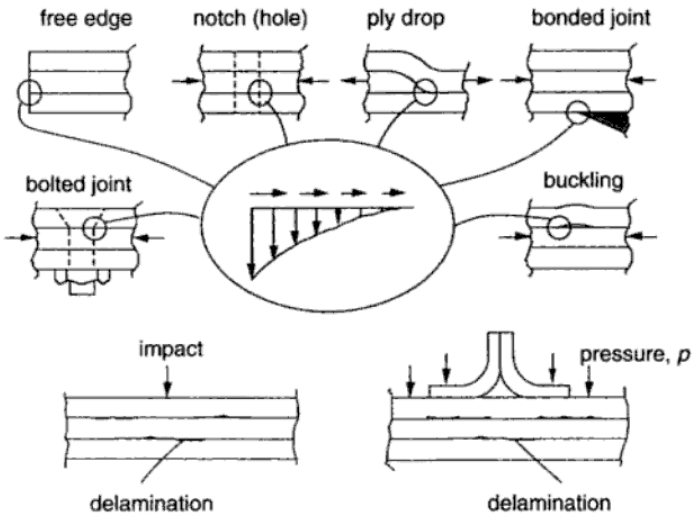

Figure 2.1: Possible sources of delamination (Hodgkinson, 2000).

Special test methods and specimen configurations have been developed for evaluating fiber composite fracture behavior with a focus on the determination of the interlaminar crack toughness. Depending on exterior loading and corresponding to the possible relative movement of the crack surfaces it can be distinguished among three methods of loading which differ in the relative movement of the crack surfaces as shown in Figure 2.2. Mode I, mode II and mixed mode I/II loading have the greatest practical significance. Mode I is the most critical loading condition and has therefore always been of great experimental interest (Grellmann and Seidler, 2007).

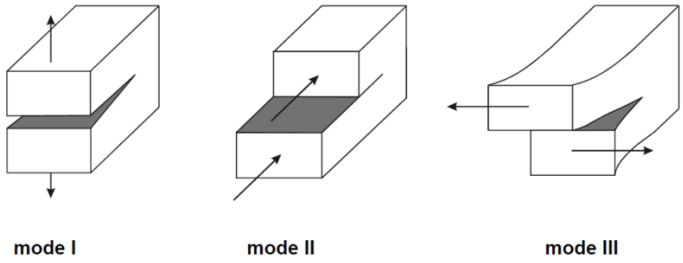

Figure 2.2: Illustration of the basic modes of crack loading, mode I (opening), mode II (in-plane shear), mode III (out-of-plane shear) (Anderson, 1991; Pinter, 2011).

2.2 Linear Elastic Fracture Mechanics

Fracture mechanics characterize the failure of materials under the influence of defects and imperfections which exist in all real components. An external loading can lead to crack growth starting from those defects. Linear elastic fracture mechanics (LEFM) is the basic scheme used for most investigations of continuous fiber reinforced polymers. LEFM has its theoretical basis in that all energy dissipation is associated with the fracture process and the deformation which occurs is linear elastic. This is beneficial since useful and simple methods can be developed in contrast to metals and polymer testing, where plasticity and non-linear effects are important in most tests (Williams, et. al., 2001).

Based on fundamental formulations of Griffith for an energetic approach to crack growth, Irwin proposed a more convenient model for solving engineering problems. The basis of this approach is that all energy dissipation is associated with the fracture process and the deformation which occurs is linear elastic. LEFM assumes that a linear elastic body contains a sharp crack and describes the change of energy which occurs when such a body undergoes an increase in crack area. The parameter describing this energy is called strain energy release rate, *G*, which is defined as the rate of energy released by the crack growth as described in Equation (1).

$$G = \left|\frac{dU}{dA}\right| \tag{1}$$

where *dU* is the change of the stored strain energy and *dA* is the increase of crack surface. To drive the crack growth, a certain energy release is needed to overcome the so called fracture resistance or critical energy release rate, G_C. Therefore, at fracture the critical energy release rate is given by:

$$G = \left|\frac{dU}{B * da}\right| = G_C \qquad (2)$$

where *a* is the crack length for a specimen of uniform thickness *B*. *G* is determined by the loading and geometry of the cracked body while G_C is a material property and is the energy per unit area necessary to create the new surface area of the crack.

An important aspect of fracture resistance is its dependency on the crack growth. Hence the plot of the critical energy release rate, G_C versus crack increment, Δa, is called the *resistance-* or *R-curve* as shown in Figure 2.3. The shape of the R-curve depends on the material behavior and to a lesser extent on the configuration of the cracked structure. A material shows a flat R-curve if the materials resistance is constant with crack growth, as illustrated by the dotted line in Figure 2.3. An ideally brittle material for example would yield a flat R-curve because the surface energy is an invariant property. When the resistance curve is flat, one can define a critical value of energy release rate *G*, unambiguously. Materials with rising R-curve (solid line in Figure 2.3) are often characterized by the value of initiation of the crack growth, but it has to be noted that this is only a characterization of the onset of crack growth and does not provide any information on the shape of the R-curve. When nonlinear material behavior accompanies fracture, however the R-curve can take on a variety of shapes. For example, ductile materials usually result in a rising R-curve, due to a plastic zone at the crack tip that dissipates energy. Usually, unidirectional carbon fiber reinforced polymers also yield a rising R-curve. This effect can be referred to nonlinearities at the crack tip and to fiber bridging which is described in clause 2.3 (Anderson, 1991; Williams, et. al., 2001).

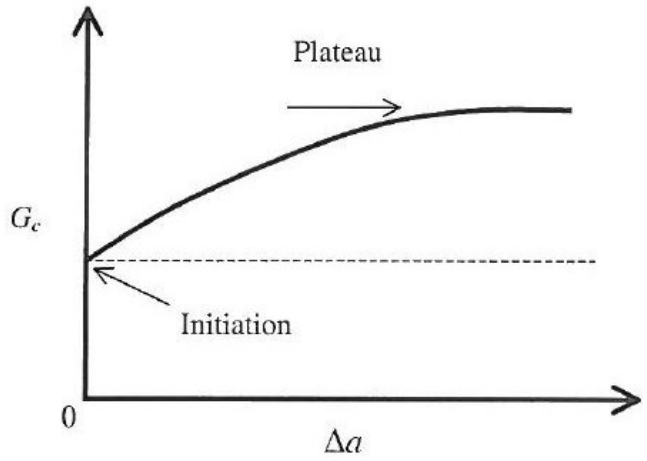

Figure 2.3: Resistance- or R-curve, a complete description of the fracture toughness of a material (Williams, et. al., 2001).

The initiation value is usually the lowest and is thus judged to be most critical. Many R-curves tend to level out to a plateau value which can be seen as an upper limit for G_C. If the initial value is the highest, this leads to an immediate catastrophic failure of the whole specimen as it was shown by Johnson and Pavlick. Especially at low temperatures the R-curve can have an inverted shape (Johnson and Pavlick, 2005). Every type of specimen geometry used, has to be calibrated so that load or energy measurements at fracture can be converted to G_C. By measuring the specimen's compliance C (= inverted stiffness) as a function of crack length a, Equation (1) can be converted to:

$$G = \frac{P^2}{2B} * \frac{dC}{da} \tag{3}$$

where P is the load applied to the specimen (Williams, et. al., 2001).

Another approach to determine the materials fracture toughness besides the energetic way is to describe the local stress field around the crack tip based on concepts of elastic theory. According to this approach the stresses are singular directly at the crack tip ($r \rightarrow 0$, see Figure 2.4). This leads to the formation of a plastic zone in front of the crack tip and contrary to LEFM, to an elastic-plastic comportment. The stress distribution around any crack in a structure is similar and depends only on the parameters r and the angle measured from the crack line. The difference between one cracked component and another lies in the magnitude of the stress field parameter, which is defined as the stress intensity factor, K. As long as the plastic zone is small compared to the smallest length of the specimen, LEFM can be applied (Hertzberg, 1996).

$$K = \sigma * \sqrt{\pi * a} * f(a/w) \tag{4}$$

where: σ……stress
a……crack length
w……width of the specimen
f(a/w)……dimensionless correction factor

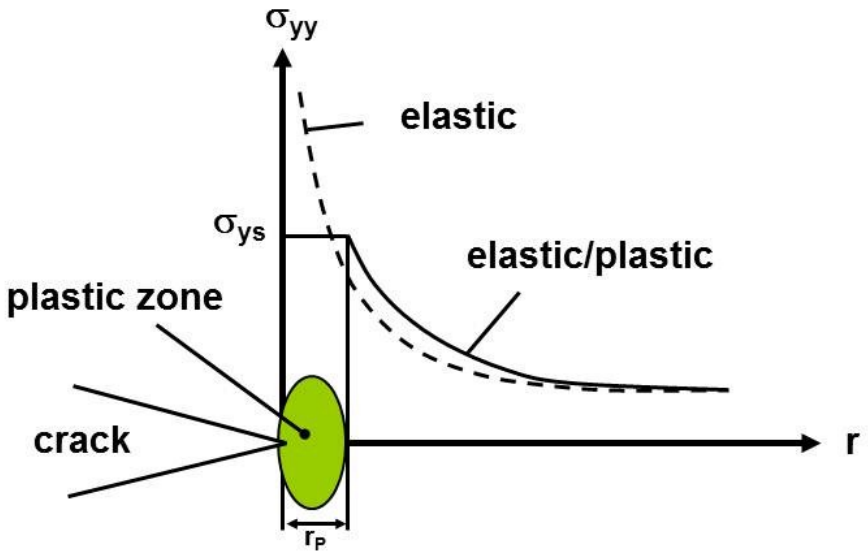

Figure 2.4: Schematic illustration of the local stress field near the crack tip (Pinter, 2011).

For metals and polymers, fracture toughness is often described in terms of the critical stress intensity factor, K_C. For linear elastic isotropic materials K_{IC} and G_{IC} are related by the following expression for the plain strain case,

$$G_I = \frac{{K_{IC}}^2}{E} * (1 - \nu^2) \tag{5}$$

and for plain stress:

$$G_I = \frac{{K_{IC}}^2}{E} \tag{6}$$

where: E……Young's modulus

v……Poisson's ratio

The energy release rate, *G*, and the stress intensity factor, *K*, are used most commonly to describe the fracture toughness of fiber reinforced polymers. The energy release rate quantifies the change in potential energy that accompanies an increment of crack extension, while *K* characterizes the stresses, strains and displacements near the crack tip. That means that *G* describes a global behavior and *K* is a local parameter. For a typical aerospace aluminum alloy with a K_{IC} of 35 MPa $m^{1/2}$, Equation (5) yields a G_{IC} of 16 kJ m^{-2}, which is considerably higher than the measured G_{IC} value of 0.27 ÷ 1.74 kJ m^{-2} for composite laminates. This shows their affinity to delamination. In general, for the characterization of the delamination behavior of fiber reinforced materials, the energy release rate approach is used. As

the fiber-matrix compound is not isotropic, a complex stress field develops at the crack tip which is difficult to describe by using the stress intensity factor *K* (Hertzberg, 1996; Hodgkinson, 2000; Williams, et. al., 2001; Sjörgen and Asp, 2002).

2.3 Interlaminar fatigue crack growth in Continuous Fiber Reinforced Polymer Composites

The concept of LEFM has been successfully implemented and applied to describe interlaminar crack growth in laminated fiber composites under fatigue loading conditions (Anderson, 1991). Crack propagation is mostly described in terms of the energy release rate, *G*, related to the crack growth rate per cycle, *da/dN* (Brunner, et. al., 2009). By monitoring the maximum and minimum load within a loading cycle, the maximum and minimum strain energy release rates G_{max} and G_{min} can be determined. The cyclic strain energy release rate is then given by

$$\Delta G = G_{max} - G_{min} \tag{7}$$

Figure 2.5 is a schematic plot of *da/dN* versus ΔG, which illustrates typical fatigue crack growth behavior in fiber reinforced polymer composites. The curve contains three distinct regions. At intermediate ΔG values, the curve is linear (Figure 2.5, section II), but the crack growth rate deviates from the linear trend at high and low ΔG levels (Figure 2.5, sections I and III). In section III of Figure 2.5 the crack growth rate accelerates as G_{max} approaches G_c, the critical strain energy release rate of the material. At the other extreme, in section I, *da/dN* approaches zero at a threshold value, G_{th} (Anderson, 1991).

The linear region of the *da/dN* versus ΔG plot in Figure 2.5 can be described by the following power law:

$$\frac{da}{dN} = A * \Delta G^m \tag{8}$$

where *A* and *m* are experimentally determined material constants. The relationship of Equation (8) is widely known as Paris law and shows that the fatigue crack growth depends only on ΔG (Anderson, 1991).

If the *da/dN* curve is shifted to higher values of ΔG the material is more resistant to fatigue delamination. This means that higher loading levels are necessary to initiate

fatigue crack growth. Further a smaller slope of the curve, as illustrated in Figure 2.5, indicates slower crack propagation and therefore longer life cycles can be realized (Pinter, 1994). In this regard laminates can clearly be distinguished, but a comparison of the slopes cannot be used for a ranking of materials with respect to their delamination resistance performance. This method is only suitable for local comparisons at certain loading levels, but no conclusions can be drawn on the value of ΔG at which G_{th} or G_c is reached (Stelzer, et. al., 2011).

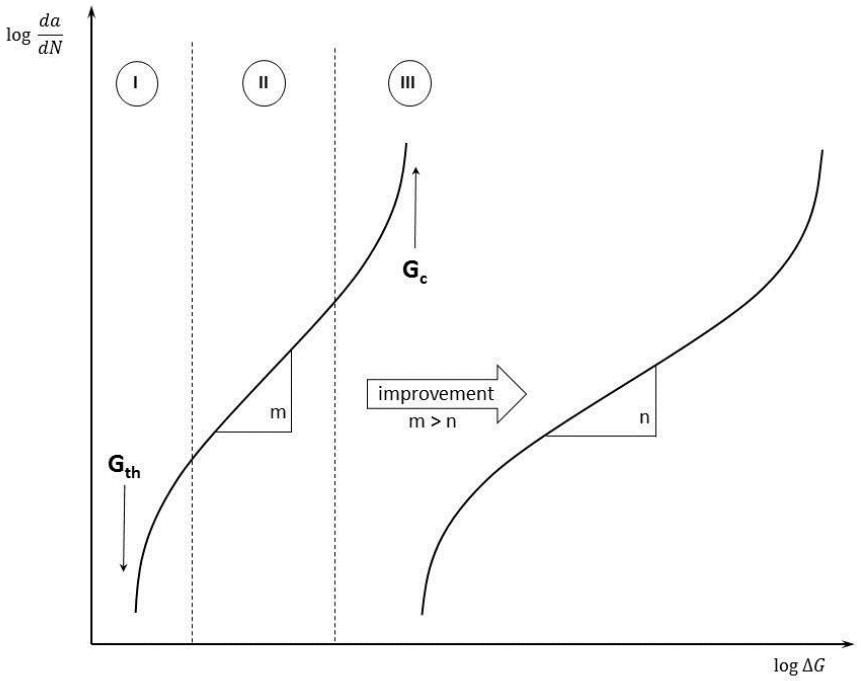

Figure 2.5: Schematic illustration of a fatigue crack propagation curve (Pinter, 1994).

There are two different approaches for measuring the interlaminar fatigue crack growth. On the one hand the test can be performed under displacement control where the crack opening displacement is held constant throughout the test (Brunner, et. al, 2009), or on the other hand the force can be controlled and maintained at a constant level (Cvitkovich, 1995; Pinter, 1994). By taking a look at the so called Paris plot, one can see the difference in determining the crack propagation behavior between the two methods (Figure 2.6). While force controlled tests start with very small crack propagation rates and end in catastrophic failure, tests performed with displacement control start just below the critical energy release rate with high crack propagation rates and slow down as the crack grows. This means by maintaining a constant displacement during the test, the energy release rate decreases. According to the decline of the energy release rate the crack propagation rate slows down until

the crack finally stops growing. This test method allows rough results within reasonable time to be obtained (minimum test duration between 8 and 10 hours). In order to detect threshold values however, the test duration has to be increased significantly as crack propagation even after 20 million cycles has been reported (Brunner, et. al., 2009).

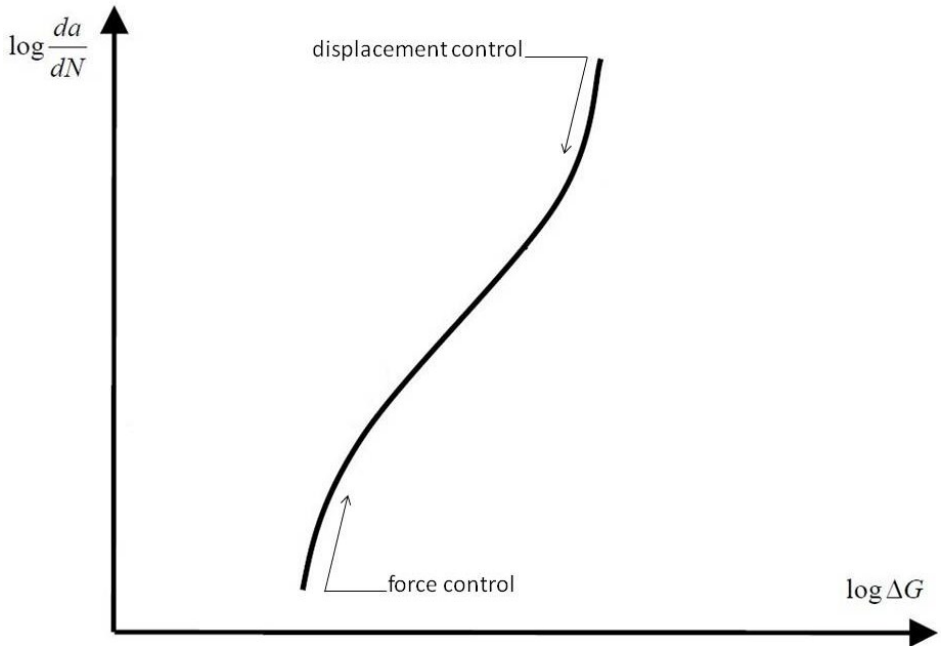

Figure 2.6: Determining the interlaminar crack propagation behavior by either force control or displacement control.

In general threshold values used in a no-growth design concept have to be regarded critically. Especially at low frequencies or large displacements the determination of such values may require long test duration. It is not yet clear if such threshold values exist or whether they appear due to limited experimental measurement resolution when keeping in mind that a crack growth rate of 10^{-6} mm/cycle equates to a growth of one nanometer per cycle. Hence it is questionable if a threshold actually exists. As described by Stelzer et al. noise in the load signal of the testing machine leads to significant scatter in the Paris plot, especially at low delamination rates. That means that the determination of Paris plots at low delamination rates may be affected by measurement resolution of the load-cell (Stelzer, et. al., 2011).

An important factor of influence on the energy release rate, especially under mode I loading conditions, is the occurrence of fiber bridging. Fiber bridging is a phenomenon that is commonly observed in fracture in nearly all types of fibrous

composites. Figure 2.7 shows in principle fibers bridging the gap between the fracture faces directly behind the crack tip. As the delamination extends, these fibers gradually become strained and subsequently divert some of the available strain energy away from the crack tip (Russell and Street, 1988). In general, bridging is a positive attribute of fracture in composites because more energy has to be applied to the system in order to propagate the bridged crack. Fiber bridging does not typically occur between plies of different orientations, but unidirectional laminates tend to fiber bridging. Tests to determine interlaminar fracture toughness are usually performed using unidirectional lay-ups. Hence crack propagation measurements may not be representative of the behavior in an actual structure, as due to fiber bridging the strain energy release rate is overestimated (Gregory and Spearing, 2004).

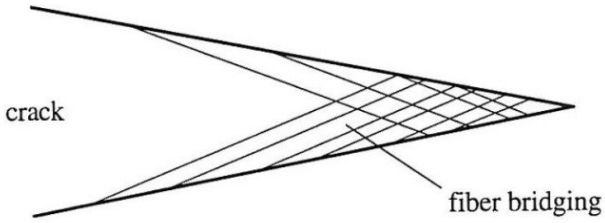

Figure 2.7: Fibers bridging from one crack surface to the other (Cvitkovich, 1995).

According to Russell and Street it is more difficult to quantify the effects of fiber bridging under fatigue loading conditions on the crack propagation rate compared to the quasi-static case. While maintaining constant displacement during a fatigue test the energy release rate keeps decreasing. According to the decline of the energy release rate the crack propagation rate also slows down until the crack finally stops growing. Hence, any decrease in *da/dN* due to fiber bridging may be obscured by the decrease of the energy release rate because of the constant displacement in a fatigue test (Russell and Street, 1988). A method to overcome this problem, proposed by Russell and Street, is to carry out testing under conditions of constant ΔG. Then, only *da/dN* needs to be monitored and plotted against crack length, *a*, for different values of ΔG. The tests were carried out on Double Cantilever Beam (DCB) specimens and the experimental arrangement is shown in Figure 2.8. An elastic spring inserted in series with the specimen automatically increases the opening displacement of the specimen as the crack extends. Because the compliance of the spring is twice as high as the initial specimen compliance, no immediate reduction of ΔG occurs and after several millimeters of crack growth it is necessary to gradually

increase the piston displacement in order to maintain ΔG constant (Russell and Street, 1988).

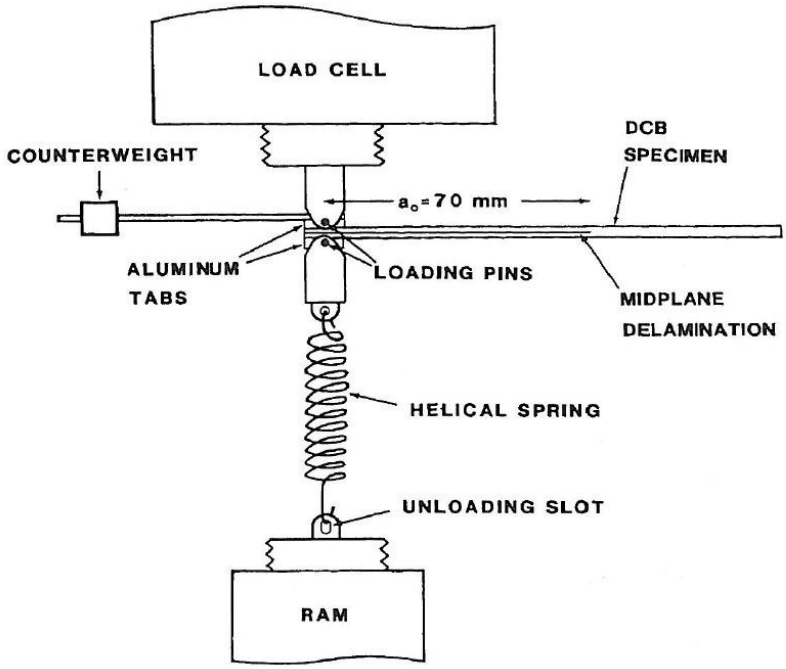

Figure 2.8: Experimental arrangement for constant ΔG interlaminar fatigue after Russell and Street (Russell and Street, 1988).

In 1994 Hojo et al. investigated different methods for the measurements of fatigue crack growth threshold. Since the exponents in the power law of Equation (8) for carbon fiber reinforced polymers are much higher than those for conventional metallic materials, the evaluation of the delamination fatigue threshold is of great relevance (Hojo, et. al., 1994a; 1987). At first, results of the delamination growth onset method indicated a large scatter, and the threshold values depended on the definition of the growth onset. Thereupon constant energy release rate tests indicated that the crack propagation rate *da/dN* decreases with the increment of crack length what can be referred to the occurrence of fiber bridging. The *da/dN* at zero increment of crack length was expressed as a power function of the maximum energy release rate. Below *da/dN* = 10^{-6} mm/cycle, non-propagating cracks indicated the existence of the growth threshold. The threshold values obtained from G_{max}-constant tests were the most conservative ones which were not affected by fiber bridging. Subsequently a new simple test method was proposed, which is the iteration of load-shedding tests. The threshold values converged after several tests, and the threshold value agreed with that obtained by the constant maximum energy release rate test (Hojo, et. al., 1994b).

The goal of this thesis, concerning mode I measurements, was to implement ΔG-constant tests by controlling the test parameters through immediate processing in the machine's software. The decrease in crack propagation rate and finally the arrest in a classic mode I test under displacement control usually happen within a few millimeters. Keeping the energy release rate constant by increasing the machines displacement with the growing crack allows testing the specimen over a wider area and to obtain more significant results. This could also be used for a quick material comparison as the slope of the linear region in a Paris-plot can be estimated by performing three tests at different levels of ΔG within reasonable time. Figure 2.9

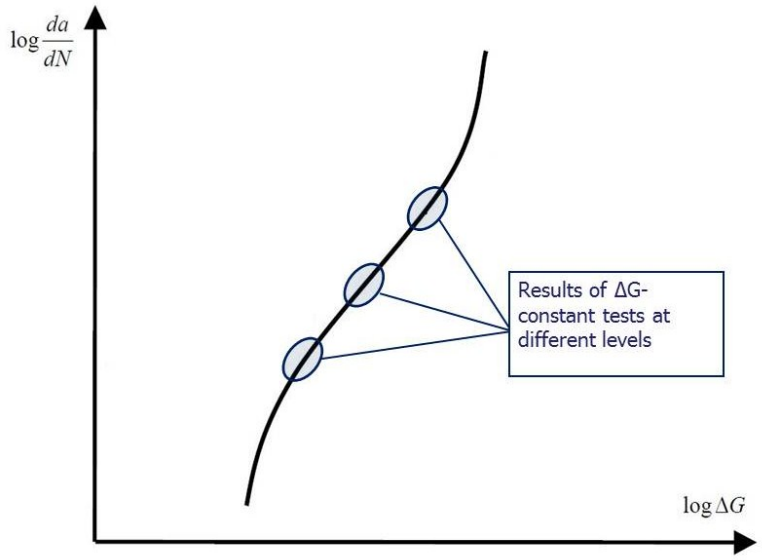

Figure 2.9: Schematic illustration of the results of ΔG constant tests in the Paris plot.

The general development of mode I fatigue testing was based on the quasi-static mode I test ISO 15024. For mode II shear load fatigue, test development cannot be based on an existing quasi-static ISO standard. A variety of mode II setups have been proposed for quasi-static testing. Essential criteria for fatigue test development are, as it was in mode I development, the applicability in an industrial test environment, simple test setup and data analysis (Brunner, et. al., 2010).

Figure 2.10 shows different test setups for quasi-static mode II delamination testing. The end-notched flexure (3ENF) test was originally carried out using three-point loading (Figure 2.10a) which has the great disadvantage of unstable crack propagation below a ratio of crack length to span length of a/L = 0.55 and yields only initiation values of G_{IIC}. For this reason it is not widely considered suitable for an international standard, but is being pursued as an initiation test by the American

Society for Testing and Materials (ASTM) (Martin and Murri, 1990; Asp, et al., 2001; Sjörgen and Asp, 2002; Blackman, et al., 2006; Argüelles, et al., 2010). In the stabilized 3ENF (Figure 2.10b) test the crack shear displacement has to be measured and this value is then used to control the real-time loading of the test specimen. For an international standardization this method was considered to be too complex (Davies, et al., 1998; Blackman, et al., 2006). Other studies have been performed using the 4ENF (Figure 2.10c) test which allows the full resistance curve (R-curve) to be deduced for the composite (Blackman, et al., 2005), but friction has a more significant influence compared for example to 3ENF. Furthermore the calibrated end-loaded split (C-ELS, Figure 2.10d) setup is used for testing under mode II loading conditions. Two main conclusions for C-ELS tests were drawn from earlier studies by the European Structural Integrity Society (ESIS), Technical Committee 4 on Polymers and Polymer Composites (TC4). Firstly, it is very difficult to measure the crack length accurately during mode II delamination in the absence of any applied beam opening displacement. Secondly, the clamping of the sample, as required in the C-ELS test, appeared to introduce variability (Blackman, et al., 2006). An advantage of the C-ELS setup is that the same test rig can be used for a fixed-ratio Mixed-mode I/II test, the so called Asymmetric Double Cantilever Beam (ADCB) test. Fatigue Mixed-mode I/II tests using the ADCB setup provide a fixed ratio of mode I to mode II of 4 to 3 (Brunner, et al., 2010). Despite all advantages and disadvantages as described above, for fiber reinforced polymer composite laminates the calibrated end-loaded split test is preferred to the both ENF setups. The ESIS, TC4 on Polymers and Polymer Composites, has applied this method extensively and its applicability for fatigue testing shall be investigated (Blackman, et al., 2006).

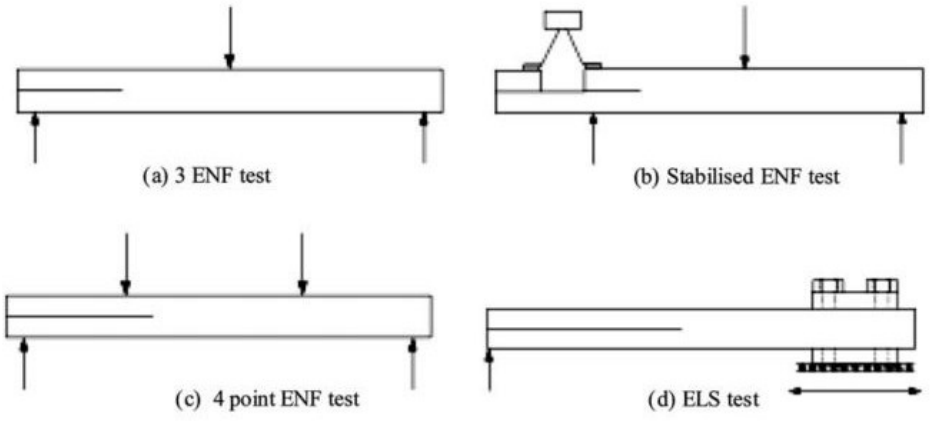

Figure 2.10: Diagram of various mode II delamination test setups (Blackman, et al., 2006).

Regarding the 3ENF test setup under fatigue load it has to be taken in account that the specimen has to be fixed against shifting sideways. Because the specimen delaminates at one end only, it will deflect asymmetrically, resulting in small side forces which tend to shift the specimen on the roller fixture of the 3ENF setup (Martin and Murri, 1988). Martin and Murri applied a restraining bar that was free to rotate as the specimen deforms during the test (Figure 2.11 (a)). To prevent the specimen from sliding in the three-point bending fixture during fatigue testing Cvitkovich used an additional roller at the opposite of the load introduction point which was fixed to the original roller with lock nuts and clamped hand tight (Figure 2.11 (b)). Stelzer mounted an elastic wire between the loading roller and the end of the specimen which had to be notched beforehand (Figure 2.11 (c)).

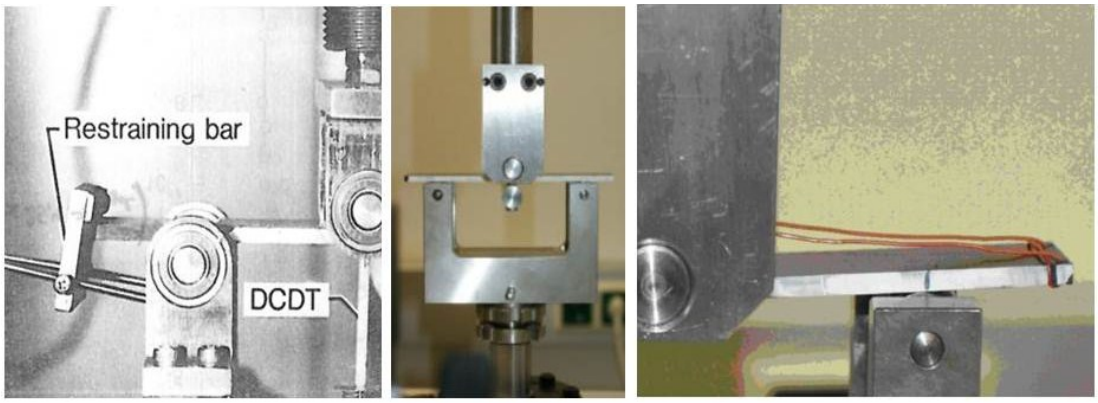

Figure 2.11: Different approaches to eliminate the shifting effect during 3ENF fatigue testing (Martin and Murri, 1988; Cvitkovich, 1995; Brunner, et al., 2010)

The scope of this thesis regarding mode II measurements was to design a C-ELS fixture and to realize first tests. Further, the reproducibility and the differences to 3ENF test results were investigated. Finally a comparison of 3ENF- and C-ELS-tests for an actual Round Robin was performed and the results are presented.

3. Experimental

3.1 Materials and Specimens

All of the test specimens were unidirectional reinforced laminates with either epoxy or polyetheretherketone (PEEK) serving as matrix material and were conditioned to +23°C and 50% relative humidity for at least one week before testing. For testing under mode I loading conditions with extensometer control (see clause 3.2.1) two types of epoxy resin from BASF AG (Ludwigshafen, Germany) were used. The used types were Rigidite 5276 (R5276) and Rigidite 5259 (R5259) which are both toughness-modified types. The carbon fibers used for these specimens were of the type Celion G30-500 12K produced by BASF Structural Materials (Charlotte, USA). The tested specimens differed from the proposed specimen according to ISO 15024. In deviation from the standard, the crack starter film had a length of 20 mm. As the tests with attached extensometer were performed with grips as shown in Figure 3.8, the specimens had to be notched for clamping. The dimensions of these specimens were 150x20x8 mm (LxBxH, see also Table 3.1), and a notch with 17 mm depth and 3 mm height was cut into the specimen (Figure 3.1) with an IsoMet® 4000 Linear Precision Saw (Buehler, Illinois, USA) which is pictured in Figure 3.2. It is important not to cut further than the starter film because otherwise the crack would not automatically initiate in the mid-layer of the specimen.

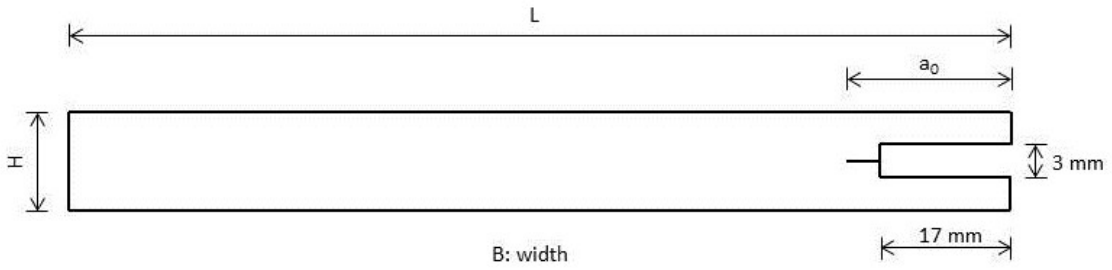

Figure 3.1: Notched specimen for ∆G constant tests with attached extensometer.

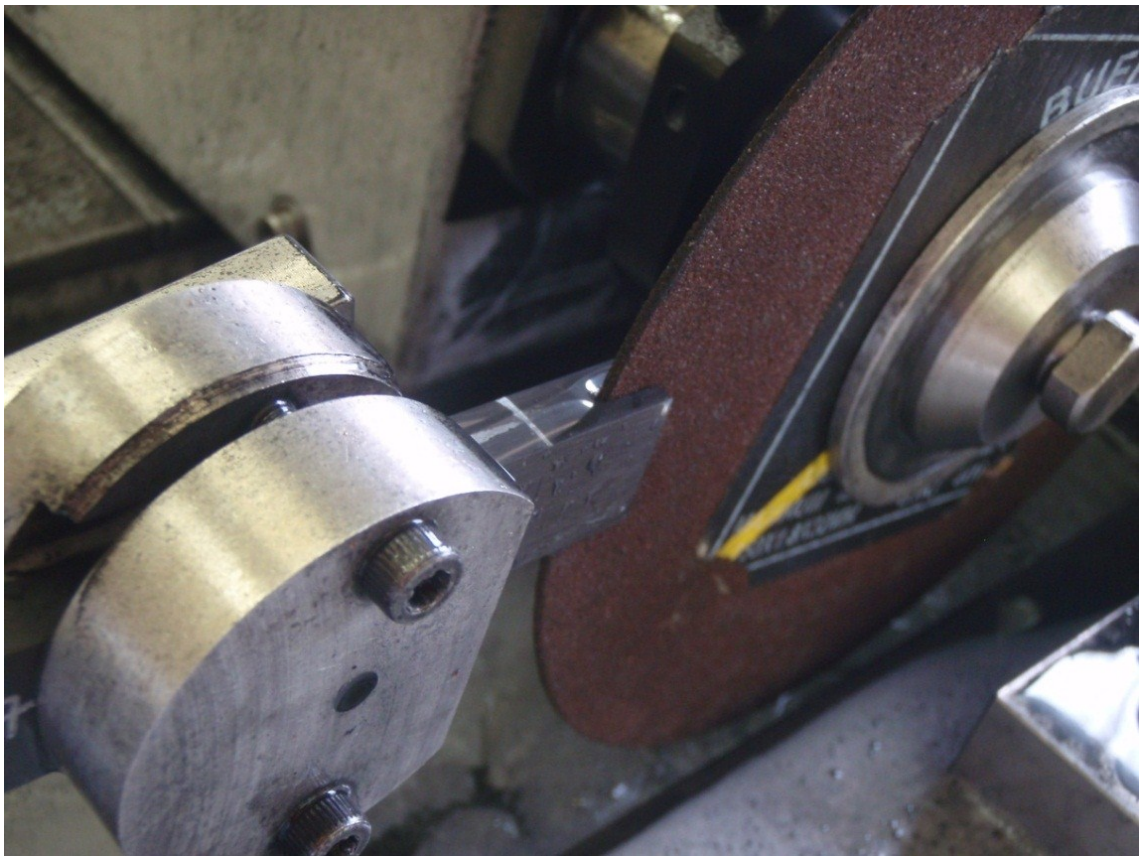

Figure 3.2: IsoMet® 4000 Linear Precision Saw for notching the specimens.

After cutting the notch into the specimens they were put into a drying chamber for a few hours to eliminate the humidity, which was incorporated during cutting due to the cooling water. After opening the crack to the initial crack length the next step was to apply the marking to facilitate reading the crack length during the fatigue test by spraying white lacquer to the edge of the specimen. After the lacquer dried up, the specimen was marked every 5 mm with a sliding caliper, beginning at the initial crack length as shown in Figure 3.3.

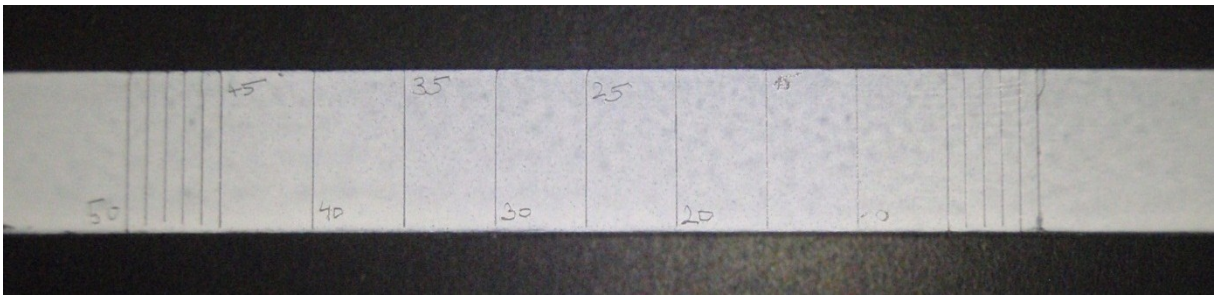

Figure 3.3: Markers for determining the crack length for tests under extensometer control.

For measurements under mode I loading conditions with compliance control (see clause 3.2.2) and mode II testing, on the one hand specimens with R5259 matrix and Celion G30-500 12K fibers and on the other hand specimens with PEEK matrix were tested. The thermoplastic matrix was of PEEK from ICI (Östringen, Germany) with carbon fibers of the type AS4 by Hercules Inc. (Magna, USA) with characteristics similar to the Celion G30-500 12K fiber. The dimensions of these specimens were 120x20x3 mm (LxBxH, see also Table 3.1). The length of the starter film for the specimens of PEEK was 20 mm and the ones of Rigidite 30 mm. The load was applied via aluminum loading blocks that were mounted to the specimens as shown in Figure 3.4. The crack lengths were recorded using a travelling microscope with 40x magnification. In order to increase the contrast for determining the position of the crack, typewriter correction fluid was applied.

For measurements under mode II loading conditions a thin layer of typewriter correction fluid was also applied to one edge of the specimen. Furthermore, the specimens were marked with a fine ball-pen at increments of 2.5 mm as shown in Figure 3.5.

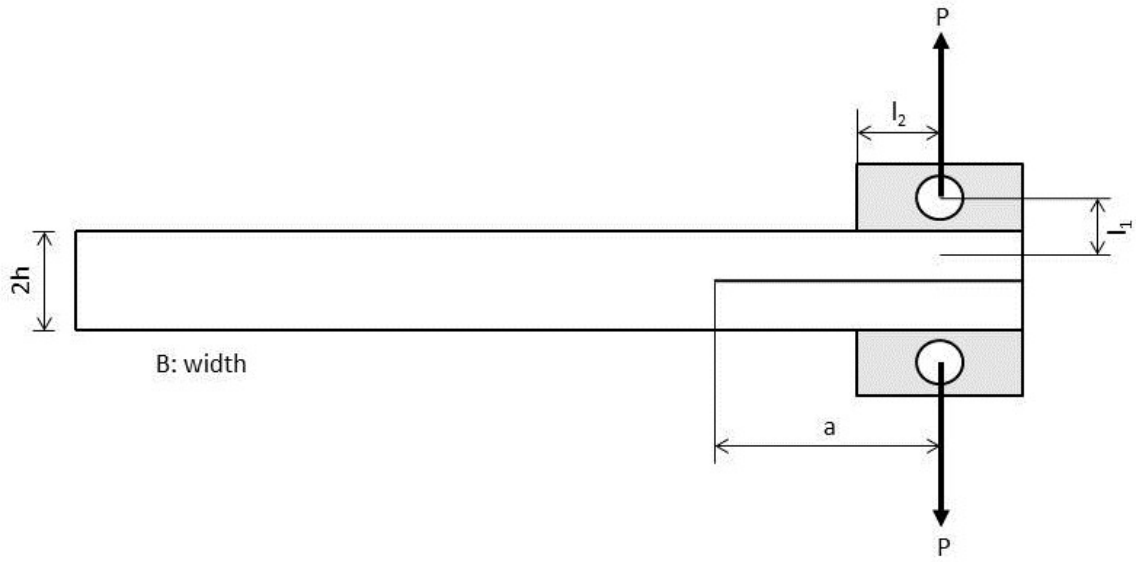

Figure 3.4: DCB specimen with loading blocks for mode I loading.

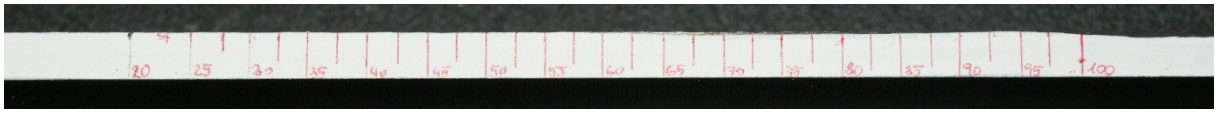

Figure 3.5: Specimen marked at increments of 2.5mm from 20÷100 mm crack length (measured from the load-line) for mode II loading.

The laminates for the mode II round robin measurements had the denotation IM7 - 977/2 and were supplied by CYTEC Industries Inc (Cytec Industries Inc., New Jersey, USA). The specimens used for the round robin measurements had the dimensions 150x20x4 mm (LxBxH, see also Table 3.1) and had a length of the starter film of 60 mm. Typewriter correction fluid and markings at increments of 2.5 mm were applied as described above.

For all specimens under both, mode I and mode II loading, the overall length of the specimen was measured to the nearest mm. The width, *b,* was measured at three evenly spaced points along the length of the specimen. The thickness, *2h,* was measured at six points, three at each edge of the specimen. For mode I and mode II C-ELS tests, the lengths l_1 and l_2 had to be measured (Figure 3.4 and Figure 3.6). Additionally for mode II C-ELS tests the length l_3 and the height *H* had to be determined (Figure 3.6).

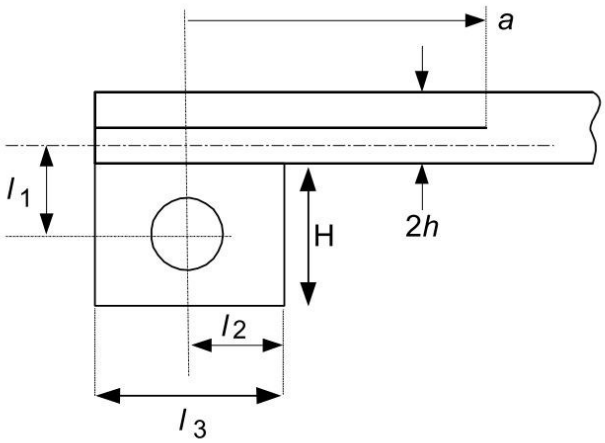

Figure 3.6: Load-block dimensions for C-ELS specimen (Blackman and Brunner, 2009).

Table 3.1: Overview of the different types of specimens used.

Test method	Length [mm]	Width [mm]	Height [mm]
Extensometer Control	120	20	8
Compliance Control	120	20	3
Round Robin	150	20	4

3.2 Experimental Procedure for Mode I Fatigue Loading

3.2.1 Extensometer Control

A new approach for ΔG constant tests is monitoring the exact opening of the beams of the specimen via an extensometer applied to the DCB specimen. Based on the extensometer data of the beam opening the crack length can be determined. Figure 3.7 illustrates the test setup in principle that was applied to a servo-hydraulic testing machine (MTS Systems Corporation, USA). No loading blocks or hinges are used, but grips like they were developed at the KTH Royal Institute of Technology of Stockholm, Sweden (see Figure 3.8).

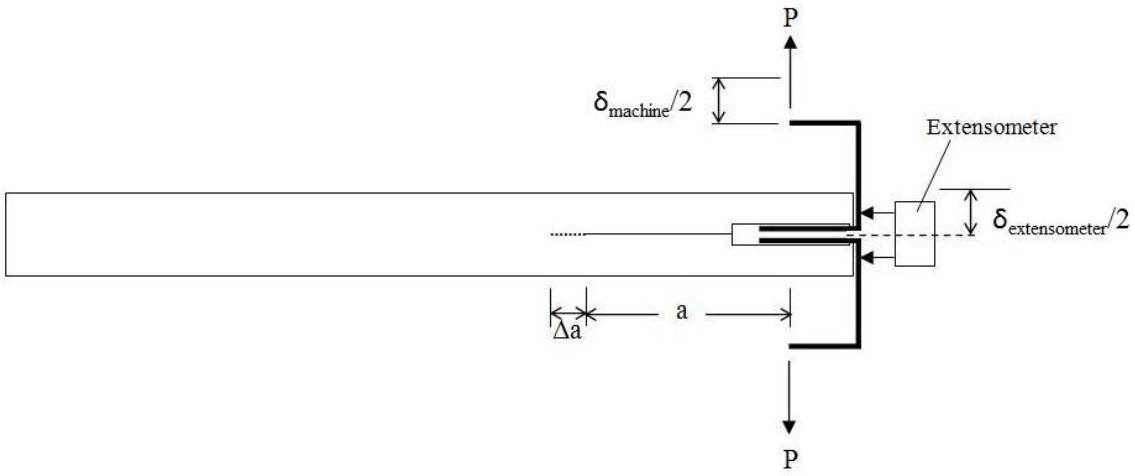

Figure 3.7: Schematic setup of mode I beam opening control (Canteli, 2010).

At first a monotonic mode I test is performed in order relate the displacement of the extensometer to the crack length. Therefore load-displacement values are recorded under displacement control. At certain values of crack length that are visually observed, the corresponding displacement is read. For each crack length the extensometer value can now be found and plotted in a diagram that yields a linear relationship. The principle of this calibration method is shown in Figure 3.9. The monotonic test also provides the critical energy release rate G_{IC} at which the delamination starts. Based on $G_{IC,}$ the level of the constant energy release rate G for the fatigue test can be chosen (for example 80% of G_{IC}). The fatigue tests were performed at an R-ratio of 0.1 and a frequency of 5 Hz.

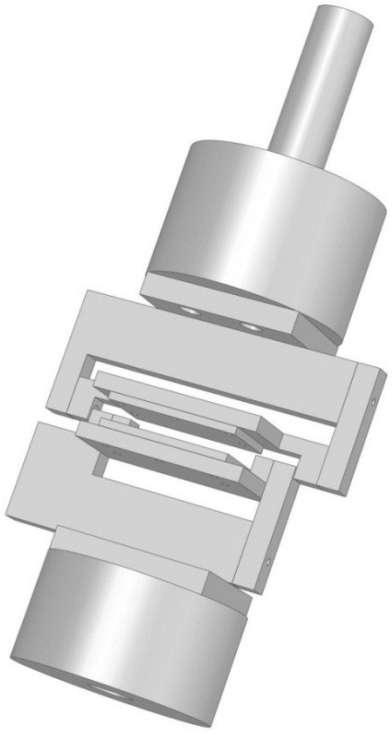

Figure 3.8: Grips for clamping a notched DCB specimen.

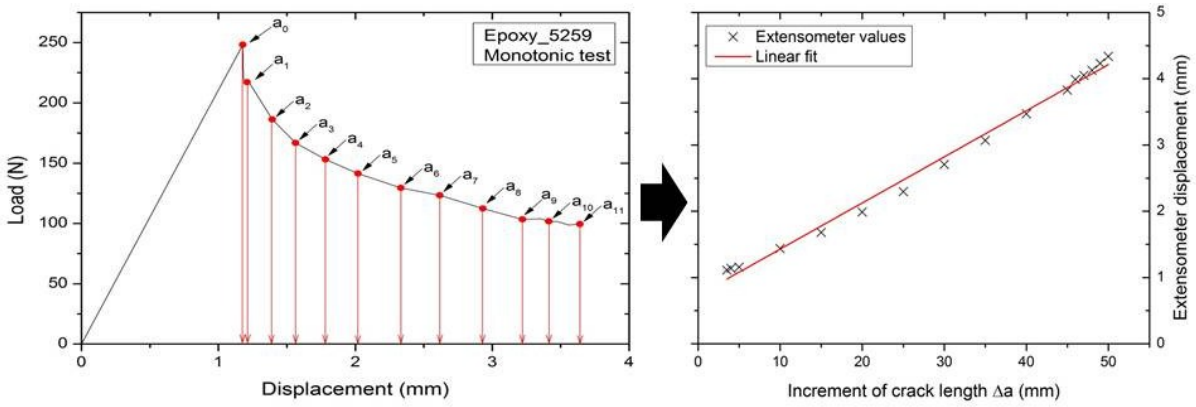

Figure 3.9: Correlation between crack length and displacement of the attached extensometer obtained from a monotonic test.

As the fatigue tests are not performed at the critical energy release rate, G_{IC}, but at lower loading levels, the displacement values from the monotonic test are reduced. The displacement values for example, may be reduced to 80 % of G_{IC}. Despite testing under displacement control it is assumed that an increase of crack length leads to a deflection in the signal of the extensometer. Such a peak in the signal of the extensometer is correlated with the crack length and the machine displacement is

increased according to the desired value of *G*. In a preliminary calculation the required displacement to maintain the desired value of *G* at different increments of crack lengths is calculated. In the control software of the testing machine a procedure is implemented that uses the signal of the extensometer as reference. The software procedure consists of several steps, where each step is linked to a certain range of crack length. While the machine displacement is constant within a step, the energy release rate descends as the crack advances. As it is assumed that during crack growth there is a short moment where the beam displacement has a positive deflection, the increase of displacement can be triggered by monitoring the extensometer signal. If the crack length and hence the extensometer reaches the maximum limit value of the corresponding step, the machine control switches to the next step where the machine displacement is adjusted so that the resulting energy release rate *G* stays at its demanded constant value.

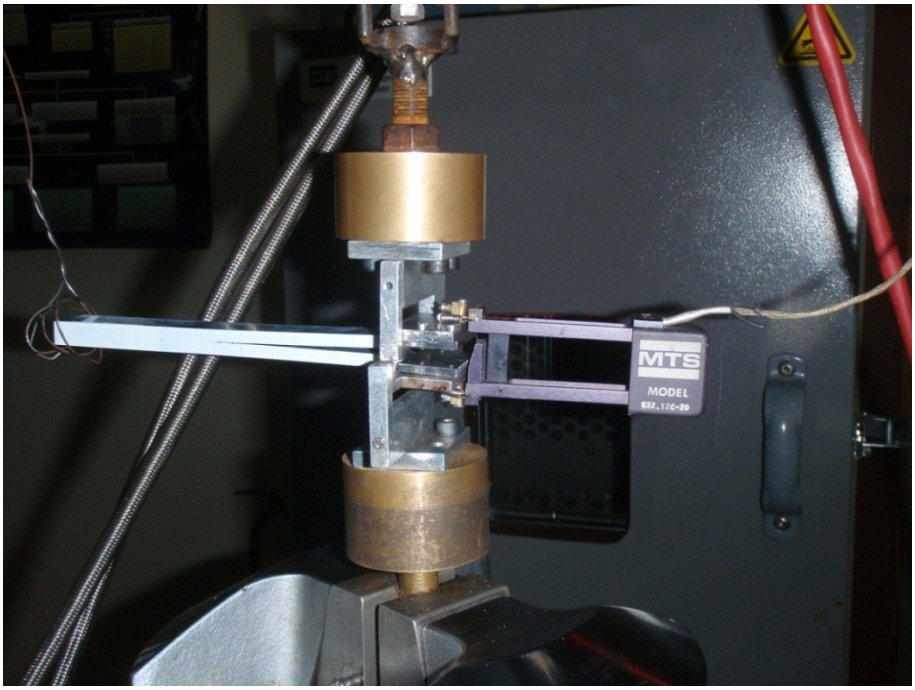

Figure 3.10: Test setup for ∆G constant measurements with beam opening control.

In Figure 3.10 one can see the test setup with the extensometer (MTS 632.12C, 25 mm gauge length, MTS Systems Corporation, USA) mounted on the two separated beams of the specimen. To monitor the crack length during the test a camera (PULNIX TM-7CN, JAI Inc., USA) was connected via USB to a computer where the crack length was observed in order to check if it correlates with the actual step of the software procedure (Figure 3.11).

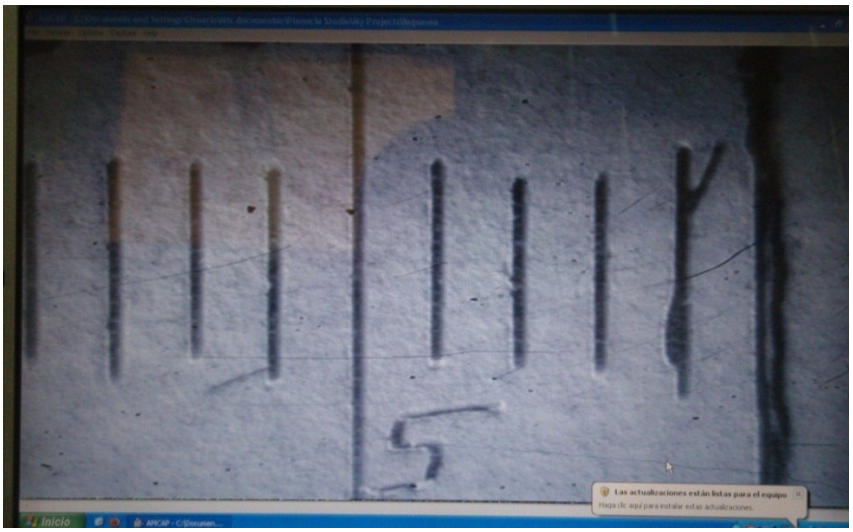

Figure 3.11: Marked cheek of a specimen on the screen of a PC connected to a PULNIX TM-7CN camera.

3.2.2 Compliance Control

Another approach to realize ΔG constant tests is to use the compliance of the specimen to deduce the crack length and hence to readjust the machine displacement to maintain a predefined value of the energy release rate *G*. These tests were performed with an MTS 831 servo hydraulic testing machine. Through conventional mode I fatigue tests the calibration data for calculating the parameters for the ΔG constant tests was obtained. Due to the linear relationship of the compliance and the crack length in a logarithmic diagram (Figure 3.12), it is possible to calculate the corresponding crack length for each value of compliance out of the relation in Equation (9).

$$C = d * a^k \tag{9}$$

The compliance can also be written as the quotient of the machine displacement δ and the load *P*.

$$C = \frac{\delta}{P} \tag{10}$$

Based on the measured compliance the crack length can be calculated as:

$$a = \left(\frac{\delta}{P}\right)^{\frac{1}{k}} * d^{-\frac{1}{k}} \tag{11}$$

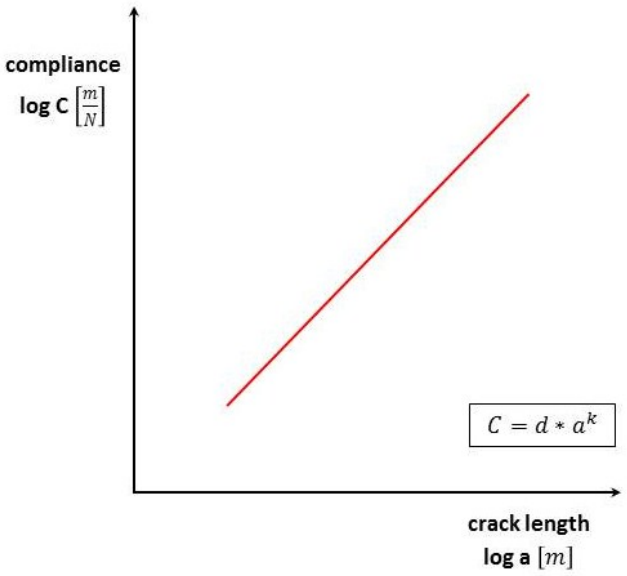

Figure 3.12: Linear Relationship between compliance and crack length in a double logarithmic diagram.

In the machine control software a template was created which was similar to the one for the Extensometer Control tests. As it is not possible to control the machine displacement in real-time, based on the calculated compliance, several steps are defined to readjust the machine displacement after the crack has advanced a certain increment. Starting from the initial crack length a_0, a step for every three millimeters of crack propagation is defined. The compliance of the corresponding crack length at the end of each step is set as limit value for the machine control. That means the compliance is set as control parameter and every time the measured compliance exceeds the limit value of the current step, the machine switches into the next step automatically. The machine displacement in each step is held at an R-ratio of 0.1 at a loading frequency of 5 Hz. The calculation of the steps begins with Equation (10) which is transformed to:

$$P = \frac{\delta}{C} \tag{12}$$

Furthermore the compliance *C* is substituted by Equation (9) which is obtained from the diagram shown in Figure 3.12.

$$P = \frac{\delta}{d * a^k} \tag{13}$$

For defining the steps, the calculation of the energy release rate *G* is done through the simple beam theory (BT):

$$G = \frac{3 * \delta * P}{2 * b * a} \tag{14}$$

With Equation (13) the energy release rate *G* is calculated as:

$$G = \frac{3 * \delta^2}{2 * b * d * a^{k+1}} \tag{15}$$

To keep the energy release rate constant, for every increment of crack length the corresponding machine displacement is calculated, where *G* is set to the desired level (e.g. 1000 J/m²) and the crack length is varied from zero to the final crack length in increments of 3 millimeters.

$$\delta = \sqrt{\frac{2 * G * b * d * a^{k+1}}{3}} \tag{16}$$

To define the compliance-limits at the end of each step, the compliance at the final crack length of each increment is calculated with Equation (9). The trend of the energy release rate *G* during a compliance controlled test is pictured in Figure 3.13. As the crack propagates within a step, the energy release rate is decreasing. By the time the crack reaches the end of the step increment the compliance reaches the limit value so that the machine control switches to the next step.

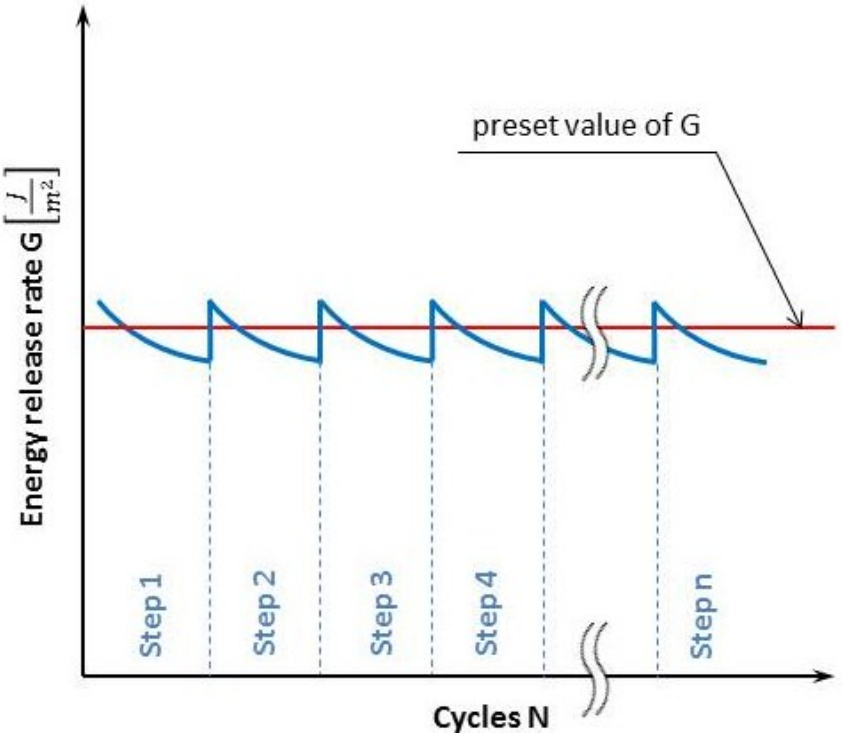

Figure 3.13: Behavior of the energy release rate G passing through the previously programmed steps in the control software of the machine.

To check if the actual crack length correlates with the calculated crack length and related compliance, a travelling microscope with 40x magnification was attached to the test rig. To facilitate the detection of the crack tip on the edge of the specimen it was covered with a thin layer of brittle white ink and illuminated by cold light.

Succeeding experiments were transferred to another servo-hydraulic machine of the type MTS 858, a horizontal tabletop testing machine (Figure 3.14), in order to perform tests by regulating directly the value of *G*. The reason therefore was the more modern machine control software (MTS model 793.00 System Software) as it is possible to control the value of the energy release rate by regulating the displacement. By realizing this type of control it is no longer necessary to define steps and limit values of compliance. The so called Dual Compensation Control mode requires two feedback signals, a more stable primary feedback (for proportional–integral–derivative control with first-order derivative filter – PIDF-closed-loop control), and a secondary feedback (for command compensation). In the present case the primary feedback is the displacement signal. If Equation (11) is used with Equation (14), the energy release rate can be calculated in real-time as

$$G = \frac{3 * \delta * P}{2 * b} * \left(\frac{\delta}{P}\right)^{-\frac{1}{k}} * d^{\frac{1}{k}} \qquad (17)$$

where δ and P are the output signals of the machine. Based on this calculated value the software command regulates the displacement to a preset constant value of G_{max} and G_{min}.

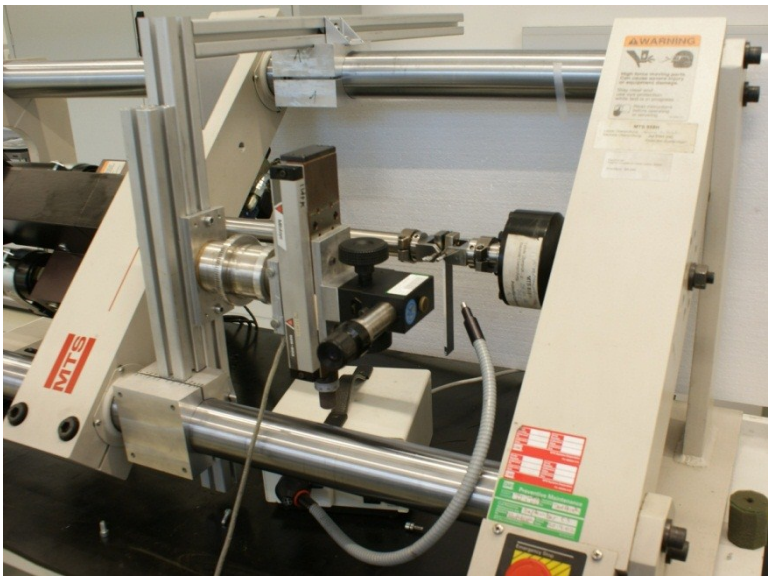

Figure 3.14: MTS 858, servo-hydraulic tabletop system with test setup for G_i-constant tests.

3.2.3 Calculation of the Crack Propagation Rate, da/dN

There are two possibilities to determine the crack propagation rate *da/dN*. The simplest way to evaluate *da/dN* is to calculate the slope of the straight line connecting two adjacent points on the plot of crack length vs. number of cycles by using Equation (18).

$$\frac{da}{dN} = \frac{a_{i+1} - a_i}{N_{i+1} - N_i} \tag{18}$$

The more precise 7-Point method is described in ASTM E647 – 00. This incremental polynomial method for computing *da/dN* involves fitting a second order polynomial (parabola) to sets of (2*m*+1) successive data points, where *m* can take values of 1, 2 or 3. The regression parameters determined by the least squares method, that is minimization of the square of deviations between observed and fitted values of delamination length. Since this method is not able to describe the delamination rates between the first and the last pair of data points, these have to be evaluated using the secant, or point-to-point method which is described in Equation (18). For the second and the second to last set of data points the 3-point method is used (*m*=1) which means the regression polynomial is applied to the first and last three data points and evaluated for the medium point (i.e., the second or second to last). Analogous for the third and third to last data point (*m*=2) the 5-point method, and for all further data (*m*=3) the 7-point method is used. A schematic illustration of this incremental polynomial method is depicted in Figure 3.15 (Pinter and Stelzer, 2010).

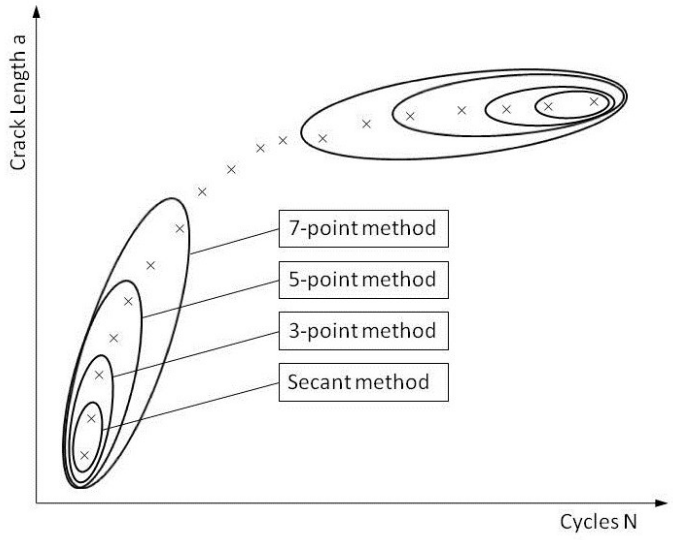

Figure 3.15: Schematic illustration of an a-N plot for determining the crack propagation rate (Pinter, 1994).

3.2.4 Calculation of the Energy Release Rate, G_I

The energy release rate *G* under mode I loading was calculated using the Corrected Beam Theory (CBT) and the Modified Compliance Calibration (MCC; Equation (22)). For both Methods a compliance calibration is required.

The Corrected Beam Theory (Equation (19)) takes into account the influence of large movements of the piston by using the correction factor *F* (Equation (20)) and the influence of the loading blocks is taken into account by the use of the correction factor *N* (Equation (21)). *Δ* is a correction to the crack length to take account of the imperfectly clamped beam boundary condition, and is defined as the intercept on the x-axis of a plot of cube root of compliance versus crack length, as shown in Figure 3.16 (Williams, 1989; Davies, et al., 1998).

$$G_I = \frac{3 * \delta * P}{2 * b * (a + \Delta)} * \frac{F}{N} \tag{19}$$

$$F = 1 - \frac{3}{10} * \left(\frac{\delta}{a}\right)^2 - \frac{2}{3} * \left(\frac{\delta * l_1}{a^2}\right) \tag{20}$$

$$N = 1 - \left(\frac{l_2}{a}\right)^3 - \frac{9}{8} * \left[1 - \left(\frac{l_2}{a}\right)^2\right] * \frac{\delta * l_1}{a^2} - \frac{9}{35} * \left(\frac{\delta}{a}\right)^2 \tag{21}$$

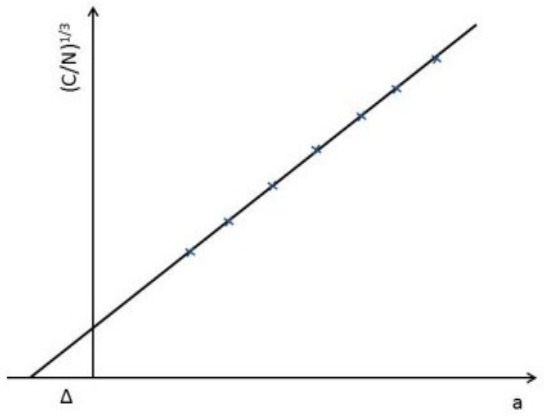

Figure 3.16: Determination of the correction factor Δ for the corrected beam theory (ISO 15024:2001).

The second method was proposed by the Japanese Industrial Standards group (JIS), which is shown in Equation (22) where *m* is a coefficient derived experimentally from a plot of $(BC)^{2/3}$ versus *a/2h* (Figure 3.17) (Davies, et al., 1998). The source code for the data analysis using MatLab (MathWorks, Inc.) is presented in section 9.

$$G_I = \frac{3 * m}{2} * \left(\frac{P}{B}\right)^2 * \left(\frac{B * C}{N}\right)^{\frac{2}{3}} * F \qquad (22)$$

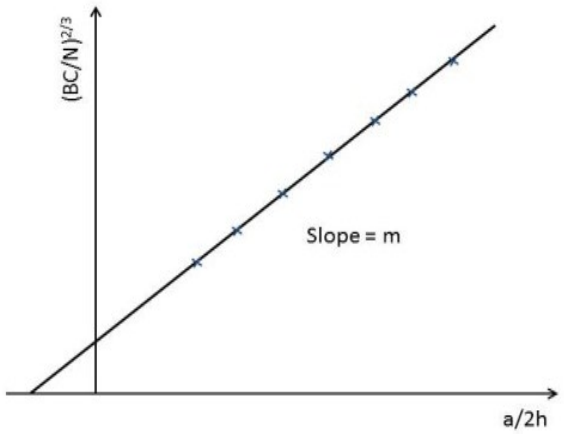

Figure 3.17: Plot for determining the coefficient m for the modified compliance calibration method (ISO 15024:2001).

3.3 Experimental Procedure for Mode II Fatigue Loading

3.3.1 3ENF Test

The experiments under three-point bending 3ENF loading were performed on a servo-hydraulic test system MTS 831 (MTS Systems Corporation, USA). The test setup is illustrated schematically in Figure 3.18. An angle cut out of polymer was mounted to the test device to avoid shifting of the specimen as shown in Figure 3.19. The marked specimens (as described in section 3.1) were mounted to the test rig so that the end without delamination lay flat to the fixation angle.

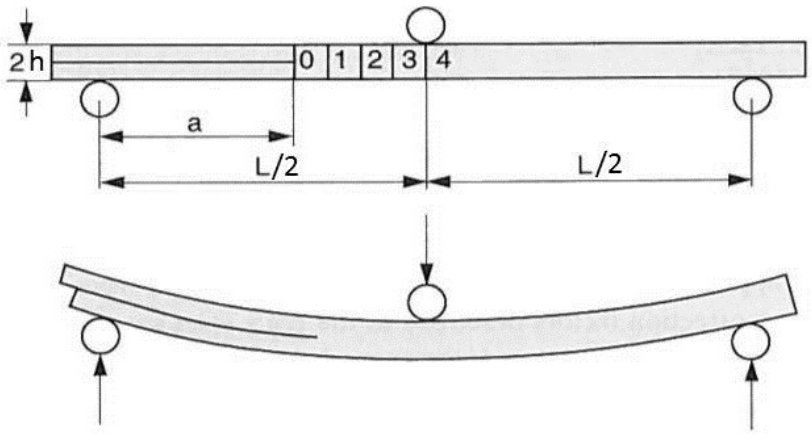

Figure 3.18: Schematic illustration of the 3ENF test setup (Grellmann and Seidler, 2007).

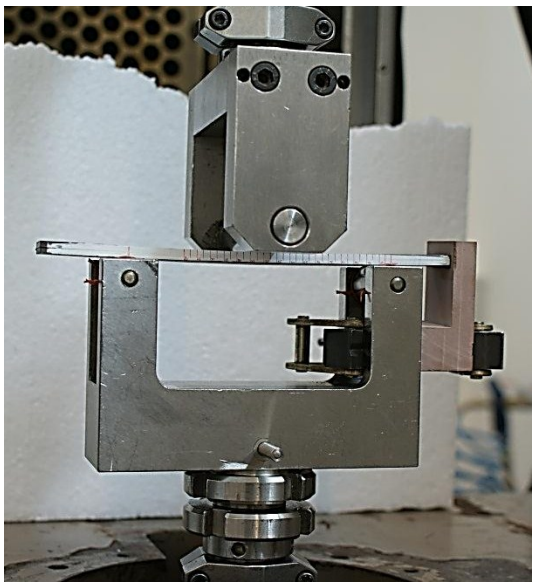

Figure 3.19: 3ENF test device with restraint against shifting of the specimen.

For at least one specimen of each material the critical energy release rate, G_{IIC}, was determined by performing a quasi-static test. Therefore the specimen was loaded monotonically with a loading rate of 1mm/min and the load-displacement curve was plotted (Figure 3.20). The displacement at which the maximum load is reached was used to calculate the critical energy release rate. For the fatigue test a maximum displacement, δ_{max}, was chosen right after the value at which the delamination initiated in order to start the fatigue test just below the critical energy release rate, G_{IIC}.

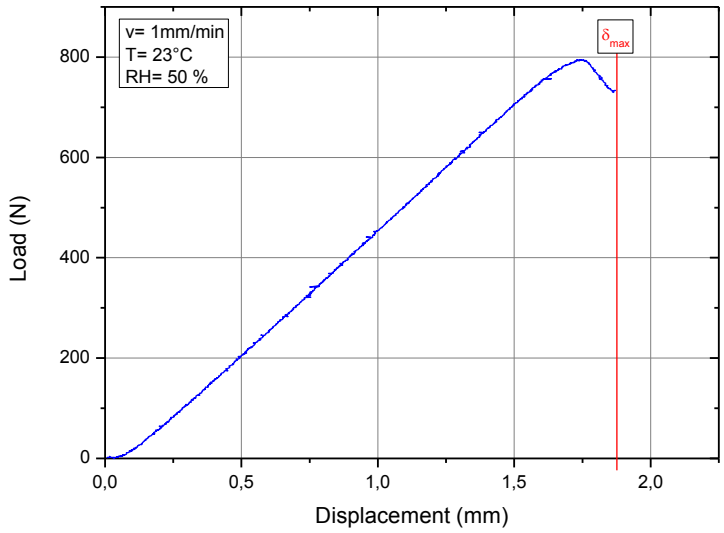

Figure 3.20: Load-displacement curve from a monotonic test to determine the critical energy release rate and the displacement for the fatigue test.

The fatigue tests were performed at an R-ratio of 0.1 and a frequency of 3 Hz. Load and displacement values were recorded throughout the test for a subsequent data analysis as described in section 3.3.5. At high crack propagation rates at the beginning of the test, the crack length was visually measured in small intervals (e.g. every 500 ÷ 1000 cycles). As the crack propagation rate decreased, the reading of the crack length was reduced to once per hour and later to twice a day.

3.3.2 C-ELS Test

A servo-hydraulic testing machine of the type MTS 831 (MTS Systems Corporation, USA) was used in displacement control mode. The test setup is schematically described in Figure 3.21. It is important that the clamping arrangement can slide

easily in a horizontal direction with a fixed loading point in order to transmit loads only in vertical direction.

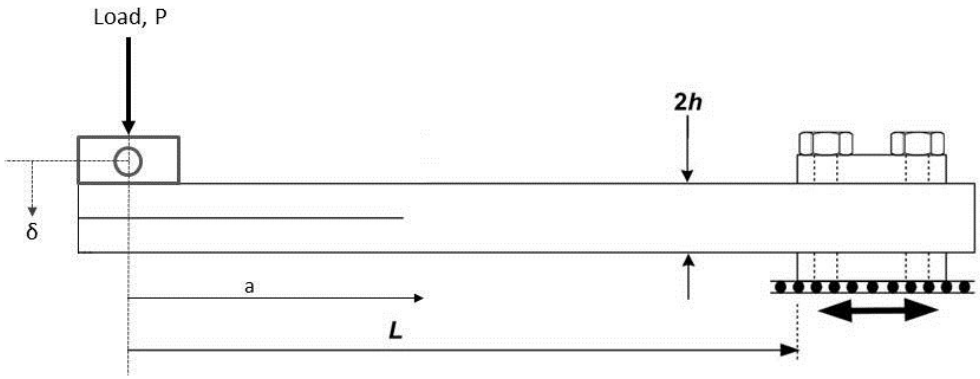

Figure 3.21: Schematic illustration of the mode II C-ELS test setup (Blackman and Brunner, 2009).

The in-house designed fixture is shown in Figure 3.22, where the horizontal mounting is realized by the use of linear ball bearings. The specimens were clamped using a torque wrench to apply a consistent pressure. The clamping torque was chosen to be 5 Nm.

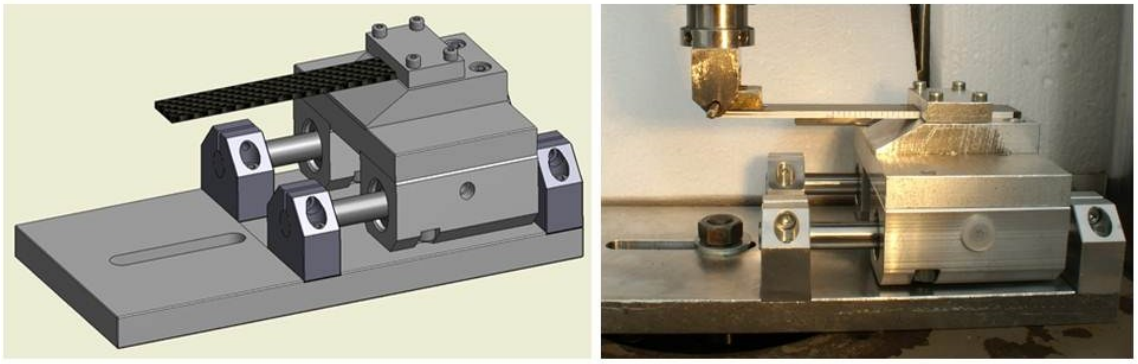

Figure 3.22: C-ELS fixture constructed at the chair of Material Science and Testing of Plastics at the Montanuniversitaet Leoben, Austria.

For every material tested, a so called clamp calibration has to be performed to measure the compliance of the test setup with an un-cracked specimen, as proposed in the ESIS TC4 protocol (Blackman and Brunner, 2009). Therefore a specimen is positioned in the clamping fixture, so that it is fixed with the starter film fully within the clamp as shown in Figure 3.23. Via the loading block, which has to be applied to the end without starter film, the load is introduced. At first the specimen is clamped at a free length of L = 100 mm and the applied clamping pressure is recorded. Further the specimen is loaded at a displacement rate of 1 mm/min and the load-displacement

data is recorded to a maximum of 250 N. When the maximum load is reached, the specimen is unloaded at 10 mm/min. This procedure is repeated with the beam clamped at free lengths of 100, 90, 80, 70, 60 and 50mm (Blackman and Brunner, 2009).

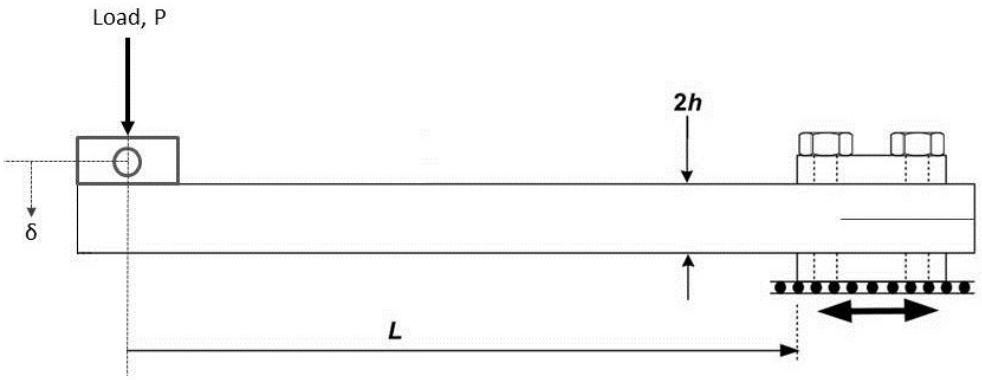

Figure 3.23: Clamp calibration setup with the delamination fully within the clamp (Blackman and Brunner, 2009).

The specimens mounted for fatigue testing were pre-cracked to eliminate the influence on delamination initiation due to the starter film. Before performing a fatigue test a quasi-static test was carried out in order to determine on one hand, the displacement for the fatigue test and to receive a value for the critical energy release rate G_{IIC}. The specimens were clamped at a free length, L, so that $a_0/L \geq 0.55$ is fulfilled. Larger values than 0.55 will improve the stability of crack growth but will reduce the available length for crack propagation (Blackman and Brunner, 2009).

The fatigue tests were performed at an R-ration of 0.1 at a frequency of 3 Hz. The applied displacement was obtained from the quasi-static test. Therefore the displacement value at which the maximum loading occurred was read out from the load-displacement curve. During the test the machine displacement and the load were recorded for further data analysis as described in clause 3.3.5.

3.3.3 Determination of the Flexural Modulus

The determination of the flexural modulus was based on the DIN EN ISO 178 standard. Therefore a three-point bending test setup as shown in Figure 3.24 and Figure 3.25 was applied to a Zwick/Roell Z250 tensile test machine. As proposed in the standard the radii R_1 and R_2 were 5 mm and the span length, L, was 64 mm. The specimens were loaded with a loading rate of 2 mm/min until a maximum flexural

strain of 0.3 % was reached. For the calculation of the flexural modulus the following Equation was used:

$$E_1 = \frac{\sigma_{f2} - \sigma_{f1}}{\varepsilon_{f2} - \varepsilon_{f1}} \tag{23}$$

where σ_{f1} is the flexural stress at a flexural strain of ε_{f1}= 0.005 and σ_{f2} is the flexural stress at ε_{f2}= 0.25.

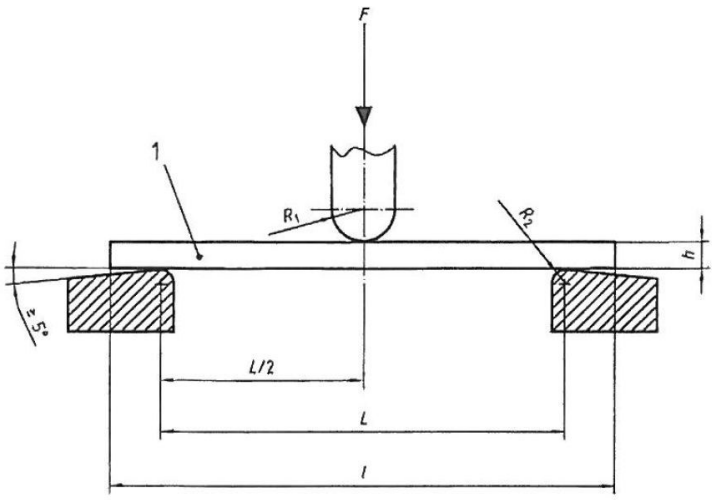

Figure 3.24: Draft of the three-point bending fixture according to DIN EN ISO 178.

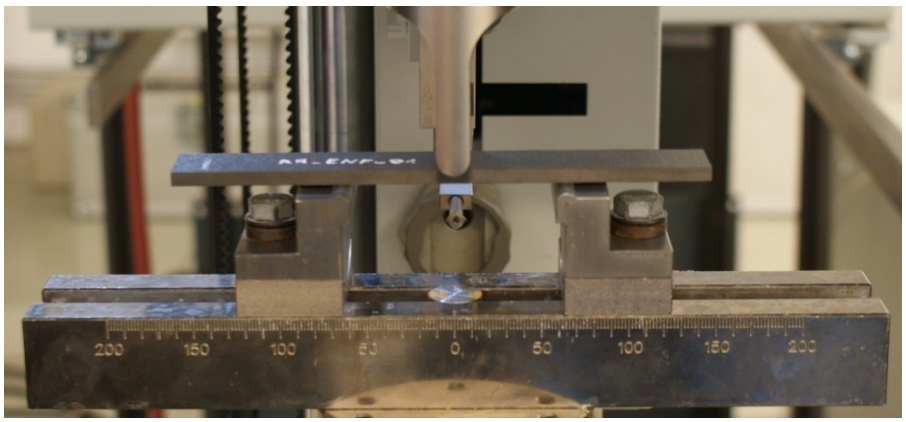

Figure 3.25: Three-point bending test setup with mounted specimen for the determination of the flexural modulus.

3.3.4 Round Robin

As there are several test setups that have been proposed for quasi-static mode II testing of fiber laminates the selection for the round robin was based on current standardization activities within ASTM and ISO. Hence the three-point bending End Notched Flexure, 3ENF, and Calibrated End Loaded Split, C-ELS, were chosen.

Before testing the specimens their length was measured. Along the length of the beam three measurements of width and thickness were taken (with an accuracy of 0.01 mm). For each specimen the flexural modulus was determined according to standard three-point bending test as described in clause 3.3.3. For all specimens tested using the C-ELS setup, a clamp calibration was performed. Therefore a loading block was applied to the uncracked end of the specimen which was carefully removed after the calibration and mounted to the other end for fatigue testing.

For tests with the 3ENF setup the specimens were monotonically pre-cracked in order to obtain a value for the displacement in the fatigue test on the one hand, and to compare the critical energy release rate, G_{IIc}, to the results of the fatigue test. The first 3ENF fatigue test was performed at a frequency of 3 Hz. Further tests of both, 3ENF and C-ELS, were performed at a frequency of 5 Hz because of the long test duration at 3 Hz. The data analysis was based on the Simple Beam Theory for 3ENF tests. For C-ELS tests the Corrected Beam Theory and the Experimental Compliance Calibration method were used.

3.3.5 Calculation of the Energy Release Rate, G_{II}

The data analysis of the 3ENF test setup is based on the German standard DIN EN 6034, which uses the Beam Theory for the determination of interlaminar fracture toughness energy under mode II loading conditions. For the calculation of G_{II} the following formula is used:

$$G_{II} = \frac{9 * P * a^2 * \delta}{2 * b * \left(\frac{1}{4}L^3 + 3a^3\right)} \qquad (24)$$

where P is the load, δ the displacement, a the crack length, b the width of the specimen and L the span length, as shown in Figure 3.18.

The G_{II} values of the C-ELS tests can be determined by three different data reduction schemes, the Experimental Compliance Method (ECM), the Simple Beam Theory (SBT) and the Corrected Beam Theory with effective crack length (CBTE). The SBT and the ECM both require experimental values of crack length to be determined and the CBTE is independent of measured crack length. SBT and CBTE require a value for the flexural modulus of the specimen which was determined via three-point bending. Alternatively the modulus can be determined from the clamp calibration procedure (Blackman and Brunner, 2009).The calculation of G_{II} is generally based on

the Irwin-Kies equation (Equation (3)). The source code for the data analysis using MatLab (MathWorks, Inc.) is presented in clause 9.

Determination of the C-ELS clamp correction

The procedure described in clause 3.3.2 is a necessary correction of the calculation of G_{II}, as the C-ELS fixture itself has a certain compliance which has to be subtracted from the measured compliance during testing a specimen. Based on the data obtained from the clamp calibration measurement, the mean values of compliance obtained from the measurements at each value of free length, *L*, is plotted in a $C^{1/3}$ versus *L* plot. Then a linear regression is performed and extrapolated back to $C^{1/3}= 0$. The value of the intercept with the *L*-axis is referred to as the clamp correction, Δ_{clamp}. The slope of the regression line can be used to determine the flexural modulus of the specimen by the following expressions:

$$slope = \left(\frac{1}{2 * b * h^3 * E_1}\right)^{\frac{1}{3}} \tag{25}$$

$$E_1 = \frac{1}{2 * b * (h * slope)^3} \tag{26}$$

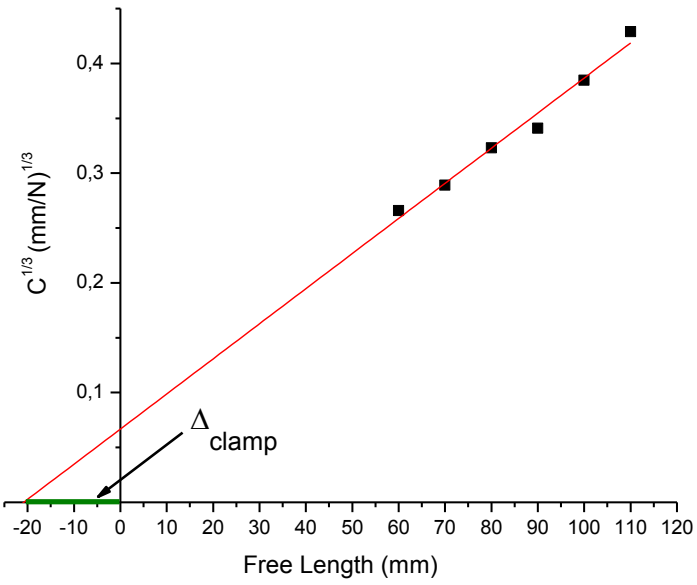

Figure 3.26: Example for the $C^{1/3}$ versus L plot for the determination of the clamp calibration. In the example given Δ_{clamp}= 20 mm.

Experimental Compliance Method (ECM)

The experimental compliance method is based on a cubic relationship between the compliance, *C,* and the measured crack length, *a*. If the values of *C* are plotted versus the cube of the measured crack length, a^3, a linear regression will yield a slope, *m*, and an intercept with the *C*-axis of C_0. This can be written as:

$$C = C_0 + m * a^3 \tag{27}$$

Equation (27) is now differentiated with respect to crack length and substituted into Equation (3). Additionally a correction factor *F* is added to correct large displacement effects in the beam. The energy release rate G_{II} can now be calculated as:

$$G_{II} = \frac{3 * P^2 * a^2 * m}{2 * b} * F \tag{28}$$

Simple Beam Theory (SBT)

The compliance, *C*, of the C-ELS specimen can be written as:

$$C = \frac{\delta}{P} = \frac{3 * a^3 + L}{2 * b * h^3 * E_1} \tag{29}$$

By differentiation of Equation (29) with respect to the crack length and substituting into Equation (3) the energy release rate is calculated as:

$$G_{II} = \frac{9 * P^2 * a^2}{4 * b^2 * h^3 * E_1} \tag{30}$$

Corrected Beam Theory using Effective Crack Length (CBTE)

For the Corrected Beam Theory with Effective Crack Length approach, the crack length is calculated using the measured compliance and the known flexural modulus E_1, which was measured in advance. This method also requires the value of the clamp correction of the C-ELS fixture. The CBTE takes in account rotations at either the crack tip or clamping point and includes corrections for the transverse shear effects in the composite arms. For the CBTE, the compliance is written as:

$$C = \frac{\delta}{P} = \frac{3 * a_e^3 + (L + \Delta_{clamp})^3}{2 * b * h^3 * E_1} * N \tag{31}$$

The term *N* is an additional correction factor to account for effects caused by the loading blocks. The definition is given below. Further the effective crack length, a_e, results in:

$$a_e = \left[\frac{1}{3} * \left\{\frac{2 * b * C * h^3 * E_1}{N} - (L + \Delta_{clamp})^3\right\}\right]^{\frac{1}{3}} \quad (32)$$

The value of effective crack length is substituted in Equation (30) and gives:

$$G_{II} = \frac{9 * P^2 * a_e^2}{4 * b^2 * h^3 * E_1} * F \quad (33)$$

where F is the term for correcting for large displacement effects in the beam.

Large displacement and load-block correction factors

Large displacements of the specimen during the test gives rise to a reduction in the moment arm. This effect has been analyzed by Williams (Williams, 1987) and it has been shown that it can be corrected via the correction factor *F*, which is given by (Blackman and Brunner, 2009):

$$F = 1 - \theta_1\left(\frac{\delta}{L}\right) - \theta_2\left(\frac{\delta * l_1}{L^2}\right) \quad (34)$$

where δ is the machine displacement, *L*, the free length of the beam and θ_1 and θ_2 are defined below. The length l_1 is defined in Figure 3.6.

The effects of bonding a load-block to the test specimen will be to stiffen the arm and additionally, the offset to the load-point will incur additional rotational effects. This effect was also analyzed by Williams (Williams, 1987) and it was shown that it may be corrected via the factor *N*, which is given by (Blackman and Brunner, 2009):

$$N = 1 - \theta_3\left(\frac{l_2}{L}\right)^3 - \theta_4\left(\frac{\delta * l_1}{L^2}\right) - \theta_5\left(\frac{\delta}{L}\right)^2 \quad (35)$$

where the length l_2 is shown in Figure 3.6 and θ_3, θ_4 and θ_5 are defined below.

$$\theta_1 = \frac{3}{20} * \left[\frac{15 + 50\left(\frac{a}{L}\right)^2 + 63\left(\frac{a}{L}\right)^4}{\left[1 + 3\left(\frac{a}{L}\right)^3\right]^2}\right] \quad (36)$$

$$\theta_2 = \frac{-3\left(\frac{L}{a}\right) * \left(1 + 3\left(\frac{a}{L}\right)^2\right)}{1 + 3\left(\frac{a}{L}\right)^3} \quad (37)$$

$$\theta_3 = \frac{4}{1 + 3\left(\frac{a}{L}\right)^3} \quad (38)$$

$$\theta_4 = -\frac{9}{4} * \frac{\left\{\left[1 - \left(\frac{a}{L}\right)\right]\left[1 + 3\left(\frac{a}{L}\right)^3\right] + 4\left(\frac{a}{L}\right)^2\left[1 - \left(\frac{l_2}{a}\right)^2\right]\left[1 + 3\left(\frac{a}{L}\right)^2\right]\right\}}{\left[1 + 3\left(\frac{a}{L}\right)^3\right]^2} \quad (39)$$

$$\theta_5 = \frac{36}{35} * \frac{1 + \frac{3}{8}\left(\frac{a}{L}\right)^3 * \left[35 + 70\left(\frac{a}{L}\right)^2 + 63\left(\frac{a}{L}\right)^4\right]}{\left[1 + 7\left(\frac{a}{L}\right)^3\right]^3} \quad (40)$$

4. Results and Discussion

4.1 Mode I

4.1.1 Extensometer Control

Out of the monotonic tests, where the displacement of the machine and the extensometer is correlated to the crack length, the displacement values for the critical energy release rate, G_{IC}, at each crack length are obtained. The values of the machine displacement at the critical energy release rate are illustrated in Figure 4.1 by the black 100%-line. In order to perform fatigue tests at loading levels lower than $G_{IC,}$ the displacement values obtained from the monotonic test are reduced for example to 65%. The 100%-line in Figure 4.1 shows the machine displacement at each increment of crack length and the colored lines show the reduced values for further fatigue testing. The same procedure of reducing the displacement values is applied to the extensometer data.

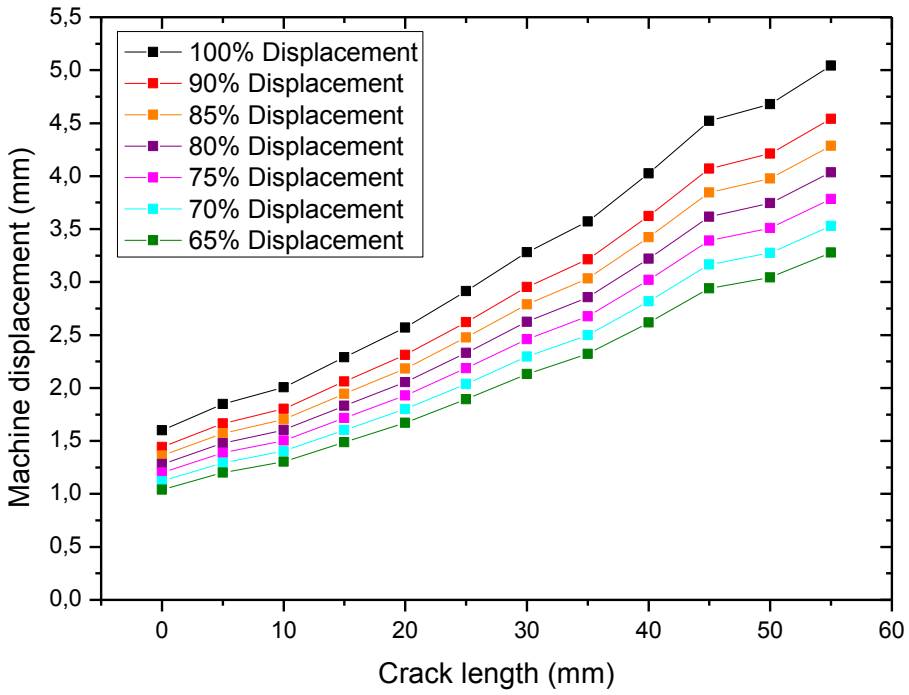

Figure 4.1: Correlation of machine displacement and crack length increment of a monotonic test.

These values are then transferred to a table where the different steps are defined (Table 4.1). As the calibration data from the monotonic test is available for crack increments of 5 millimeters, the intermediate steps are generated by linear interpolation. The maximum extensometer values in Table 4.1 are the detector limits that trigger the change to the next step if reached. The values of extensometer and displacement are implemented in the control software of the machine. The load values in Table 4.1 are those obtained from the monotonic test without any modification. The listed values of crack length in the last column serve as a reference to check if the actual crack length is in accordance with the actual step.

Table 4.1: Example for the steps implemented in the control software of the testing machine with the extensometer signal as threshold value to switch from one step to the other for crack lengths from 20 to 37mm.

Material 5276 at 23ºC and 65% of G_{IC}							
	EXTENSOMETER (mm)		**DISPLACEMENT (mm)**		**LOAD (N)**		**a (mm)**
	MAX	MIN	MAX	MIN	MAX	MIN	
ramp	0,5 mm in 10 sec.						0
Fatigue20	1,878	1,733	1,67	0,17	146,74	14,67	20-22
Fatigue22	**2,022**	1,878	1,78	0,18	146,81	14,68	22-25
Fatigue25	2,171	2,022	1,89	0,19	146,89	14,69	25-27
Fatigue27	**2,320**	2,171	2,01	0,20	140,18	14,02	27-30
Fatigue30	2,435	2,320	2,13	0,21	133,46	13,35	30-32
Fatigue32	**2,550**	2,435	2,23	0,22	127,87	12,79	32-35
Fatigue35	2,731	2,550	2,32	0,23	122,27	12,23	35-37
…	…	**…**	…	…	…	…	…

In the following the results of tests at 65% and 75% of the displacement from the monotonic test are presented. As during a ΔG constant test the relation between the crack length and the number of cycles should be linear, it is obvious in both, Figure 4.2 and Figure 4.3, that within one step the crack propagation rate drops significantly. It is a not an easy task to control the test in order to pass through all of the predefined steps. Either the crack advances too fast and leaves some steps out which leads to catastrophic failure of the specimen due to wrong displacement values for the current crack length, or the limit for changing into the subsequent step is not reached and the crack stops growing. Regarding the energy release rate in Figure 4.2 a strong decrease within the steps can be observed. The maximum number of

cycles did not exceed 150000 because at crack length of more than 50 mm the extensometer limits were hardly ever reached.

In general the tests with extensometer control did not work out as well as expected. There are several approaches which could give an explanation for the failure of many of the conducted tests. First and foremost it has to be stated that the forerun tests to develop the test method were performed with specimens of 3 millimeters thickness compared to 8 millimeters in the quoted case. The thicker specimens are more difficult to handle because they showed stiffer and more brittle comportment. In addition the starter film was only 20 millimeters long. To avoid a rapid, monotonic crack growth at the beginning of the test all specimens were pre-cracked to reduce the necessary force to advance the crack. The difficulty hereby is to open all specimens to the same initial crack length, a_0, at which the monotonic calibration was carried out. If the crack does not initiate due to fatigue loading, but abruptly as the beams are opened, the steps of the machine control do not fit to the current crack length, which is equitable to a shifting of a_0. If rapid crack growth in the beginning shifts a_0 to greater values, the force at the crack tip decreases and the crack propagates too slowly and will not reach the next limit. On the other hand it can happen that the extensometer signal has a deflection due to sudden monotonic crack growth and the test template overleaps one or more steps. The abrupt change of displacement due to skipping a step leads to cracking of the whole specimen. At small values of the initial crack length a_0, small displacements have to be realized in order to fulfill the requested level of fatigue. In consequence the difference between two steps is very small and the extensometer limits are close to each other. This makes the test control more difficult and sensitive to deflections in the displacement.

The main problem of this approach might be the determination of the limit values for the extensometer in a monotonic test. The displacement in a monotonic test is increasing steadily, but in a fatigue test crack growth occurs at a constant displacement. Based on this fact it makes the correlation of crack length in a fatigue test and extensometer values obtained from a monotonic test questionable. This might give an explanation why the limits are not reached during the test. Therefore compliance control seems to be more precise, as it is calibrated using the data of a fatigue test.

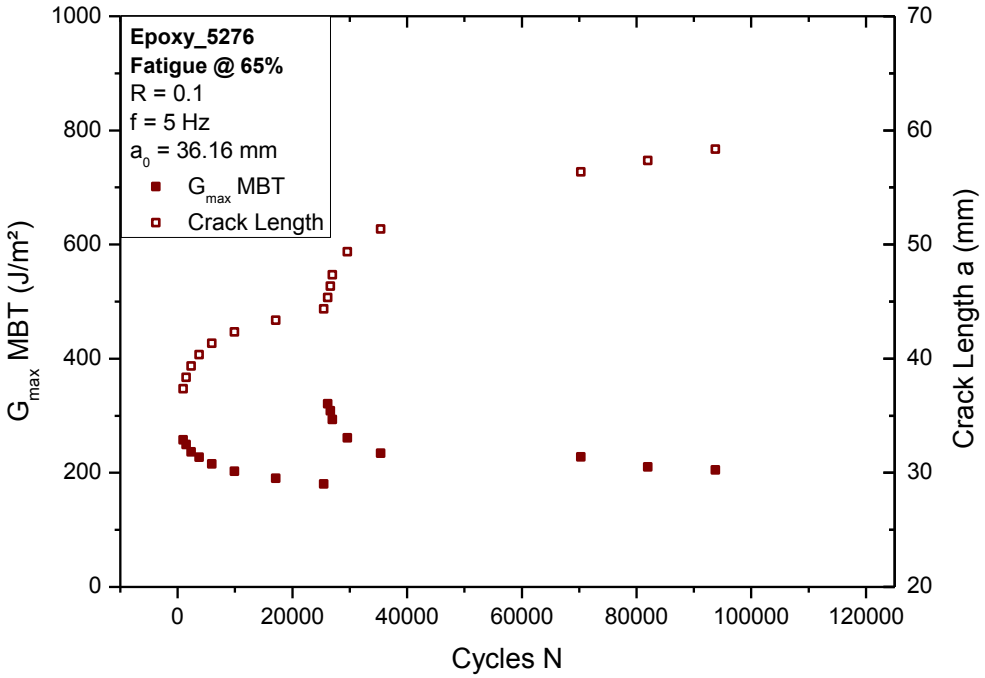

Figure 4.2: Result of a ΔG constant fatigue test at 65% of the machine displacement from $G_{IC\_monoton}$ for Epoxy_5276.

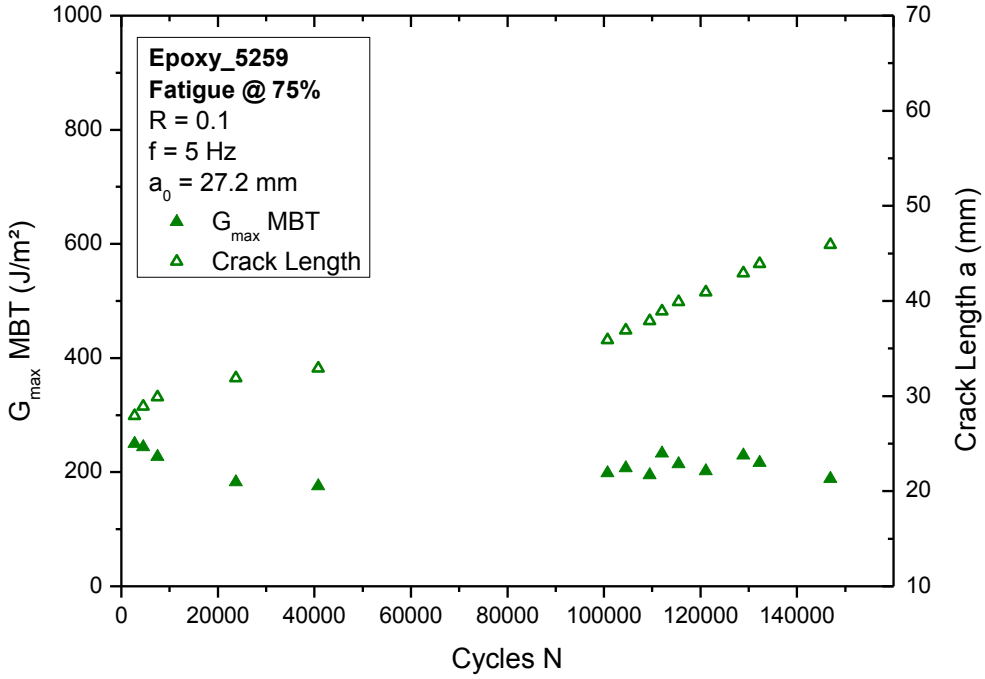

Figure 4.3: Result of a ΔG constant fatigue test at 75% of the machine displacement from $G_{IC\_monoton}$ for Epoxy_5259.

4.1.2 Compliance Control

Regarding the handling of the tests, it is easier to perform them via compliance control as the test can be controlled by measuring only the signal of the load cell and the machine displacement. Firstly tests with a frequency of 1 Hz and a preset value of the energy release rate *G* of 1000 J/m² were performed. Based on the chosen value of *G*, the parameters for each step are calculated as described in 3.2.2. The predefined steps with the corresponding displacement and compliance values are listed in Table 4.2. Starting from a crack length of 20 mm the displacement values in order to obtain an energy released rate of 1000 J/m² are calculated according to Equation (16) based on the calibration data *k* and *d*. The displacement values, δ_{min}, are calculated using the R-ration of 0.1. The column "expected force" shows the load values at the initial crack length of each step according to Equation (13). *P_limit* describes the expected force at the final crack length of a step and *C_limit* the value of compliance that leads to switching into the next step.

Table 4.2: Chart with the calculated displacement for programming the test template so that the energy release rate is held at a mean level of 1000 J/m².

Step, Crack Length	Crack Length Mean	Displacement		expected Force	Force @ Limit	Compliance @ Limit	Energy Release Rate
- [mm]	a [mm]	δ_{max} [mm]	δ_{min} [mm]	P [N]	P_limit [N]	C_limit [mm/N]	G [J/m²]
20-22	21	1,67	0,17	167,10	147,63	1,14E-02	1000
22-24	23	1,97	0,20	154,92	138,32	1,43E-02	1000
24-26	25	2,30	0,23	144,55	130,21	1,77E-02	1000
26-28	27	2,65	0,27	135,59	123,07	2,16E-02	1000
28-30	29	3,02	0,30	127,76	116,73	2,59E-02	1000
30-32	31	3,41	0,34	120,87	111,07	3,08E-02	1000
32-34	33	3,83	0,38	114,75	105,98	3,62E-02	1000
34-36	35	4,27	0,43	109,27	101,37	4,21E-02	1000
36-38	37	4,72	0,47	104,33	97,18	4,87E-02	1000
…	…	…	…	…	…	…	…

Each step covers a crack increment of 3 millimeters. By calculating the corresponding compliance at the end of each crack increment based on the slope *k* and the constant term *d* from the compliance calibration curve (see Figure 3.12), the step-limits are determined. When the increasing compliance reaches a calculated limit value, the machine switches into the next step. The displacement is increased

according to the current crack length to maintain the energy release rate at its desired value.

Figure 4.4 shows the behavior of the energy release rate, *G,* and the crack propagation rate, *da/dN,* over the number of cycles, *N*. The red horizontal line shows the pre-set value for *G*, which was in this case 1000 J/m². Figure 4.5 shows a Paris plot, comparing the results of a classic mode I test to linear fitted trend lines of each step of the *G*-constant test. It can be seen that the results of both tests match each other and that the G-constant test covers a small area of the Paris curve as predicted in Figure 2.9. Figure 4.6 and Figure 4.7 show the results of a test performed at a higher frequency (3 Hz). In this measurement the crack growth was unstable in the beginning and subsequently resulted in higher values of *G*, as some steps of the control software were overleaped and the load at the crack tip was too high for the actual crack length. A sudden increase of crack length results in scatter of the measured compliance. This can lead to switching to a new step even though the crack length has not increased in accordance to the deflection in the compliance signal. If this happens, the applied machine displacement leads to great forces at the crack tip and can lead to catastrophic failure of the specimen.

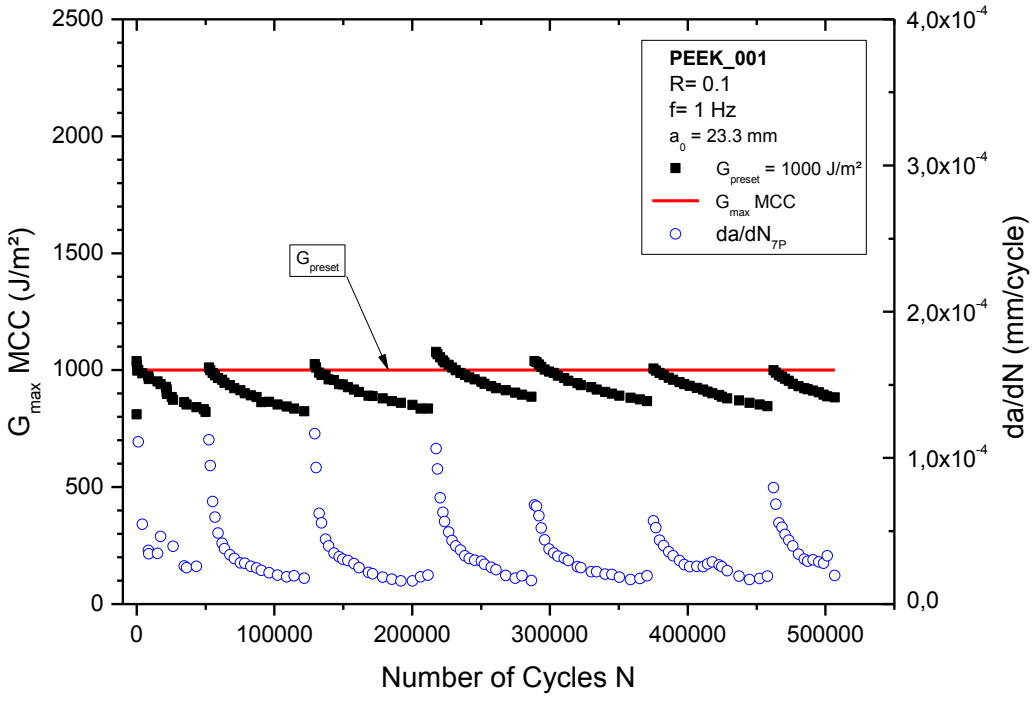

Figure 4.4: Energy release rate G and crack propagation rate versus number of cycles for a desired constant G of 1000 J/m² at a frequency of 1 Hz.

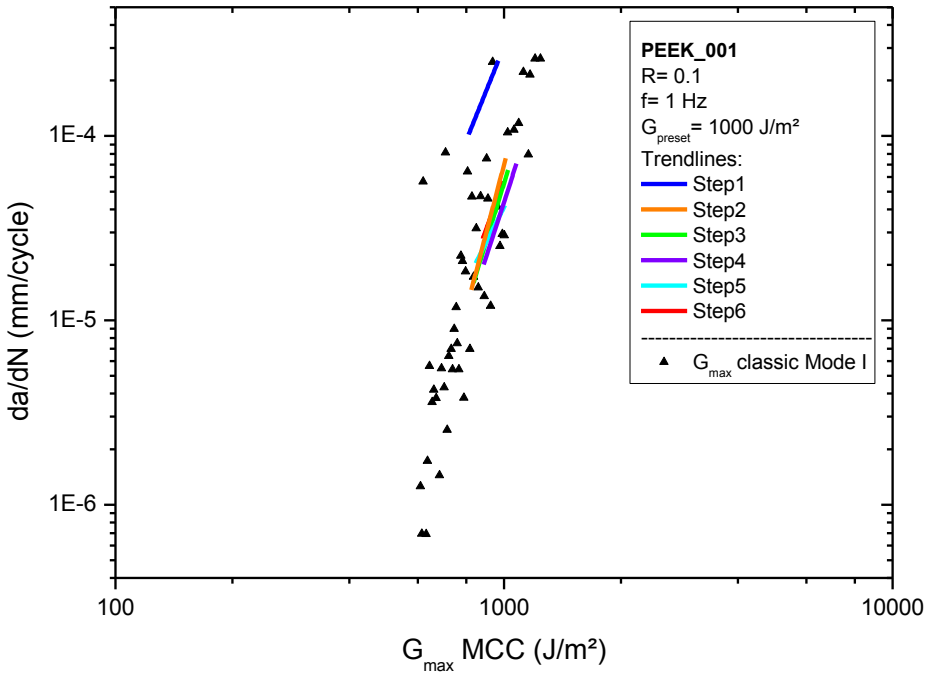

Figure 4.5: Linear fitted trend lines of the particular steps at a preset value of G= 1000 J/m² compared to a classic mode I curve at a test frequency of 1 Hz.

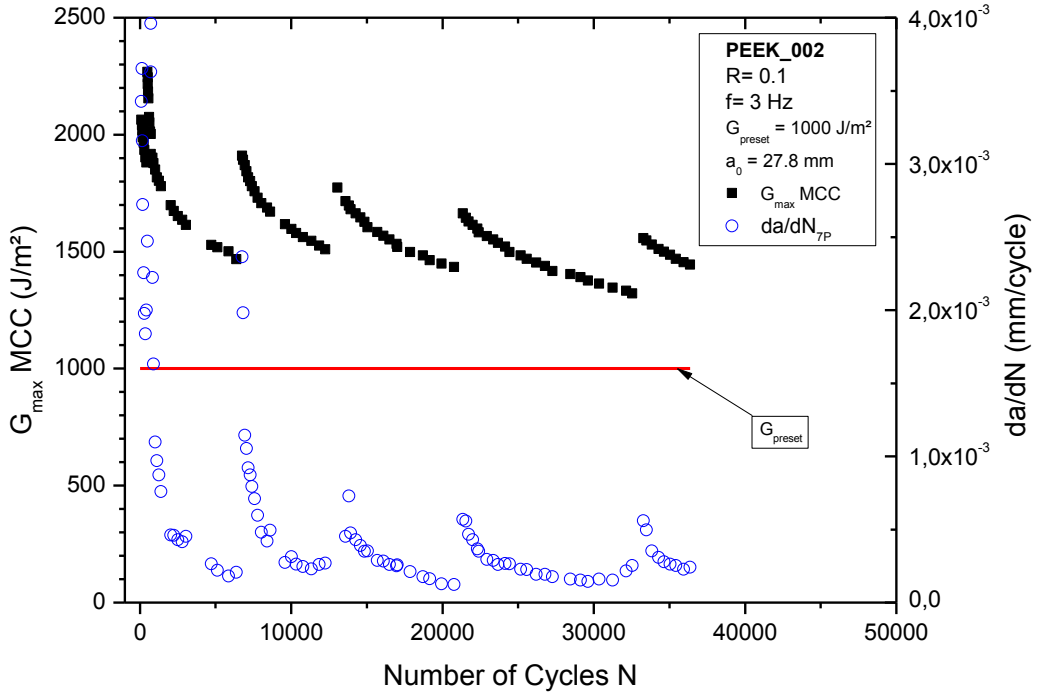

Figure 4.6: Energy release rate G and crack propagation rate versus number of cycles for a desired G of 1000 J/m² at a frequency of 3 Hz.

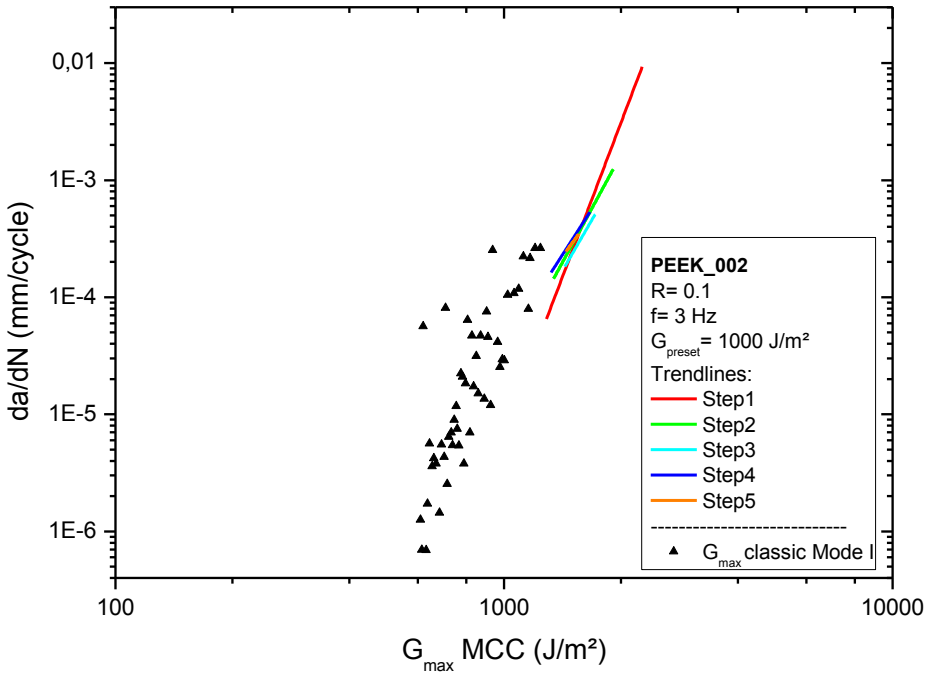

Figure 4.7: Linear fitted trend lines of the particular steps at a preset value of G= 1000 J/m²compared to a classic mode I curve at a test frequency of 3 Hz.

In order to reduce the influence of unstable crack growth, tests at a frequency of 3 Hz and lower preset energy release rate, G_{preset}= 800 J/m² were performed, but showed the same phenomenon as tests with a preset energy release rate of G_{preset}= 1000 J/m². The machine control overleaped some steps because unstable crack growth occurred which lead to peaks in the compliance signal. This phenomenon results in a machine displacement that does not fit to the actual crack length in order to achieve the preset value of *G*, as one can see in Figure 4.8. The crack never catches up with the corresponding fatigue step and so the applied displacement and hence the values of *G* are constantly too high throughout the test. Figure 4.9 shows the result of a test at a preset value of G_{preset} = 800 J/m² and a frequency of 1 Hz. The change of the frequency from 3 to 1 Hz was another attempt to reduce the occurrence of unstable crack growth. Again it can be seen that the crack growth was unstable and the preset level of *G* was not reached. The maximum number of cycles reached before the whole specimen was cracked, was less than 400000.

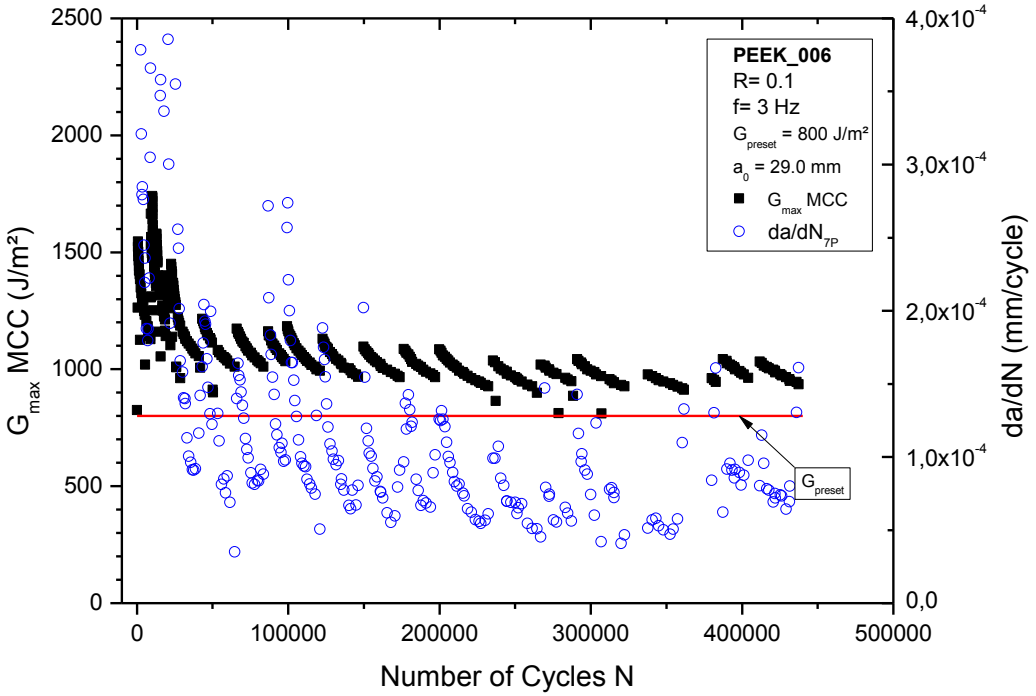

Figure 4.8: Energy release rate G and crack propagation rate over number of cycles for a desired G of 800 J/m² at a frequency of 3 Hz.

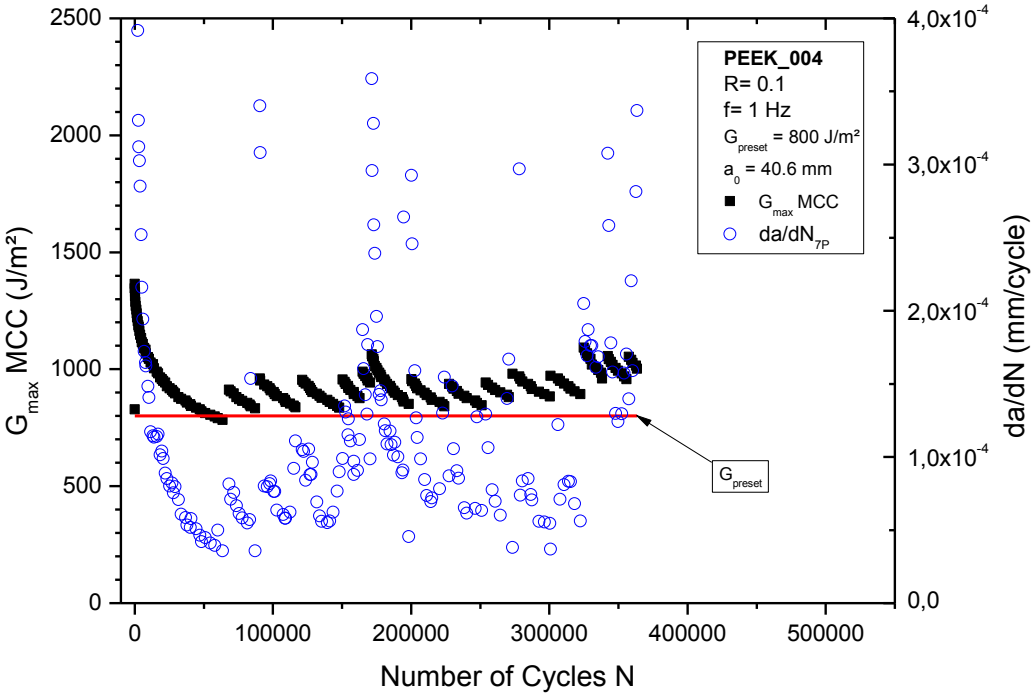

Figure 4.9: Energy release rate G and crack propagation rate versus number of cycles for a desired G of 800 J/m² at a frequency of 1 Hz.

Figure 4.10 shows the compliance calibration data of all specimens tested under compliance control with pre-defined steps in a logarithmic diagram. The table in the diagram lists the values for *k* and *d* of the allometric fit and a calculated mean value of all tests. By taking a closer look to those values for the specimens tested at an energy release rate of 1000 J/m² (PEEK_001, PEEK_002) and the ones tested at 800 J/m² (PEEK_003, PEEK_004, PEEK_005) a small difference between the values can be seen. Further Figure 4.11 and Figure 4.12 illustrate the Paris plots of the tests at a G_{preset}-level of 1000 and 800 J/m². It can be seen that the tests are not really reproducible and that a relatively high scatter occurs.

The reason for the deviating values of *G* might be found in unstable crack growth which is a problem especially with PEEK. Unstable crack growth leads to scatter in the compliance and as the steps of the machine control are defined beforehand, the machine control cannot correct discrepancies between preset and actual energy release rate during the test.

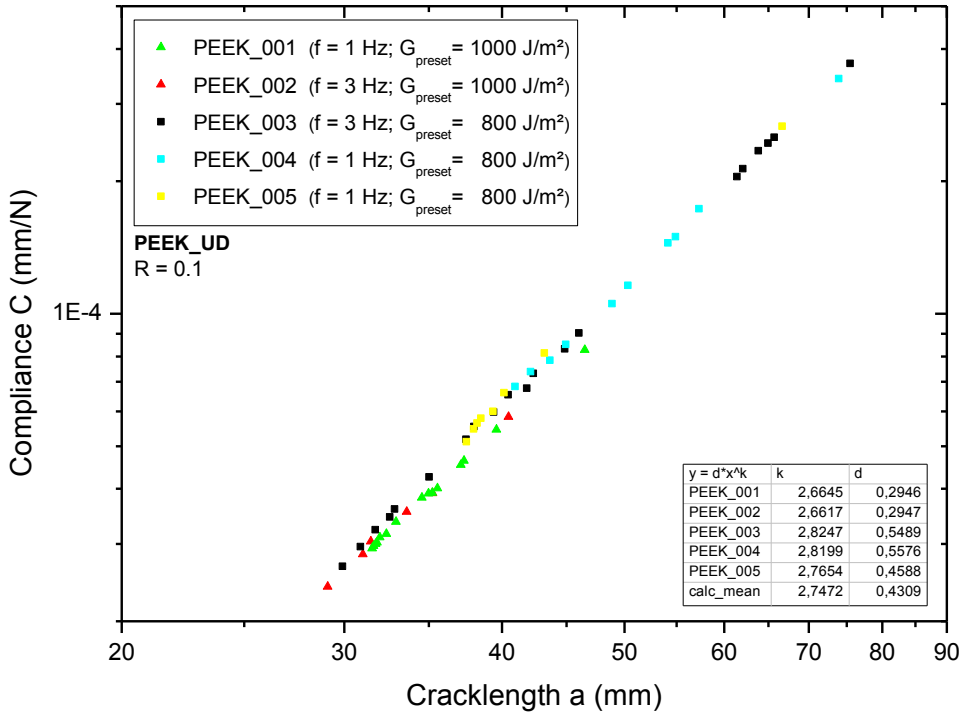

Figure 4.10: Compliance calibration data of all tested specimens.

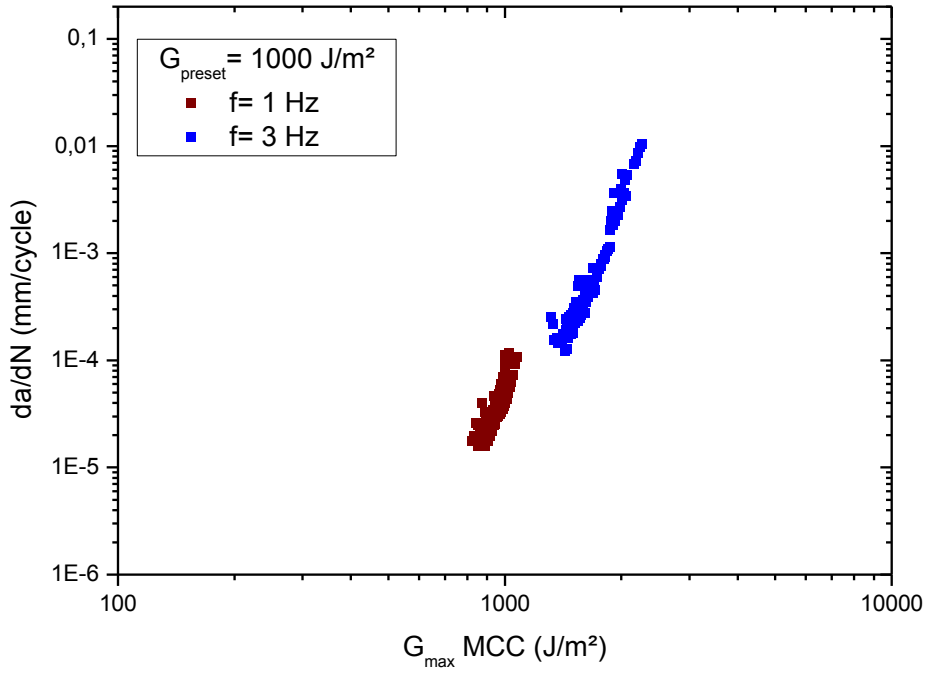

Figure 4.11: Paris plot for the tests performed at a preset G of 1000 J/m².

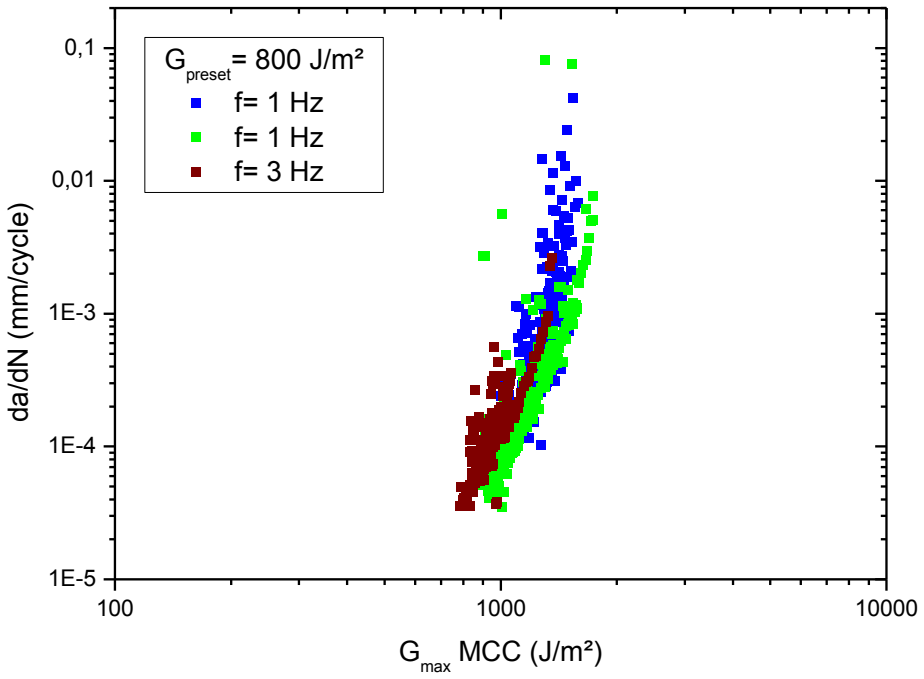

Figure 4.12: Paris plot for the tests performed at a preset G of 800 J/m².

Because of the relatively high scatter in the results of compliance controlled tests with pre-defined steps a new method was developed as described in clause 3.2.2. Testing in dual compensation mode is way more effective in keeping the energy release rate constant. Again the red horizontal line in Figure 4.13 and Figure 4.14 marks the desired value of *G*. The values for *G*, calculated in real-time by the machine's software, are marked by the black circles, respectively rectangles ($G_{I,max}$ Machine). The machine control software calculated the energy release rate according to the Simple Beam Theory (Equation (14)). Hence, none of the correction factors *F* and *N* were used in this calculation. Furthermore, the online calculation of the energy release rate was based on compliance calibration data (*k*, *d*) from former measurements, as *k* and *d* have to be implemented into the software before starting a test with a new specimen. During each test the actual crack length was measured several times to compare the calibration data implemented to the software to the actual values for *k* and *d.* Table 4.3 shows the differences between the values of *k* and *d* implemented into the software in advance (PEEK_mean) and the calibration data measured during the test of specimen PEEK_006 and PEEK_007.

Table 4.3: Comparison of the constants k and d implemented to the machine control with the calibration data measured during the test.

	k	**d**
PEEK_mean	2,7472	0,4309
PEEK_006	2,5777	0,2362
PEEK_007	2,3599	0,0975

In Figure 4.13 and Figure 4.14 one can see that the SBT using the exact values for *k* and *d* yields different results ($G_{I,max}$ SBT) because the crack length calculation and further the values of *G* are influenced. According to the results of classic mode I tests, the values for G calculated using the Modified Compliance Calibration method are significantly lower compared to the Simple Beam Theory. Further it can be seen, that there is a difference in the slope between SBT and MCC. The reason for the different slopes have not yet be found, but might be connected to the use of the correction factors *F* and *N*.

In Figure 4.13 a drop in the energy release rate occurs, beginning at 10^6 cycles. This happened because the crack length had reached a value at which the displacement

necessary to maintain an energy release rate of 1200 J/m² could not be achieved at a frequency of 3 Hz. Thus the energy release rate decreased. The final crack length of the tested PEEK_006 specimen was 54 mm, which was reached within $1.13 * 10^6$ cycles. Testing the specimen PEEK_007 (Figure 4.14), a final crack length of 38.12 mm after $2.79 * 10^6$ cycles was reached.

Figure 4.15 pictures a Paris plot of G_{max}-constant tests using dual compensation control. The results of both specimens, PEEK_006 and PEEK_007, are compared to the curve of a classic G_{max} test under mode I loading conditions. It can be seen that the crack propagation rates at the beginning of each test are fitting to the curve of the classic test. Accompanying the crack propagation the crack propagation rate decreases and PEEK_006 (Figure 4.13) even rises up again after approximately 500000 cycles. A possible explanation can be deduced regarding the trend of the R-ratio during the test. As the machine control keeps the maximum and minimum value of the energy release rate, G_I, at a constant ratio of 0.1, the ratio of the displacement values varies over the course of the test because the R-ratio could not be included as an additional control parameter in the control software. Figure 4.16 compares the R-ratio of PEEK_006 to PEEK_007. According to Hojo et.al., the crack propagation rate depends on the R-ratio. It has been shown that the crack propagation behaves inversely proportional to the R-ratio in a *da/dN* vs. G_{max} plot. As the R-ratio is lower for PEEK_006, this can give an explanation for why the crack propagation rate and further the calculated maximum energy release rate by using the MCC method yields higher values compared to PEEK_007 (Hojo, et al., 1987).

The dual compensation mode for G-constant tests definitely yielded the best results of the methods described in this thesis. As it was not possible to maintain a constant R-ratio as yet, for future experiments it would be of great importance to modify the machine control in order to keep both the energy release rate and the R-ratio constant.

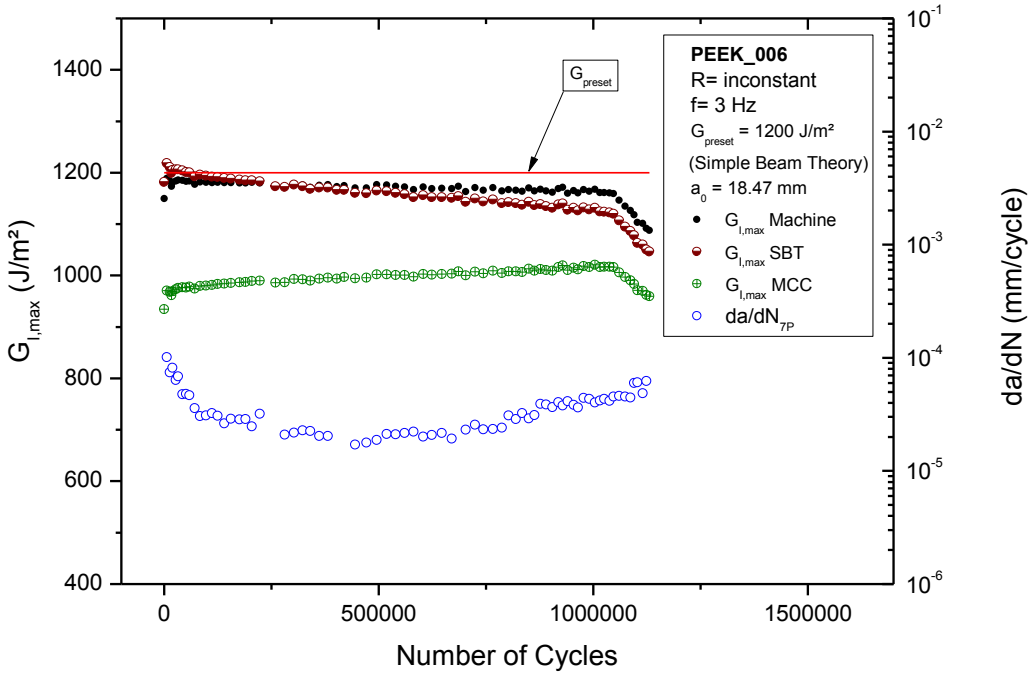

Figure 4.13: Result of a G_{max}-constant test using dual compensation control for specimen PEEK_006.

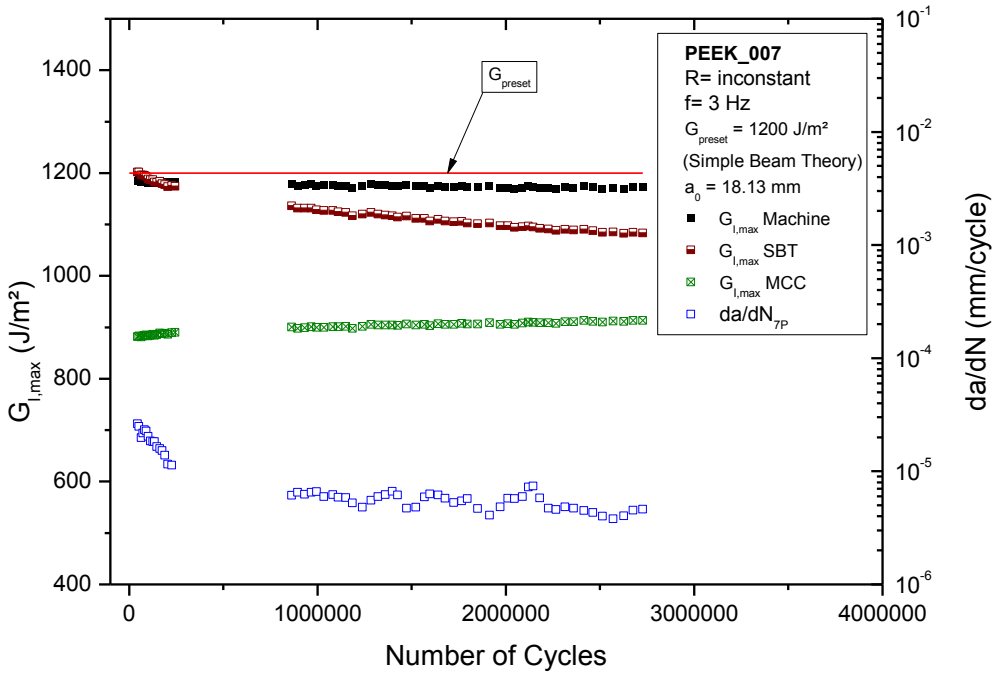

Figure 4.14: Result of a G_{max}-constant test using dual compensation control for specimen PEEK_007.

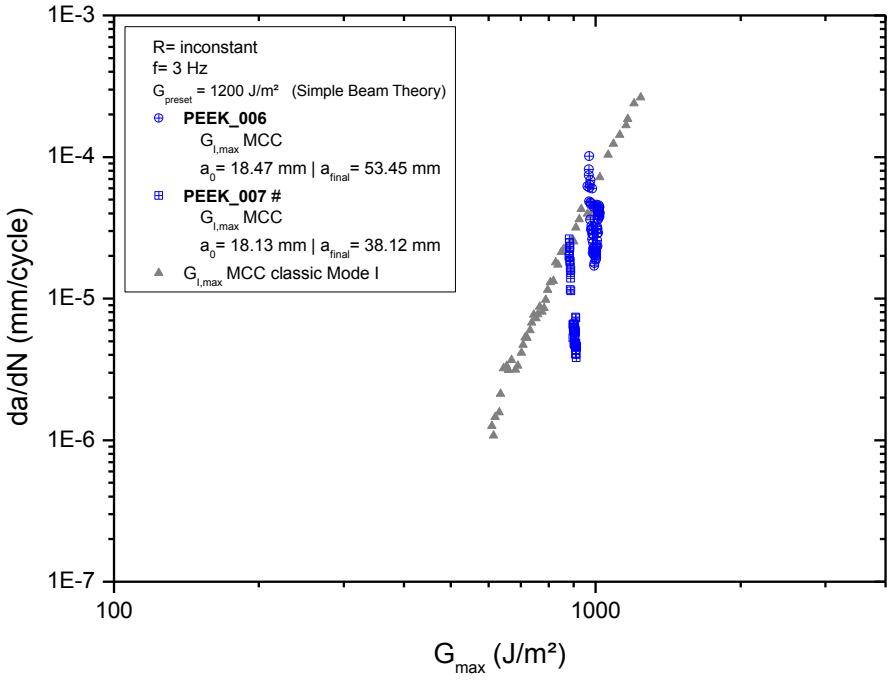

Figure 4.15: Paris plot of a G_{max}-constant test using dual compensation control compared with the result of a classic mode I test.

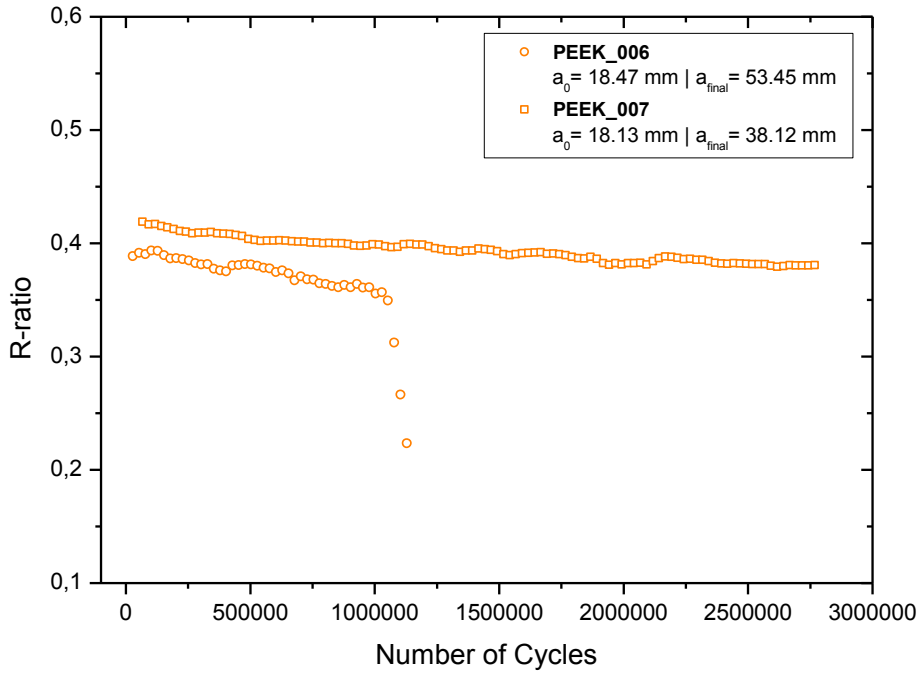

Figure 4.16: Trend of the R-ratio of a G_{max}-constant test using dual compensation control.

4.2 Mode II

4.2.1 Clamp Calibration

The fixture for the C-ELS tests was made of aluminum in a first attempt. The clamp calibration yielded a relatively high clamp correction, Δ_{clamp}, of 20.8 mm. Clamp correction factors of C-ELS test devices from other laboratories had correction factors of 10.4 mm and 15.1 mm (Blackman and Brunner, 2009). Hence the jig for clamping the specimen was reconstructed from steel. Figure 4.17 shows the results, comparing steel to aluminum and it can be seen that the clamping of steel had a stiffer comportment. A clamp calibration was performed on the jig of steel for both, PEEK and epoxy, what yielded a difference of 5.9 mm in the clamp correction between the different specimens. It has to be noted that it was not possible to include a free length of 50 mm as proposed by Blackman et.al. (Blackman and Brunner, 2009), because the C-ELS fixture could not be moved that close to the loading line due to the axle box. Specimens of epoxy had another limiting factor. The starter film had a length of 30 mm so the maximum free length was reduced compared to the specimens of PEEK with a starter film of 20 mm. Clamping the specimens at free lengths from 50 to 110 mm might have reduced the scatter significantly.

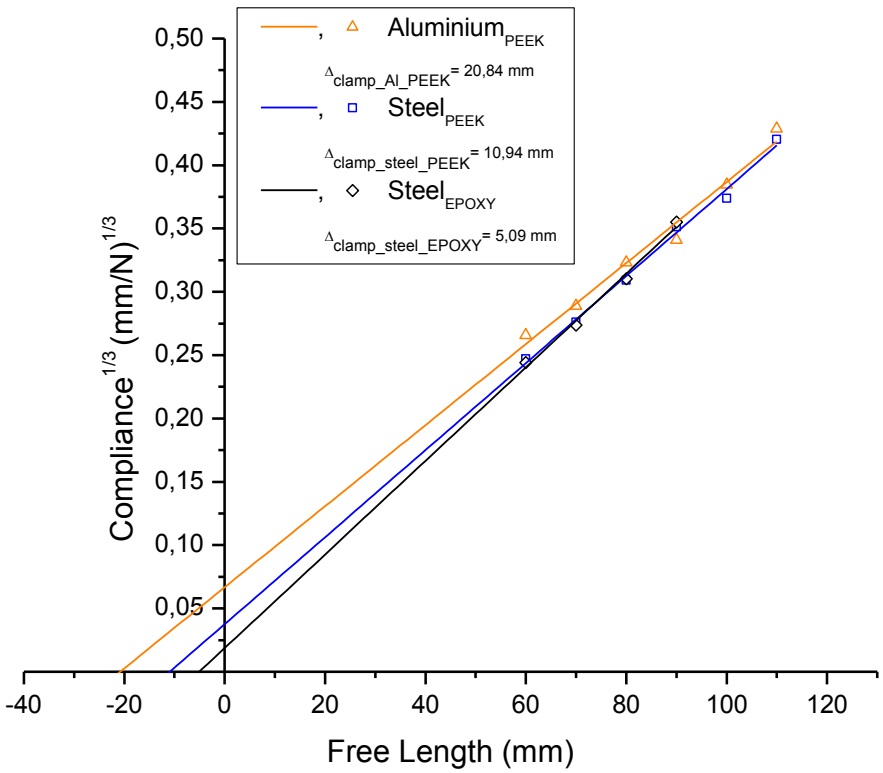

Figure 4.17: Result of the clamp calibration, comparing jigs of steel and aluminum.

4.2.2 Comparison of 3ENF Test and C-ELS Test

For every material and test setup the monotonic value of the critical energy release rate, G_{IIc}, was determined in a quasi-static test according to DIN EN 6034 for 3ENF setup and for C-ELS tests the procedure proposed by Blackman et.al. (Blackman and Brunner, 2009), was applied. These values were taken as a reference value to compare to the maximum value of G that occurred during the fatigue tests and are listed in Table 4.4.

Figure 4.18 shows the results for specimens of PEEK. The values of G_{IImax} obtained from 3ENF fatigue tests start from 5000 J/m² which is much higher compared to the fracture toughness, G_{IIc}, of 1898 J/m². Regarding the results from C-ELS tests, on the one hand the maximum values match the fracture toughness better, but on the other hand do not fit to the 3ENF results at all. Contrary to expectations the C-ELS test yields G_{IImax} values below the energy release rate G_{Imax} obtained from DCB tests under mode I loading. There is also a significant difference in the slope of the curves. Regarding the results of the monotonic tests to determine the fracture toughness, G_{IIC}, one would not expect such a big difference between 3ENF and C-ELS in a fatigue test. A possible reason for this big deviation might be the fixture against shifting of the specimen as it is shorn in Figure 3.19. Due to friction between the specimen and the restraint energy might be absorbed what would yield values for the energy release rate that are too high.

Table 4.4: Critical energy release rate, G_{IIC}, for PEEK and epoxy for 3ENF and C-ELS test setup.

	$G_{IIC\ PEEK}$ (J/m²)	$G_{IIC\ Epoxy}$ (J/m²)
3ENF	1898	988
C-ELS	2087	756

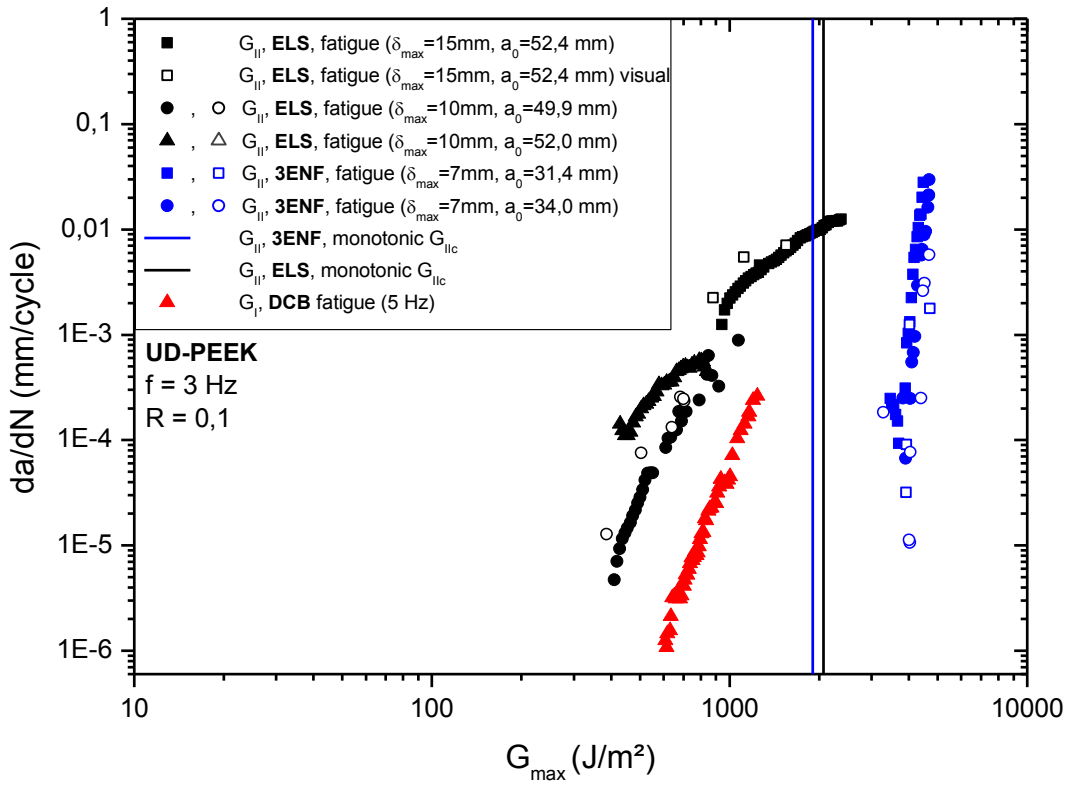

Figure 4.18: Comparison of 3ENF and C-ELS tests performed with PEEK as matrix material.

The results for epoxy are shown in Figure 4.19 which appear to match each other much better than for PEEK. Both the 3ENF and the C-ELS test yielded values of G_{IImax} that matched the fracture toughness, G_{IIc}, well. In contrary to PEEK, the values of the C-ELS fatigue test are clearly higher than the results for G_{Imax} under mode I loading conditions. What can once again be seen is the difference of the slope between the 3ENF and C-ELS curve in the Paris plot. As already stated, it would have been expected that due to the horizontal movement of the fixture and therefore greater energy consumption, the C-ELS setup would yield higher values of G compared to the 3ENF setup. To investigate if temperature differences between the two test setups due to hysteretic heating were the reason for different values of G, an infrared camera was used as described in clause 4.2.4. The results show that the temperature deviation within a specimen did not exceed 1 °C. Therefore further investigations regarding differences in friction between the two crack surfaces in the different test setups would be interesting. Also the equations for data analysis may be reviewed to take account of possible influencing factors.

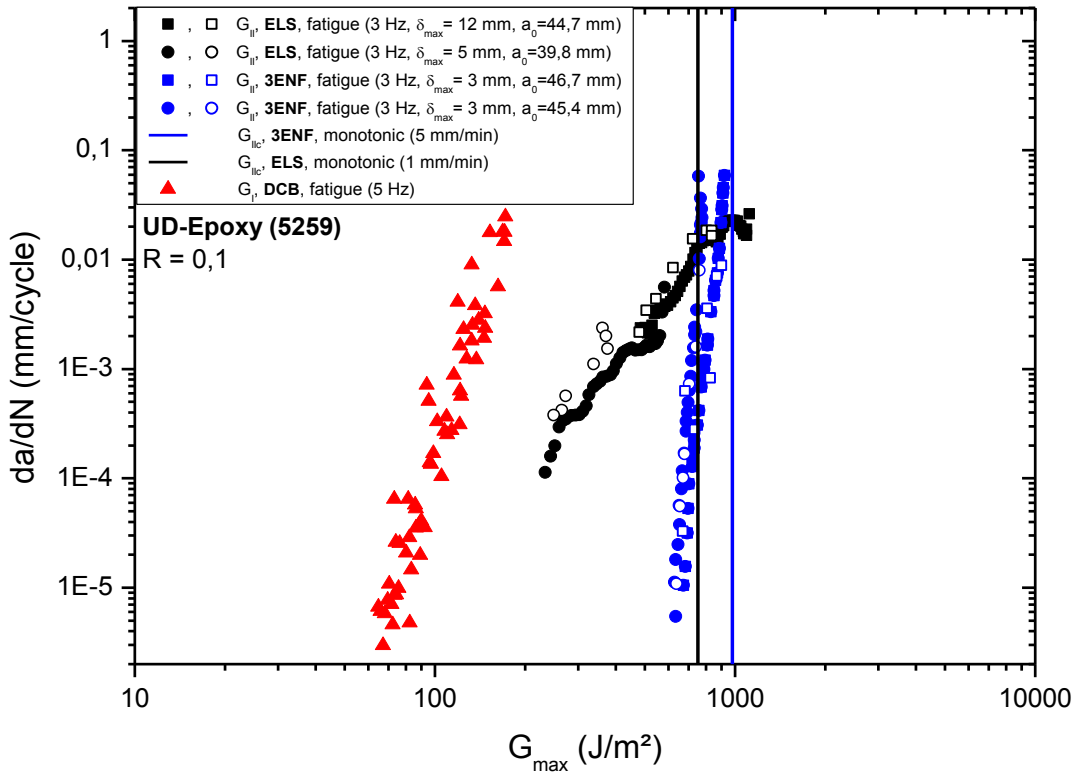

Figure 4.19: Comparison of 3ENF and C-ELS tests performed with Epoxy as matrix material.

4.2.3 Crack Length Determination

In addition it has to be said that under mode II loading conditions the determination of the crack tip can be really difficult. By the use of a travelling microscope, especially at small machine displacements, it is not always possible to assess the exact position of the crack tip. Using the C-ELS setup the crack can be opened to a defined position for the determination of the crack tip via travelling microscope. Therefor the piston of the machine moved in the opposite direction as in the fatigue test until the crack surfaces were separated to facilitate the reading of the crack tip. For 3ENF testing, in a first approach it was attempted to perform a monotonic compliance calibration in order to determine the crack length without measuring via travelling microscope in the fatigue test. Therefore a specimen was placed in the test device at different delamination lengths and loaded with a rate of 18 mm/s to simulate the loading speed of a fatigue test at a frequency of 3 Hz and a displacement of 1.5 mm. In Figure 4.20 the obtained compliance values are plotted versus the crack length. To check the applicability of this method the compliance values of a fatigue test at a

frequency of 3 Hz with an amplitude of 1.5 mm is plotted in the same diagram. It is shown that it is not possible to deduce the crack length during a fatigue test from data obtained by a monotonic compliance calibration.

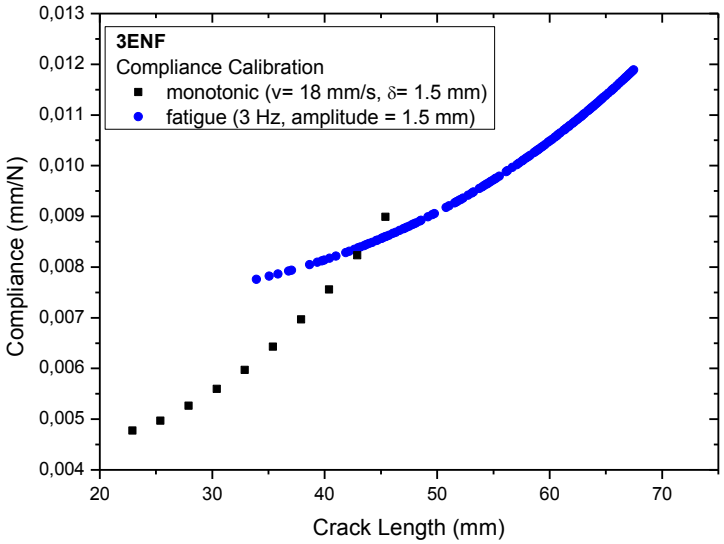

Figure 4.20: Comparison of a monotonic compliance calibration to the course of the compliance of a fatigue test.

Another attempt to detect the crack length was by using a digital image correlation system (Aramis, GOM, Braunschweig, Germany). Therefore a speckle muster was applied to the edge of the specimen using black and white spray paint (Figure 4.21). A camera with telecentric lens was placed in front of the specimen to take photos of the specimen at a frequency of 2 Hz. Subsequently the crack tip can be detected by illustrating the major strain on the specimens edge as pictured in Figure 4.22. The major strain is given in percent and referred to color scale. The crack tip can be found in Figure 4.22 at a value of about 40mm on the x-axis. In this region a rising major strain up to approximately 4 % indicates the location of the crack tip. To assess the crack tip exactly it is important to use a lense with high resolution. The avaliable telecentric lense could depict an image section of 60x60 mm, hence it was not possible to cover the whole specimen. By using a normal lense to depict the whole length of the specimen, the resolution of the edge of the specimen is too low to detect the major strain with sufficient accuracy for crack length determination. Therefore it was not possble to measure the absolute crack length, but it could be detected when the crack reached the field of view. Furthermore the clamping region of the C-ELS test was investigated with digital image correlation but no significant

local strain peaks could be observed during the test that could have been an explanation for the difference in the slope of C-ELS and 3ENF tests. Even though the method is exact, its setup is complex and the data analysis time consuming.

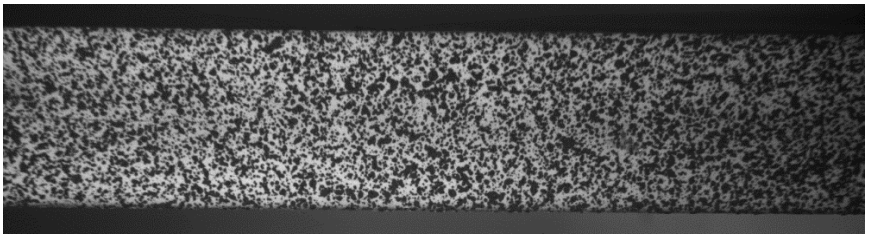

Figure 4.21: Edge of a specimen with applied speckle muster for optical strain measurement.

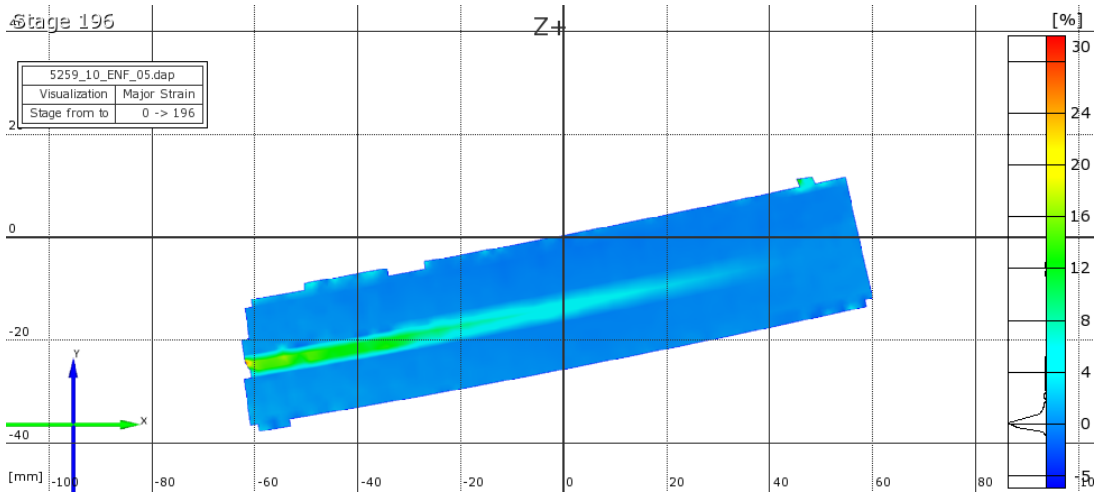

Figure 4.22: Illustration of the major strain at the edge of a specimen showing the crack tip.

4.2.4 Results for Round Robin

According to the guidelines for the mode II fatigue round robin on fiber laminates (ESIS TC4 2011) for each specimen tested under C-ELS loading conditions a preliminary clamp calibration was performed (Brunner and Stelzer, 2011). The results of these clamp calibrations are shown in Figure 4.23. Comparing the results to the previously tested epoxy specimens it can be seen that the test device yielded higher values for the clamp correction, Δ_{clamp}, using the round robin specimens with 4 mm of thickness. As the starter film of these specimens had a length of 60 mm it was not possible to perform the clamp calibration at free length greater than 80 mm. In order to be able to measure the compliance at a free length of 50 mm the slotted hole for mounting the C-ELS fixture was elongated. Nevertheless only four measurements per specimen could be performed to calibrate the C-ELS device. Therefore the

results show a certain scatter that might have been reduced by calibrating the fixture using a specimen with a shorter starter film to be able to clamp the specimen up to a free length of 110 mm.

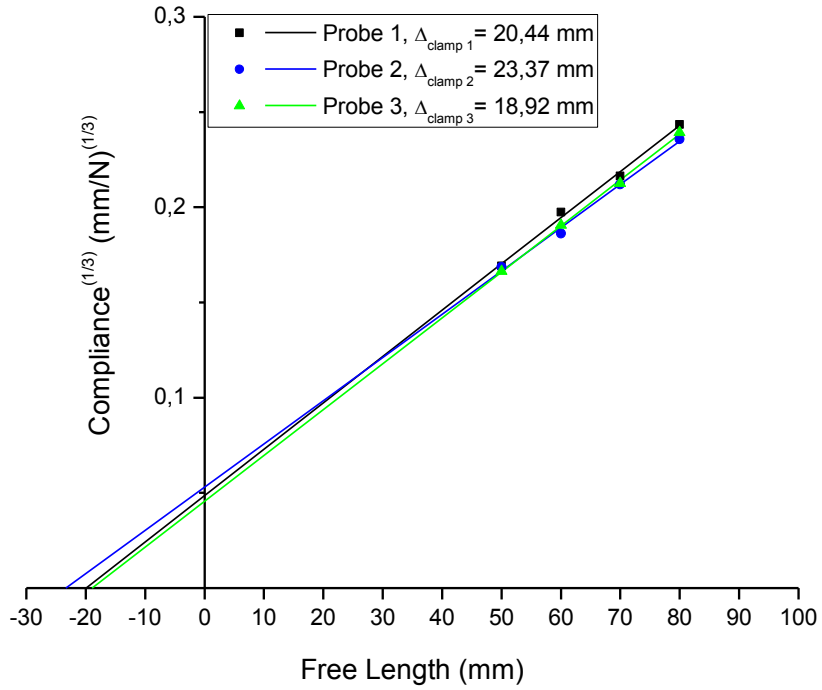

Figure 4.23: Clamp calibration of the C-ELS specimen for round robin testing.

The comparison of the results obtained from C-ELS and 3ENF tests is shown in Figure 4.24, where it can be seen that the same tendency as mentioned above occurred. The curve of the energy release rate resulting from the C-ELS test is not as steep as the one obtained from the 3ENF test. The vertical line represents the value of the fracture toughness, G_{IIc}, measured in a monotonic 3ENF test. Both the C-ELS and the 3ENF tests yielded results of G_{IImax} in the region of the monotonic value. Compared to 3ENF, the result of the C-ELS test implies that the material tends to delaminate at smaller loads, but the crack growth is slower. The result of the 3ENF test conveys the impression that higher loads are necessary to lead to crack growth but on the other hand a small increase in the applied load would rapidly lead to catastrophic failure. To investigate this difference in the results, an infrared camera (FLIR Systems, USA) was set up to measure the temperature of the specimen throughout the test for both, 3ENF and C-ELS setup. Pictures were taken in time increments of 5 minutes to observe the temperature profile of the specimen depending on the number of cycles and the crack length.

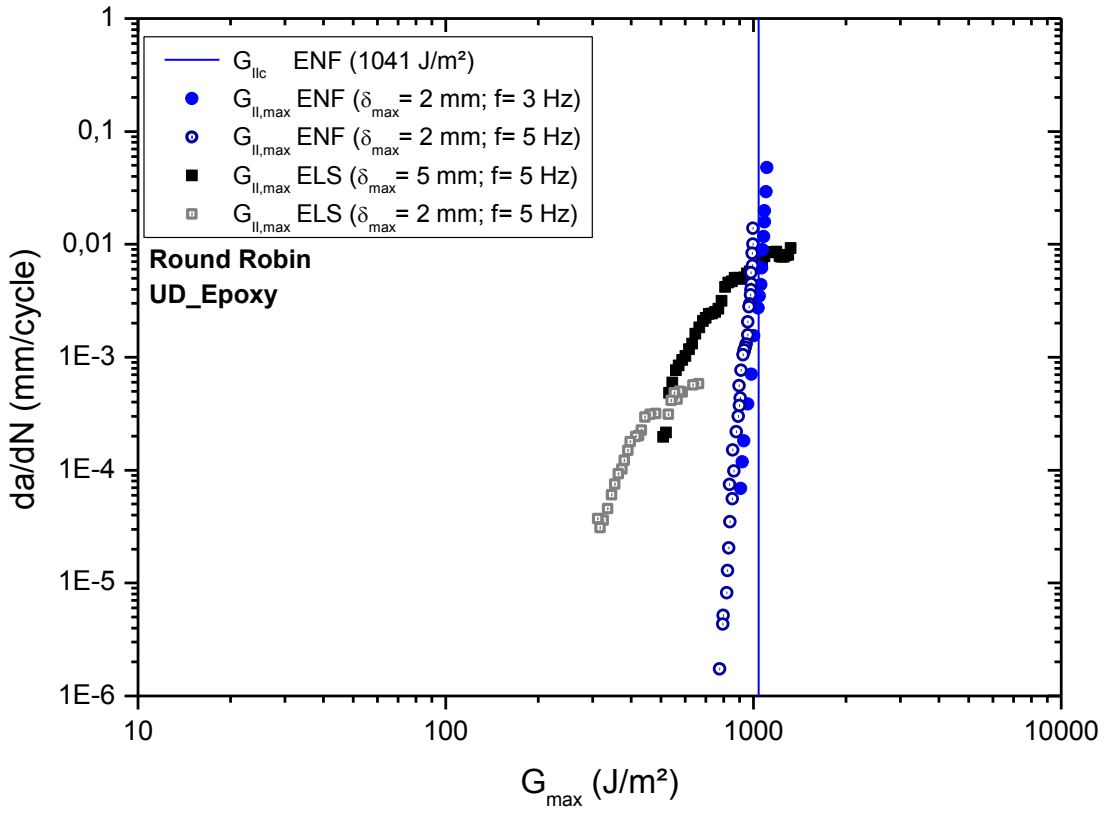

Figure 4.24: Results of 3ENF and C-ELS fatigue tests for mode II round robin.

In Figure 4.25 it can be seen that there is a region of elevated temperature under the loading point which marks the region of the crack tip as it shifts to the right, following the growing crack. The observed difference in temperature cannot be regarded as a significant result as the temperature difference over the length of the specimen does not exceed 1°C. This leads to the conclusion that no significant hysteretic heating occurs that would consume energy. A stationary state of the temperature profile is reached rapidly and Figure 4.26 a) shows the temperature profile of the specimen in 3ENF loading after 235000 cycles. It can be seen that the temperature on the left side of the loading point B is slightly higher than on the undamaged right side. The highest temperature was measured at the loading point B where the greatest bending occurred. Regarding the C-ELS fixture also after 23500 cycles in Figure 4.26 b) the temperature has the highest value at the clamping but it does not deviate more than 1°C from the lowest temperature measured on the edge of the specimen. Apart from detecting differences between the two test setups this method might be applied to detect the crack tip when external temperature influences are excluded, e.g. by the use of a temperature chamber.

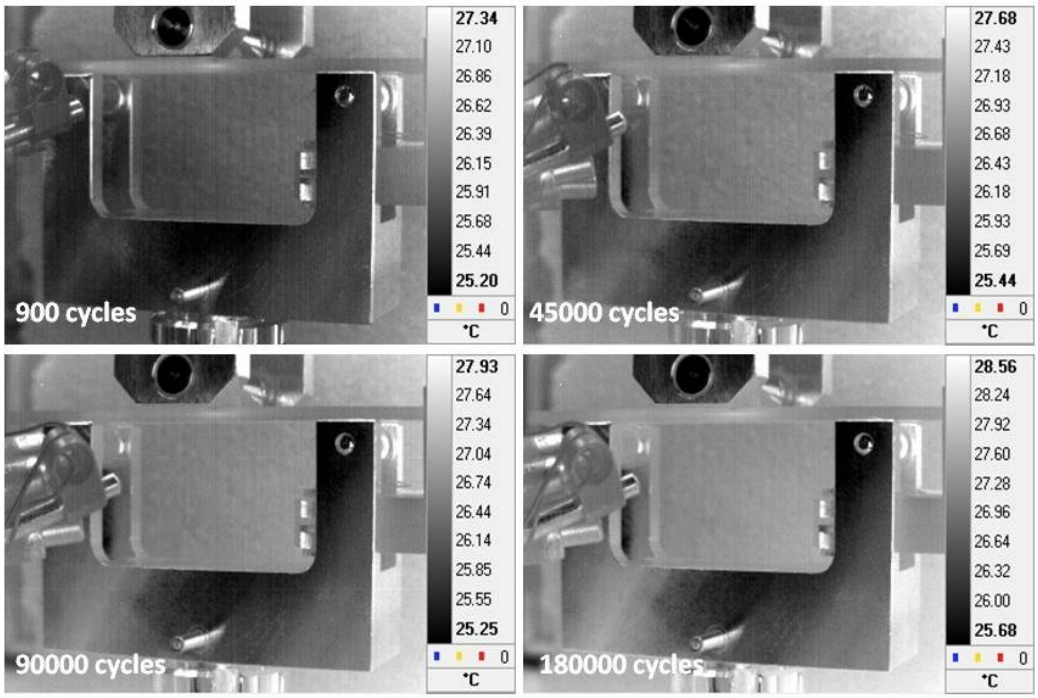

Figure 4.25: Infrared pictures of the 3ENF test at after 900, 45000, 90000 and 180000 cycles.

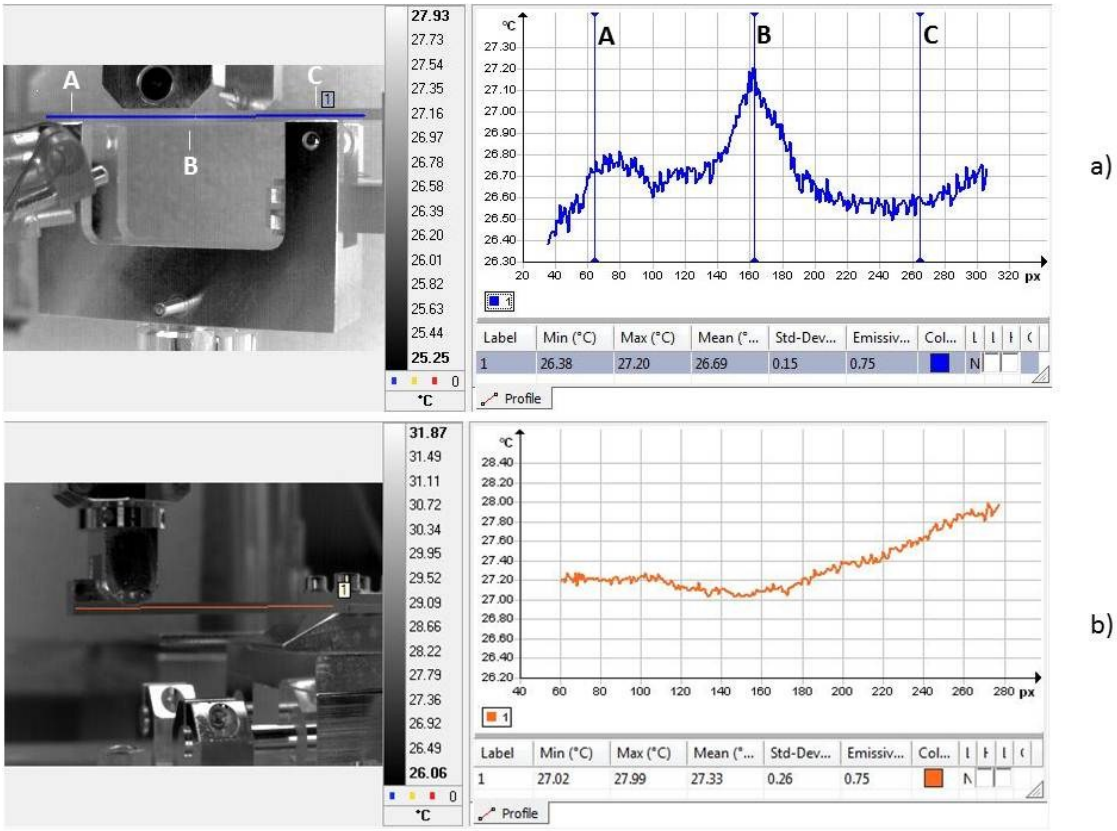

Figure 4.26: Comparison of 3ENF and C-ELS specimens during a fatigue test after approximately 235000 cycles.

5. Conclusions and Outlook

The focus within this work was twofold. On the one hand a method was developed to realize cyclic G-constant tests under mode I loading conditions. For mode II fatigue loading conditions on the other hand, a C-ELS test device was constructed and a comparison between the 3ENF and C-ELS setup within an international round robin was performed.

Regarding mode I testing first tests performed under extensometer control with defining loading steps for certain crack increments did not yield satisfying results for *G*-constant measurements. Thereupon, tests based on compliance calibration were performed which were easier to handle. These evolutionary developments lead to *G*-constant tests based on a compliance calibration by regulating the machine displacement under a so called dual compensation mode control. Finally it was possible to regulate the machine displacement in real-time according to the desired value of *G*. As a disadvantage of the dual compensation control mode it has to be stated that it was not possible to keep a constant R-ratio throughout the test. It is of great interest to maintain a constant R-ratio to exclude a possible influence on the crack propagation rate. Another factor of influence was the scatter in calibration data between the specimens as the machine control used beforehand determined mean-values. A goal for further measurements should be to implement a dual compensation mode control using the Calibrated Beam Theory or the Modified Compliance Calibration to calculate the energy release rate. Further the machine control might be modified in order to maintain a constant R-ratio.

Under mode II loading conditions the 3ENF setup and the C-ELS fixture yielded different results. The obtained curves of the energy release rate in the Paris plot differed from each other significantly. The reason for this difference could not be determined. By investigating the clamping of the C-ELS and 3ENF setup with an infrared camera no peculiarities could be observed. Measurements of the strain distribution on the edge of the specimens also did not show any apparent differences. The C-ELS test is preferable regarding the determination of the crack tip as it can be very difficult to determine the crack tip in a 3ENF test using a travelling microscope. Several methods of crack tip determination have been tested, but either they did not work out, or they were complex in their application. In further

investigations it would be of interest to measure the temperature of the specimen when performing the test in a temperature chamber to yield more exact and significant results. If the final results of the round robin tests approve this discrepancy between 3ENF and C-ELS tests it might be useful to review the formulas used for the data analysis and the applied correction factors.

6. References

Anderson, T. L. (1991). “Fracture Mechanics – Fundamentals and Applications”, CRC Press Inc., Florida, USA.

Argüelles, A.; Vina, J.; Canteli, A. F.; Bonhomme, J., (2010), Polymer Composites **31**, pp. 700-706.

Asp, L. E.; Sjörgen A.; Greenhalgh, E. S., (2001), Journal of Composites Technology and Research **23**, pp. 55-68.

Blackman, B. R.; Brunner, A. J., (2009), “Fibre-composites - The determination of the mode II fracture resistance, GIIc, of unidirectional fibre-composites using the calibrated end loaded split (C-ELS) test and an effective crack length approach”, ESIS TC4 Protocol.

Blackman, B. R.; Brunner, A. J.; Williams, J. G., (2006), Engineering Fracture Mechanics **73**, Elsevier Ltd., pp. 2443-2455.

Blackman, B. R.; Kinloch, A. J., Paraschi M., (2005), Engineering Fracture Mechanics **72**, Elsevier Ltd., pp. 877-897.

Brunner, A. J.; Murphy, N.; Pinter G., (2009), “Development of a standardized procedure for the characterization of interlaminar delamination propagation in advanced composites under fatigue mode I loading conditions”, Elsevier Ltd.

Brunner, A. J.; Stelzer, S., (2011), “Guidelines for Mode II Fatigue Round Robin on Fiber Laminates”, ESIS TC4.

Brunner, A. J.; Stelzer, S.; Pinter G., (2010), “Developement of a Test Procedure for Mode II Fatigue Delamintaion Resistance of Advanced Fiber-Reinforced Polymer-Matrix Laminates”, ECF **18**.

Canteli, A. F., (2010), “An alternative procedure for measuring the crack growth for constant energy release rate range ΔG under mode-I loading”, Department of Construction and Manufacturing Engineering, University of Oviedo, Spain.

Carlsson, L. A., (1993), In “Materials Science and Technology – Structure and Properties of Composites”, (Cahn, R.W.; Haasen, P. and Kramer, E. J., ed.), Vol. **13**, VCH, Weinheim, Germany.

Cvitkovich, M., (1995), “Polymer Matrix Effects On Interlaminar Crack Growth In Advanced Composites Under Monotonic And Fatigue Mixed-Mode I/II Loading Conditions”, Dissertation, Montanuniversität Leoben, Leoben, Austria.

Davies, P.; Blackman, B. R.; Brunner, A. J., (1998), Applied Composite Materials 5, pp. 345-364.

DIN EN ISO 178, (ISO 178:2001 + Amd. 1:2004), “Plastics – Determination of flexural properties”.

Ehrenstein, G. W., (2006), “Faserverbund-Kunststoffe”, Hanser, München.

Gregory, J. R.; Spearing, S. M., (2004), Acta Materialia Vol. **52**, (Elsevier, Ltd.), pp. 5493-5502.

Grellmann, W.; Seidler, S., (2007), “Polymer Testing”, Hanser, Munich.

Hertzberg, R. W., (1996) “Deformation and Fracture Mechanics of Engineering Materials”, John Wiley & Sons Inc., USA.

Hodgkinson, J. M., (2000), “Mechanical Testing of Advanced Fibre Composites”, Woodhead Publishing Limited, Cambridge, UK.

Hojo, M.; Matsuda, S.; Tanaka, M.; Ochiai, S.; Murakami, A., (2006), Composites Science and Technology **66**, pp. 665-675.

Hojo, M.; Ochiai, S.; Gustafson, C.-G.; Tanaka, K., (1994a), Engineering Fracture Mechanics **49**, pp. 35-47.

Hojo, M.; Tanaka, K.; Gustafson, C. G.; Hayashi, R., (1987a), Composite Science and Technology **29**, pp. 273-292.

Hojo, M.; Gustafson, C.-M.; Tanaka, K.; Hayashi, R., (1987b), In Proc. “Advanced Materials for Severe Service Applications”, (Iida, K., McEvily, A. J., ed.), Elsevier Applied Science, London and New York.

Hojo, M.; Ochiai, S.; Aoki, T.; Ito, H., (1994b), In Proc. "2nd ECCM-Composites, Testing & Standardization", pp. 553-561.

ISO 15024, (2004), Fibre-reinforced plastic composites - Determination of mode I interlaminar fracture toughness, GIc, for unidirectionally reinforced materials.

Johnson, W. S.; Pavlick, M. M., (2005), "Determination of Interlaminar Toughness of IM7/977-2 Composites at Temperature Extremes and Different Thickness", NASA, Georgia Institute of Technology, USA.

Martin, R. H.; Murri, G. B., (1988), NASA Technical Memorandum **100577**, Langley Research Center, Hampton, Virginia, USA.

Martin, R. H.; Murri, G. B., (1990), In Proc. "Composite Materials: Testing and Design", 9th Conference, pp. 251-270, American Society for Testing and Materials, Philadelphia, USA.

Pinter, G., (2011), "Bruchmechanik der Kunst- und Verbundwerkstoffe", Lecture Notes, Montanuniversität Leoben, Leoben, Austria.

Pinter, G., (1994), "Charakterisierung der interlaminaren Rissausbreitung unidirektionaler Verbundwerkstoffe unter zyklischer Modus-I Belastung", Master's Thesis, Montanuniversität Leoben, Leoben, Austria.

Pinter, G.; Stelzer, S., (2010), "Determination of Mode I Fatigue Delamination Propagation in Unidirectionally Reinforced Materials", Report, Montanuniversität Leoben, Leoben, Austria.

Pinter, G.; Stelzer, S., (2010), "ESIS TC4 Delamination of Mode I Fatigue Delamination Propagation in Unidirectional Reinforced Materials", Test Protocol, Institute of Materials Science and Testing of Plastics, Leoben, Austria.

Russell, A. J.; Street, K. N., (1988), In Proc. "Composite Materials: Testing and Design", 8th Conference, pp. 259-277, American Society for Testing and Materials, Philadelphia, USA.

Sheikh-Ahmad, J. Y., (2009), "Machining of Polymer Composites", Springer Science & Business Media, New York, USA.

Sjörgen, A.; Asp, L. E., (2002), International Journal of Fatigue **24**, pp. 179-184, Elsevier Science Ltd.

Stelzer, S.; Brunner, A.J.; Argüelles, A.; Murphy, N.; Pinter, G., (2011), In Proc. "Deformation and Fracture of Composites" (to be printed), Cambridge, UK.

Williams, J. G., (1989), Journal of Strain Analysis **24**, pp. 207-214.

Williams, J. G.; Moore, D. R.; Pavan, A., (2001), "Fracture Mechanics Testing Methods for Polymers Adhesives and Composites", ESIS Publication 28, Elsevier Science Ltd., Oxford, UK.

Williams, J.G., (1987), "Large displacement and end block effects in the DCB interlaminar test in modes I & II", Journal of Composite Materials, pp. 330-347.

7. List of Figures

8. List of Tables

9. Appendix

```
% PART 1
% Cleaning the .DAT-files obtained from the MTS control software
% Removal of the data headers.
% Saving the data for following calculations.
%--------------------------------------------------------------------------
clear all
close all

% Open a dialog box to load the data files
[fileName pathName] = uigetfile({'*.dat'; '*.txt';'*.*'}, 'Messdatei
öffnen');
try
    fid = fopen([pathName fileName]);
catch
    msgbox('Angegebenes File könnte nicht gefunden werden');
    return
end
% Separation of filename, material and specimen number
[fname fext] = strtok(fileName, '.');
[peek rest1] = strtok(fname, '_');
[nr rest2] = strtok(rest1, '_');

%--------------------------------------------------------------------------
% Delete data headers and empty lines
zeilennummer = 1;
messwerte = 1;
B = zeros(4000000, 7);          % Create an empty matrix to be filled with
                                % data
while 1
    tline = fgetl(fid);
    if (tline == -1)            % If tline =1 the end oft he document is
                                % reached
        break
    end

    if ~isempty(tline)          % check if the line is empty
        if messwerte            % begin to read data after the data header
            try
                A = cell2mat(textscan(tline, '%f %f %f %f %f %f %f'));
% Convert the data from string to numbers and write them to A
                messwerte = 1;
                B(zeilennummer, :) = A;                                  %
                zeilennummer = zeilennummer+1;
            catch
                messwerte = 0; % If cell2mat nichtscant read anything, the
                               % line is empty and is followed by a data
                               % header
            end
        end
        if strcmp(tline(1:2), 'mm')     % If a line begins with mm, the
                                        % next row contains data points
           messwerte = 1;
        end
    end

end
```

```
B = B(1:zeilennummer-1, :);
[zeilen, spalten] = size(B);
%--------------------------------------------------------------------------
% Sort the columns in the following order: Number of Cycles | Pmax |
% deltamax | Compliance |
B_sorted = zeros(zeilen, 4);
B_sorted(:,1) = B(:,7);
B_sorted(:,2) = B(:,3);
B_sorted(:,3) = B(:,1);
B_sorted(:,4) = B(:,4);
%--------------------------------------------------------------------------
% Crate a matrix with only maximum values of the peak/valley recording
pline_max = 1;
P_MAX = zeros(zeilen, 12);
P_MAX_header = {'Cycles ' 'Load ' 'Displacement ' 'Compliance '
'korrFaktor_F ' 'korrFaktor_N ' 'a_calculated ' 'Gmax_BT ' 'Gmax_CBT '
'Gmax_MCC ' 'da/dN_Sekant ' 'da/dN_7-Point '};
P_MAX_units_excel = {'[] ' '[N] ' '[mm] ' '[mm/N] ' '[] ' '[] ' '[mm] '
'[J/m^2] ' '[J/m^2] ' '[J/m^2] ' '[mm/cyc] ' '[mm/cyc]'};
P_MAX_units_meter = {'[] ' '[N] ' '[m] ' '[m/N] ' '[] ' '[] ' '[m] '
'[J/m^2] ' '[J/m^2] ' '[J/m^2] ' '[mm/cyc] ' '[mm/cyc]'};

for i = 1:zeilen
    if (B_sorted(i,3) > 5)              % LIMIT FOR MAX-VALUE: e.g. 3 mm !
        P_MAX(pline_max,1:4) = B_sorted(i,:);
        pline_max = pline_max+1;
    end
end
pline_max = pline_max-1;
P_MAX = P_MAX(1:pline_max,:);
%--------------------------------------------------------------------------
% Correction from segments to number of Cycles
for j = 1:pline_max
    cycmax = ((P_MAX(j,1))/2);
    numberofcycs = ceil(cycmax);
    P_MAX(j,1) = numberofcycs;
end
%--------------------------------------------------------------------------
% Correction from mm to m fort he following calculation
for m = 1:pline_max
    P_MAX(m,3) = (P_MAX(m,3))/1000;

    P_MAX(m,4) = (P_MAX(m,4))/1000;
end
%--------------------------------------------------------------------------
% Save the matrix for further treatment with MatLab
savefile = [pathName peek '_' nr '_Maschinendaten_meter'];
save(savefile, 'P_MAX', 'P_MAX_header', 'P_MAX_units_meter', 'pline_max');
disp('Erfolgreich abgeschlossen');
```

```
% PART 2
% This file serves to complete the values of number of cycles and crack
% length, read during the test, with load and displacement from the machine
% data. Further the constants k and d are found by performing a compliance
% calibration.
%--------------------------------------------------------------------------
close all
clear all

zeichnen = 0;
%--------------------------------------------------------------------------
% Open the file containing the optical read data.
[fileName_rl, pathName_rl] = uigetfile({'*.xlsx';'*.xls';'*.*'},
'abgelesene Werte öffnen');
try
    fid = fopen([pathName_rl fileName_rl]);
catch
    msgbox('Angegebenes File konnte nicht gefunden werden!');
    return
end
% Import the Excel-file and separate data and headerrldata =
xlsread([pathName_rl fileName_rl], 'Tabelle1');
%--------------------------------------------------------------------------
% Load the previously cleaned machine data
[peek rest1] = strtok(fileName_rl, '_');
[nr rest2] = strtok(rest1, '_');
try
    load([pathName_rl peek '_' nr '_Maschinendaten_meter']);
catch
    msgbox('Die gesäuberten Maschinendaten konnten nicht gefunden werden');
    return
end
%--------------------------------------------------------------------------
% Round the number of cycles to integral numbers and convert the crack
% length from mm to m.
[zeilen_rl spalten_rl] = size(rldata);
for i = 1:zeilen_rl
    rldata(i,2) = fix(rldata(i,2));

    rldata(i,3) = rldata(i,3)/1000;
end
%--------------------------------------------------------------------------
% Complete the crack visual data
VIS_header = {'Cycles N' 'Cracklength a' 'Force Pmax' 'Displacement delta'
'Compliance C' 'log_a' 'log_C'}; % Header
VIS = zeros(zeilen_rl, 7); % crate Matrix for visual data

for j = 1:zeilen_rl
   VIS(j,1) = rldata(j,2);              % Cycles
   VIS(j,2) = rldata(j,3);              % Crack Length in meter
   for ii = 1:pline_max
       zet = P_MAX(ii,1);
       switch zet
           case VIS(j,1)
                VIS(j,3) = P_MAX(ii,2);
                VIS(j,4) = P_MAX(ii,3);
                break
           case VIS(j,1)+1
                VIS(j,3) = P_MAX(ii,2);
                VIS(j,4) = P_MAX(ii,3);
                break
           case VIS(j,1)+2
```

```
                VIS(j,3) = P_MAX(ii,2);
                VIS(j,4) = P_MAX(ii,3);
                break
            case VIS(j,1)+3
                VIS(j,3) = P_MAX(ii,2);
                VIS(j,4) = P_MAX(ii,3);
                break
        end
    end
    VIS(j,5) = VIS(j,4)/VIS(j,3);        % Compliance
    VIS(j,6) = log10(VIS(j,2));
    VIS(j,7) = log10(VIS(j,5));
end
%-------------------------------------------------------------------------
% Plot the diagran log_C vs. Log_a including the trend line for the
% determination of k and d
gerade = polyfit(VIS(:,6),VIS(:,7),1);
k = gerade(1);
d = 10^(gerade(2));
xwerte = VIS(1,6):0.01:VIS(zeilen_rl,6);
ausglg_x = (xwerte');
[zei spa] = size(ausglg_x);
ausglg_y = zeros(zei,spa);
for xw = 1:zei
    ausglg_y(xw) = k * ausglg_x(xw,1) + gerade(2);
end
%plot
if zeichnen == 1
    fig = plot(VIS(:,6), VIS(:,7), ausglg_x, ausglg_y);
    xlabel('log a');
    ylabel('log C');
    title('Compliance Calibration');
    ka = num2cell(k);
    de = num2cell(d);
    text(-1.4,-3.7,['k = ' ka],'HorizontalAlignment','left');
    text(-1.4,-3.8,['d = ' de],'HorizontalAlignment','left');
end
%-------------------------------------------------------------------------
% Savind data for further calculation
savefile = [pathName_rl peek '_' nr '_Kalibrierdaten_meter'];
save(savefile, 'k', 'd', 'peek', 'nr', 'P_MAX', 'P_MAX_header',
'P_MAX_units_meter', 'pline_max');
% Saving as Excel table
EXCEL_header = {'Cycles N' 'Cracklength a' 'Force Pmax' 'Displacement'
'Compliance'};
EXCEL_units = {'[]' '[mm]' '[N]' '[mm]' '[mm/N]'};
EXCEL = zeros(zeilen_rl,5);
EXCEL(:,1) = VIS(:,1);
EXCEL(:,3) = VIS(:,3);
EXCEL(:,5) = VIS(:,5);
for m = 1:zeilen_rl
    EXCEL(m,2) = VIS(m,2)*1000;
    EXCEL(m,4) = VIS(m,4)*1000;
end
[namexls, extxls] = strtok(fileName_rl, '.');
xlswrite([pathName_rl namexls '_erweitert'], EXCEL_header, 'Tabelle1',
'A1');
xlswrite([pathName_rl namexls '_erweitert'], EXCEL_units, 'Tabelle1',
'A2');
xlswrite([pathName_rl namexls '_erweitert'], EXCEL, 'Tabelle1', 'A3');

disp('Erfolgreich abgeschlossen');
```

```
% PART 3
% MODE I
% Calculation of the energy release rate G and the crack propagation rate
% based on the machine- and calibration data.
%--------------------------------------------------------------------------
close all
clear all
% Switch to enable/disable the plotting of the diagrams
zeichnen = 0;

% Dialog box to select the calibration data
[fileName, pathName] = uigetfile({'*.mat';'*.*'}, 'Kalibrierdaten_meter
öffnen');
try
    load([pathName fileName]);
catch
    msgbox('Angegebenes File konnte nicht gefunden werde!');
    return
end
%--------------------------------------------------------------------------
% Load the dimensions of the specimen
try
    PK_abmessungen = xlsread([pathName 'PK_Abmessungen.xlsx'], 'Tabelle1');
    breite = PK_abmessungen(1,1);
    hoehe = PK_abmessungen(2,1);
    l1 = PK_abmessungen(3,1);
    l2 = PK_abmessungen(4,1);
catch
    msgbox('Probekörperabmessungen konnten nicht gefunden werden! Es werden
folgende Werte benutzt: B=20mm; 2h=3mm; l1=4mm; l2=0mm','Achtung', 'warn');
    breite = 0.02;
    hoehe = 0.003;
    l1 = 0.004;
    l2 = 0;
end
%--------------------------------------------------------------------------
% Calculation oft he crack length using the compliance calibration
% a=(delta/P)^(1/k)*d^(1/k)
for f = 1:pline_max
    P_MAX(f,7) = ((P_MAX(f,3)/P_MAX(f,2))^(1/k))*(d^(-(1/k)));
end
%--------------------------------------------------------------------------
% Use only rows where the crack length increment is greater than 0.1 mm
last = 2;
for next = 2:pline_max
   if (P_MAX(next,7) - P_MAX(last-1,7))> 0.0001
       P_MAX(last,:) = P_MAX(next,:);
       last = last+1;
   end
end
last = last-1;
P_MAX = P_MAX(1:last,:);
%--------------------------------------------------------------------------
% Calculation of the correction factors F and N
for g = 1:last
    % F = 1 - 3/10*(delta/a)^2 - 2/3*(delta*l1/a^2)
    P_MAX(g,5) = 1 - (3/10)*((P_MAX(g,3)/P_MAX(g,7))^2) -
    (2/3)*((P_MAX(g,3)*l1)/((P_MAX(g,7))^2));
    % N = 1 - (l2/a)^3 - 9/8*[1 - (l2/a)^2]*(delta*l1/a^2) -
    % 9/35*(delta/a)^2
```

```
    P_MAX(g,6) = 1 - ((l2/P_MAX(g,7))^3) - (9/8)*(1-
    ((l2/P_MAX(g,7))^2))*(P_MAX(g,3)*l1/((P_MAX(g,7))^2)) -
    (9/35)*((P_MAX(g,3)/P_MAX(g,7))^2);
end
%-------------------------------------------------------------------------
% Calculation of G using the simple Beam Theory (BT)
% G(BT) = 3*P*delta / 2*b*a
for h = 1:last
    P_MAX(h,8) = (3*P_MAX(h,2)*P_MAX(h,3)) / (2*breite*P_MAX(h,7));
end
%-------------------------------------------------------------------------
% Calculation of G using Corrected Beam Theory (CBT)
% a) Diagram (C/N)^(1/3) vs. a
cn13 = 1:last;
aforCBT = 1:last;
for index = 1:last
    cn13(index) = ((P_MAX(index,4)/P_MAX(index,6))^(1/3));
    aforCBT(index) = P_MAX(index,7);
end
% b) Trendline
gerade_CBT = polyfit(aforCBT,cn13,1);
x_wert_CBT = -0.01:0.001:0.08;
x_wert_CBT = x_wert_CBT';
[zei spa] = size(x_wert_CBT);
y_wert_CBT = zeros(zei,spa);
for xy = 1:zei
    y_wert_CBT(xy,1) = gerade_CBT(1)*x_wert_CBT(xy,1) + gerade_CBT(2);
end
% c) Section Delta on the x-axis
x_abschnitt = -gerade_CBT(2)/gerade_CBT(1);
if x_abschnitt < 0
    delta_CBT = abs(x_abschnitt);
else
    delta_CBT = 0;
end

if zeichnen == 1
    plot(aforCBT,cn13,x_wert_CBT,y_wert_CBT);
    axis([-0.010 0.080 0 0.1])
    xlabel('Cracklenght a [m]')
    ylabel('(C/N)^(^1^/^3^)')
    title('Modyfied Beam Theory')
    C = num2cell(delta_CBT);
    text(0.020,0.07,['\Delta = ' C],'HorizontalAlignment','left')
end

% d) Calculation
for m = 1:last
    P_MAX(m,9) = (3*P_MAX(m,2)*P_MAX(m,3)*P_MAX(m,5)) /
(2*breite*(P_MAX(m,7)+delta_CBT)*P_MAX(m,6));
end
%-------------------------------------------------------------------------
% Calculation of G using Modified Compliance Calibration (MCC)
% a) Diagramm (BC/N)^(1/3) über a/h
bcn13 = 1:last;
abyh = 1:last;
for n = 1:last
    bcn13(n) = ((breite*P_MAX(n,4)/P_MAX(n,6))^(1/3));
    abyh(n) = (P_MAX(n,7)/hoehe);
end
% b) Trendline
gerade_MCC = polyfit(abyh,bcn13,1);
```

```
x_wert_MCC = -0.10:0.001:0.080;
x_wert_MCC = x_wert_MCC';
[zeil spal] = size(x_wert_MCC);
y_wert_MCC = zeros(zeil,spal);
for xyz = 1:zeil
    y_wert_MCC(xyz,1) = gerade_MCC(1)*x_wert_MCC(xyz,1)+gerade_MCC(2);
end

if zeichnen == 1
    figure
    plot(abyh,bcn13, x_wert_MCC, y_wert_MCC);
    axis([-0.01 0.08 0 0.1])
    xlabel('a/h')
    ylabel('(B*C/N)^(^1^/^3^)')
    title('Modyfied Compliace Calibration')
    CC = num2cell(gerade_MCC(1));
    text(0.02,0.07,['m = ' CC],'HorizontalAlignment','left')
end

% c) Calculation
steig = gerade_MCC(1);
for o = 1:last
    P_MAX(o,10) = (3*steig)/(2*hoehe) * ((P_MAX(o,2)/breite)^2) *
(((breite*P_MAX(o,4))/P_MAX(o,6))^(2/3)) * P_MAX(o,5);
end
%--------------------------------------------------------------------------
% Separation of the data in one matrix for each step
mainIndex = 2;
runIndex = 1;
SplitMatrix = struct('cycle', {}, 'crackLength', {});
objectIndex = 1;

SplitMatrix(1).cycle = P_MAX(1, 1);
SplitMatrix(1).crackLength = P_MAX(1, 7);

while 1
    if (abs(P_MAX(mainIndex, 3)- P_MAX(mainIndex - 1, 3)) > 0.0004)

        objectIndex = objectIndex + 1;
        runIndex = 1;

    end
        SplitMatrix(objectIndex).cycle(runIndex) = P_MAX(mainIndex, 1);
        SplitMatrix(objectIndex).crackLength(runIndex) = P_MAX(mainIndex,
7);
        mainIndex = mainIndex + 1;
        runIndex = runIndex + 1;

    if(mainIndex > size(P_MAX, 1))
        break;
    end
end

%--------------------------------------------------------------------------
% Calculation of da/dN using 7-point method
bufferVar = zeros(0);
for i=1:length(SplitMatrix)
    if (length(SplitMatrix(i).cycle) > 1)
        punkte = length(SplitMatrix(i).cycle);
        A_N = zeros(length(SplitMatrix(i).cycle), 2); % Matrix with crack
                                                      % length and cyycles
```

```
        A_N(:,1) = SplitMatrix(i).cycle;
        A_N(:,2) = SplitMatrix(i).crackLength;
        dadN = (1:punkte);
        for z = 1:punkte
            switch z
                case 1
                    dadN(z) = (A_N(z+1,2)-A_N(z,2))/(A_N(z+1,1)-A_N(z,1));
                case punkte
                    dadN(z) = (A_N(punkte,2)-A_N(punkte-
                    1,2))/(A_N(punkte,1)-A_N(punkte-1,1));
                case 2
                    pt = [A_N(z,1);A_N(z,2)];
                    subserie_N = A_N(z-1:z+1,1);
                    subserie_a = A_N(z-1:z+1,2);
                    fit = polyfit(subserie_N, subserie_a, 2);
                    steigung_in_pt = 2*fit(1)*pt(1)+fit(2);
                    dadN(z)= steigung_in_pt;
                case punkte-1
                    pt = [A_N(z,1);A_N(z,2)];
                    subserie_N = A_N(z-1:z+1,1);
                    subserie_a = A_N(z-1:z+1,2);
                    fit = polyfit(subserie_N, subserie_a, 2);
                    steigung_in_pt = 2*fit(1)*pt(1)+fit(2);
                    dadN(z)= steigung_in_pt;
                case 3
                    pt = [A_N(z,1);A_N(z,2)];
                    subserie_N = A_N(z-2:z+2,1);
                    subserie_a = A_N(z-2:z+2,2);
                    fit = polyfit(subserie_N, subserie_a, 2);
                    steigung_in_pt = 2*fit(1)*pt(1)+fit(2);
                    dadN(z)= steigung_in_pt;
                case punkte-2
                    pt = [A_N(z,1);A_N(z,2)];
                    subserie_N = A_N(z-2:z+2,1);
                    subserie_a = A_N(z-2:z+2,2);
                    fit = polyfit(subserie_N, subserie_a, 2);
                    steigung_in_pt = 2*fit(1)*pt(1)+fit(2);
                    dadN(z)= steigung_in_pt;
                otherwise
                    pt = [A_N(z,1);A_N(z,2)];
                    subserie_N = A_N(z-3:z+3,1);
                    subserie_a = A_N(z-3:z+3,2);
                    fit = polyfit(subserie_N, subserie_a, 2);
                    steigung_in_pt = 2*fit(1)*pt(1)+fit(2);
                    dadN(z)= steigung_in_pt;
                end
        end

        bufferSize = length(bufferVar) + 1;

        for j=1:length(dadN)
           bufferVar(bufferSize) = dadN(j);
           bufferSize = bufferSize + 1;
        end
    else
        bufferSize = length(bufferVar) + 1;
        bufferVar(bufferSize) = NaN;
    end
end
%-------------------------------------------------------------------------
% Write da/dN to P_MAX
for zzz = 1:length(bufferVar)
```

```
    P_MAX(zzz,12) = bufferVar(zzz)*1000; % converting to mm/cycle
end
%--------------------------------------------------------------------------
% Write data to text file for analysis with Origin
fid = fopen([pathName peek '_' nr '_kalibrierte Berechnung_meter'
'.txt'],'wt');
fprintf(fid,'%s', P_MAX_header{:} );
for i = 1:size(P_MAX,1)
    fprintf(fid,'\n%s',num2str(P_MAX(i,:)));
end
fclose(fid);

disp('Erfolgreich abgeschlossen');
```

```
% PART 4
% MODE II C-ELS
% Calculation of the energy release rate G and the crack propagation rate
% based on the machine- and calibration data.
%--------------------------------------------------------------------------
close all
clear all
% Dialog box to select the calibration data
[fileName, pathName] = uigetfile({'*.mat';'*.*'}, 'Kalibrierdaten_meter
öffnen');
try
    load([pathName fileName]);
catch
    msgbox('Angegebenes File konnte nicht gefunden werde!');
    return
end
%--------------------------------------------------------------------------
% Load the dimensions of the specimen
try
    PK_abmessungen = xlsread([pathName 'PK_Abmessungen.xlsx'], 'Tabelle1');
    breite = PK_abmessungen(1,1)/1000;
    hoehe = PK_abmessungen(2,1)/1000;
    l1 = PK_abmessungen(3,1)/1000;
    l2 = PK_abmessungen(4,1)/1000;
    l3 = PK_abmessungen(5,1)/1000;
    H = PK_abmessungen(6,1)/1000;
    L_einspann = PK_abmessungen(7,1)/1000;
    Emodul = PK_abmessungen(8,1)*1000*1000;
catch
    msgbox('Probekörperabmessungen konnten nicht gefunden werden! Es werden
folgende Werte benutzt: B=20mm; 2h=3mm; l1=4mm; l2=0mm; l3=0mm, H=0mm,
','Achtung', 'warn');
    breite = 0.02;
    hoehe = 0.003;
    l1 = 0.004;
    l2 = 0;
    l3 = 0;

end
hhalbe= hoehe/2;
format short;
%--------------------------------------------------------------------------
% Calculation the crack length using the compliance calibration
for f = 1:pline_max
    P_MAX(f,7) = ((P_MAX(f,4)-c0)/m)^(1/3);
end
%--------------------------------------------------------------------------
% Only use rows were the crack length increment is greater than 0.1 mm
last = 2;
for next = 2:pline_max
   if (P_MAX(next,7) - P_MAX(last-1,7))> 0.0001
       P_MAX(last,:) = P_MAX(next,:);
       last = last+1;
   end
end
last = last-1;
P_MAX = P_MAX(1:last,:);
%--------------------------------------------------------------------------
% Calculation of the correction factors F and N
PHI = zeros(last,5);
for g = 1:last
```

```
    PHI(g,1)= 3/20*((15 + 50*((P_MAX(g,7)/L_einspann)^2) +
    63*((P_MAX(g,7)/L_einspann)^4))/((1+3*((P_MAX(g,7)/L_einspann)^3))^2));

    PHI(g,2)= (-3*(L_einspann/P_MAX(g,7))*(1+3*((P_MAX(g,7)
     /L_einspann)^2)))  / (1+3*((P_MAX(g,7)/L_einspann)^3));

    PHI(g,3)= 4 / (1+3*((P_MAX(g,7)/L_einspann)^3));

    PHI(g,4)= (-9/4) * ( (1-(P_MAX(g,7)/L_einspann))*(1+3*
     ((P_MAX(g,7)/L_einspann)^3)) + 4*((P_MAX(g,7)/L_einspann)^2)*(1-
     ((l2/P_MAX(g,7))^2))*(1+3*((P_MAX(g,7)/L_einspann)^2))) /
     ((1+3*((P_MAX(g,7)/L_einspann)^3))^2);

    PHI(g,5)= (36/35) * (1+(3/8)*((P_MAX(g,7)/L_einspann)^3)*
     (35+70*((P_MAX(g,7)/L_einspann)^2)+63*((P_MAX(g,7)/L_einspann)^4))) /
     ((1+7*((P_MAX(g,7)/L_einspann)^3))^3);
end

for gg = 1:last
     % F:
     P_MAX(gg,5) = 1 - PHI(gg,1)*((P_MAX(gg,3)/L_einspann)^2) -
      PHI(gg,2)*((P_MAX(gg,3)*l1)/(L_einspann^2));
     % N:
     P_MAX(gg,6) = 1 - PHI(gg,3)*((l2/L_einspann)^3) -
      PHI(gg,4)*((P_MAX(gg,3)*l1)/(L_einspann^2)) -
      PHI(gg,5)*((P_MAX(gg,3)/L_einspann)^2);
end
%-------------------------------------------------------------------------
% Calculation of G using the Experimental Compliance Caliibration
for h = 1:last
    P_MAX(h,8) = ((3*(P_MAX(h,2)^2)*(P_MAX(h,7)^2)*m)/(2*breite)) *
     P_MAX(h,5);
end
%-------------------------------------------------------------------------
% Calculation of G using the Corrected Beam Theory (CBT)
% a) a_effective
delta_clamp = -0.00509; %Steel/EPOXY
for i = 1:last
    P_MAX(i,10) = ((1/3)*(2*breite*P_MAX(i,4)*(hhalbe^3)*Emodul -
(L_einspann + delta_clamp)^3))^(1/3);
end
% d) Calculation
for m = 1:last
    P_MAX(m,9) =
((9*(P_MAX(m,2)^2)*(P_MAX(m,10)^2))/(4*(breite^2)*(hhalbe^3)*Emodul)) *
P_MAX(m,5);
end
%-------------------------------------------------------------------------
% Calculation of da/dN using the 7-point method
punkte = last;
A_N = zeros(punkte, 2);   % Matirix with crack length and cycles
A_N(:,1) = P_MAX(:,1);
A_N(:,2) = P_MAX(:,7);
dadN = (1:punkte);
for z = 1:punkte
    switch z
        case 1
            dadN(z) = (A_N(z+1,2)-A_N(z,2))/(A_N(z+1,1)-A_N(z,1));
        case punkte
            dadN(z) = (A_N(punkte,2)-A_N(punkte-1,2))/(A_N(punkte,1)-
             A_N(punkte-1,1));
        case 2
```

```
            pt = [A_N(z,1);A_N(z,2)];
            subserie_N = A_N(z-1:z+1,1);
            subserie_a = A_N(z-1:z+1,2);
            fit = polyfit(subserie_N, subserie_a, 2);
            steigung_in_pt = 2*fit(1)*pt(1)+fit(2);
            dadN(z)= steigung_in_pt;
        case punkte-1
            pt = [A_N(z,1);A_N(z,2)];
            subserie_N = A_N(z-1:z+1,1);
            subserie_a = A_N(z-1:z+1,2);
            fit = polyfit(subserie_N, subserie_a, 2);
            steigung_in_pt = 2*fit(1)*pt(1)+fit(2);
            dadN(z)= steigung_in_pt;
        case 3
            pt = [A_N(z,1);A_N(z,2)];
            subserie_N = A_N(z-2:z+2,1);
            subserie_a = A_N(z-2:z+2,2);
            fit = polyfit(subserie_N, subserie_a, 2);
            steigung_in_pt = 2*fit(1)*pt(1)+fit(2);
            dadN(z)= steigung_in_pt;
        case punkte-2
            pt = [A_N(z,1);A_N(z,2)];
            subserie_N = A_N(z-2:z+2,1);
            subserie_a = A_N(z-2:z+2,2);
            fit = polyfit(subserie_N, subserie_a, 2);
            steigung_in_pt = 2*fit(1)*pt(1)+fit(2);
            dadN(z)= steigung_in_pt;
        otherwise
            pt = [A_N(z,1);A_N(z,2)];
            subserie_N = A_N(z-3:z+3,1);
            subserie_a = A_N(z-3:z+3,2);
            fit = polyfit(subserie_N, subserie_a, 2);
            steigung_in_pt = 2*fit(1)*pt(1)+fit(2);
            dadN(z)= steigung_in_pt;
        end
end
%-------------------------------------------------------------------------
% Calculation of da/dN using the secant mehtod
dadN_sek = zeros(punkte,1);
for zsek = 2:punkte
    dadN_sek(zsek) = (A_N(zsek,2)-A_N(zsek-1,2))/(A_N(zsek,1)-A_N(zsek-
1,1));
end
%-------------------------------------------------------------------------
% Write da/dN to P_MAX
for zzz = 1:last
    P_MAX(zzz,12) = dadN(zzz)*1000; % umrechnen auf mm/Zyklus
    P_MAX(zzz,11) = dadN_sek(zzz)*1000; % umrechnen auf mm/Zyklus
end
%-------------------------------------------------------------------------
% Write data to text file for analysis with Origin
fid = fopen([pathName peek '_' nr '_kalibrierte Berechnung_meter'
'.txt'],'wt');
fprintf(fid,'%s', P_MAX_header{:} );
for i = 1:size(P_MAX,1)
    fprintf(fid,'\n%s',num2str(P_MAX(i,:)));
end
fclose(fid);

disp('Erfolgreich abgeschlossen');
```

```
% PART 5
% MODE II 3ENF
% Calculation of the energy release rate G and the crack propagation rate
% based on the machine- and calibration data.
%--------------------------------------------------------------------------
close all
clear all
[fileName, pathName] = uigetfile({'*.mat';'*.*'}, 'Kalibrierdaten_meter
öffnen');
try
    load([pathName fileName]);
catch
    msgbox('Angegebenes File konnte nicht gefunden werde!');
    return
end
%--------------------------------------------------------------------------
% Load the dimensions of the specimen
try
    PK_abmessungen = xlsread([pathName 'PK_Abmessungen.xlsx'], 'Tabelle1');
    breite = PK_abmessungen(1,1)/1000;
    hoehe = PK_abmessungen(2,1)/1000;
    Emodul = PK_abmessungen(8,1)*1000000;
catch
    msgbox('Probekörperabmessungen konnten nicht gefunden
werden!','Achtung', 'warn');
    return

end
zweiL = 0.1;
L = 0.05;
%--------------------------------------------------------------------------
% Calculation of the crack length using the compliance calibration
for f = 1:pline_max
    P_MAX(f,5) = ((P_MAX(f,4)-c0)/m)^(1/3);
end
%--------------------------------------------------------------------------
% Only use rows were the crack length increment is greater than 0.1 mm
last = 2;
for next = 2:pline_max
   if (P_MAX(next,5) - P_MAX(last-1,5))> 0.0001
       P_MAX(last,:) = P_MAX(next,:);
       last = last+1;
   end
end
last = last-1;
P_MAX = P_MAX(1:last,:);
%--------------------------------------------------------------------------
% Calculation of G using the Beam Theory (BT)
for h = 1:last
    P_MAX(h,6) = (9*P_MAX(h,2)*P_MAX(h,3)*(P_MAX(h,5)^2))/
     (2*breite*(2*(L^3)+3*(P_MAX(h,5)^3)));
end
%--------------------------------------------------------------------------
% Calculation of da/dN via 7-point method
punkte = last;
A_N = zeros(punkte, 2);    % Matrix with crack length and cycles
A_N(:,1) = P_MAX(:,1);
A_N(:,2) = P_MAX(:,5);
dadN = (1:punkte);
for z = 1:punkte
    switch z
        case 1
```

```
            dadN(z) = (A_N(z+1,2)-A_N(z,2))/(A_N(z+1,1)-A_N(z,1));
        case punkte
            dadN(z) = (A_N(punkte,2)-A_N(punkte-1,2))/(A_N(punkte,1)-
A_N(punkte-1,1));
        case 2
            pt = [A_N(z,1);A_N(z,2)];
            subserie_N = A_N(z-1:z+1,1);
            subserie_a = A_N(z-1:z+1,2);
            fit = polyfit(subserie_N, subserie_a, 2);
            steigung_in_pt = 2*fit(1)*pt(1)+fit(2);
            dadN(z)= steigung_in_pt;
        case punkte-1
            pt = [A_N(z,1);A_N(z,2)];
            subserie_N = A_N(z-1:z+1,1);
            subserie_a = A_N(z-1:z+1,2);
            fit = polyfit(subserie_N, subserie_a, 2);
            steigung_in_pt = 2*fit(1)*pt(1)+fit(2);
            dadN(z)= steigung_in_pt;
        case 3
            pt = [A_N(z,1);A_N(z,2)];
            subserie_N = A_N(z-2:z+2,1);
            subserie_a = A_N(z-2:z+2,2);
            fit = polyfit(subserie_N, subserie_a, 2);
            steigung_in_pt = 2*fit(1)*pt(1)+fit(2);
            dadN(z)= steigung_in_pt;
        case punkte-2
            pt = [A_N(z,1);A_N(z,2)];
            subserie_N = A_N(z-2:z+2,1);
            subserie_a = A_N(z-2:z+2,2);
            fit = polyfit(subserie_N, subserie_a, 2);
            steigung_in_pt = 2*fit(1)*pt(1)+fit(2);
            dadN(z)= steigung_in_pt;
        otherwise
            pt = [A_N(z,1);A_N(z,2)];
            subserie_N = A_N(z-3:z+3,1);
            subserie_a = A_N(z-3:z+3,2);
            fit = polyfit(subserie_N, subserie_a, 2);
            steigung_in_pt = 2*fit(1)*pt(1)+fit(2);
            dadN(z)= steigung_in_pt;
        end
end
%-------------------------------------------------------------------------
% Calculation of da/dN via secant method
dadN_sek = zeros(punkte,1);
for zsek = 2:punkte
    dadN_sek(zsek) = (A_N(zsek,2)-A_N(zsek-1,2))/(A_N(zsek,1)-A_N(zsek-
1,1));
end
%-------------------------------------------------------------------------
for zzz = 1:last
    P_MAX(zzz,8) = dadN(zzz)*1000; % convert to mm/cycle
    P_MAX(zzz,7) = dadN_sek(zzz)*1000; % convert to mm/cycle
end
%-------------------------------------------------------------------------
% Write data to text file for analysis with Origin
fid = fopen([pathName peek '_' nr '_kalibrierte Berechnung_meter'
'.txt'],'wt');
fprintf(fid,'%s', P_MAX_header{:} );
for i = 1:size(P_MAX,1)
    fprintf(fid,'\n%s',num2str(P_MAX(i,:)));
end
fclose(fid);
disp('Erfolgreich abgeschlossen');
```